Modeling and offline simulation of thermal spray coating process for gas turbine applications

Vom Fachbereich Maschinenbau
der Technischen Universität Darmstadt

zur Erlangung des Grades
eines Doktors der Naturwissenschaften
(Dr. rer. nat.)

genehmigte Dissertation von
Dipl. Physiker Alexandr Sadovoy
aus Saporoshje

Darmstadt 2014
D17

Referent: Prof. Dr. -Ing. Matthias Oechsner
Korreferent: Prof. Dr. rer. nat. habil. Prof. h. c. Dr. h. c. Ralf Riedel
Tag der Einreichung: 03.12.2013
Tag der Prüfung: 15.04.2014

Erklärung

Hiermit erkläre ich, dass ich die vorgelegte Dissertation selbstständig verfasst und nur die angegebenen Hilfen verwendet habe.

Content

Zusammenfassung

Moderne Beschichtungen für komplexe Heißgaskomponenten wie Turbinenschaufeln haben sehr strenge Anforderungen an die Schichtdickenverteilung. Die Erfüllung dieser Anforderungen ist entscheidend für die Leistung und die Lebensdauer der Komponenten. Die meisten Hochtemperaturschutzschichten werden mit thermischen Spritzverfahren aufgetragen. Obwohl vielen wissenschaftlichen und technischen Forschungen werden die Besonderheiten der Spritzprozessen und ihre Beziehung zu finalen Schichteigenschaften nicht vollständig verstanden. In der Praxis werden die Beschichtungsprozessparameter, um erwünschten Schichteigenschaften zu erreichen, durch „trials and errors“ Ansatz mit Verwendung von verschiedenen Prozessüberwachungstechniken etabliert. Entsprechende Versuche werden in der Regel in den Produktionsanlagen mit Industrieroboter erfolgt, was macht diesen Ansatz sehr teuer und zeitaufwendig. Zur Vereinfachung und Beschleunigung des Schichtentwicklungsprozess wurden verschiedene Modelle und Softwarewerkzeuge entwickelt, um die Beschichtungsprozesse zu simulieren und die Schichteigenschaften vorherzusagen. Diese Modelle sind überwiegend auf ausgewählte Aspekte vom Beschichtungsprozess fokussiert. Hierbei gibt es zurzeit kein Model, um eine zuverlässige Vorhersage der Dicke einer kompletten Schicht auf realen Substratoberflächen, insbesondere von den komplexen Turbinenkomponenten, zu ermöglichen.

In dieser Arbeit wurde ein theoretisches Modell, basierend auf physikalischen Prinzipien entwickelt, um die Dickenverteilung von thermisch gespritzten Schichten zu simulieren. Dabei wurde der Massenkonservierungsprinzip mit der Anwendung der geometrischen Überlegungen angewandt um den Pulverspritzstrahl und die daraus resultierende Beschichtungsmuster zu modellieren. Einfluss der Prozessbedingungen auf die grundlegenden Spritzmuster wie das Spritzfleck und das Spritzprofil wurde theoretisch untersucht. Eine analytische Beziehung wurde zwischen der Dickenverteilung im Spritzfleck, Profil und der Dicke der resultierenden Schichtlage auf den flachen und zylindrischen Substraten entwickelt. Die Modellergebnisse und Annahmen wurden in den entsprechenden Experimenten überprüft und bestätigt.

Wesentliche Aspekte der Prozessmodellierung für die Entwicklung von Off-Line-Programmierung (OLP) Software zur Roboterprogrammierung mit numerischer Simulation von resultierenden Schichtdicken auf beliebigen Substratoberflächen wurden diskutiert. Die Umsetzung des entwickelten Models in RobCad Software für die Simulation von Wärmedämmschicht (WDS) auf einer Gasturbinenschaufel wurde präsentiert und diskutiert. Die Anwendung der Schichtdickensimulation in Kombination mit OLP-Technik ermöglicht ein vollständiger digitaler Prozess von Beschichtungsprozessentwicklung.

Abstract

Modern thermal spray coatings for complex hot gas components such as turbine blades and vanes have very strict requirements for the distribution of thickness. Meeting the requirements is critical for the performance and the lifetime of components. In particular, thickness of the thermal barrier coatings (TBC) determines a temperature gradient through the coating, which provides a thermal protection of cooled substrate and influences thermo-mechanical properties. The majority of high temperature protective coatings are applied with thermal spray techniques. Although there are many scientific and technical studies, all peculiarities of the thermal spray process and their relation to final coating properties are not completely understood. In practice, the parameters of the deposition process to produce coatings with required characteristics are established by a “trials and errors” approach with involvement of various process control techniques. These trials are usually done in production booths with an industrial robot, which makes this approach in most cases very expensive and time-consuming. In order to simplify and speed up the coating development, various models and software tools were developed to simulate the deposition process and predict specific coating properties. These models are predominantly focused on some selected aspects of the coating deposition. At the same time, there is no available model to provide a reliable prediction of thickness of the final coating layer on a particular substrate.

In this paper, a self consistent model based on physical principles is developed to simulate a thickness distribution of thermally sprayed coatings. In particular, the mass conservation principle with the application of geometric considerations was applied to model the spray jet and the resulting coating pattern. An influence of the process conditions on the basic spray patterns represented by spray spot and spray profile is theoretically investigated. An analytic relationship between thickness distribution in the spray spot, spray profile and thickness of the corresponding coating layer produced by a motion of the spray gun over a flat and cylindrical substrate was established, and corresponding results were discussed. The model results and assumptions were verified in the corresponding experiments.

The application of the model was outlined for an arbitrary free-form substrate surface. Some aspects of coating process modeling, related to development of the off-line programming (OLP) software tools to perform robot programming with simultaneous numerical simulation of the resulting coating thickness are discussed. An example of implementation of the developed model into RobCad software to predict thickness distribution of a TBC coating on a gas turbine blade is presented and discussed. Application of the coating deposition model in combination with the OLP technique enables a full-cycle digital coating program development, considerably optimizing development time and costs.

1 Motivation and problem definition

1.1 Motivation and problem analysis

Nowadays most components for industrial and aircraft gas turbines require protective coatings to meet performance and operational lifetime requirements. The most critical components of the gas turbine are rotary blades and stationary vanes, which undergo severe thermal and mechanical loads in a corrosive and oxidizing environment. The environmental and thermal protection of these components is achieved by the application of thermal barrier coatings (TBC). These coatings represent multilayer systems, which consist of a metallic oxidation protective layer and ceramic thermal barrier layer. The majority of TBC systems are applied with various thermal spray techniques. The function of TBC systems, their characteristics and deposition methods are discussed in this thesis in Chapters 2.1 and 2.2. Physical processes involved in coating deposition are very complex. The summary of theoretical and experimental work devoted to deposition process study is presented in Chapter 2.3. Nevertheless of a lot of scientific and technical efforts, all peculiarities of the thermal spray process and their relation to final coating properties are not completely understood. This makes it difficult to achieve technically important coating characteristics such as thickness, roughness, porosity and microstructure on real components to be coated. One of the most important characteristics of the TBC is a coating thickness and its distribution on a particular component. Usually a uniform thickness distribution for a whole component or for its selected areas is required by the particular component design. Thickness distributions on gas turbine components, and especially on turbine blades and vanes, have very narrow tolerances and their fulfillment is strictly controlled in the coating production process.

As pointed out in Chapter 2.4, thermally sprayed coating layers are produced by motion of the spray gun, typically driven by an industrial robot. The required thickness distribution in the coating layer is achieved by development of a specific robot motion path for the component to be coated. Common practice in the process of the spray path development is an iterative trials and errors approach which involves a spray trial, lab inspection of the resulting thickness distribution and adjustment of the spray paths segments to improve the spraying result. This approach can be applied to components with a relatively simple surface geometry. But it becomes much more difficult to develop a spray path for components with a complex 3D shape, such as turbine blades and vanes, due to an increased number of manual operations involved, and due to a large number of iterations to achieve the desired

thickness distribution. Furthermore, these iterative trials are usually done in the production booths, which makes this approach in most cases very expensive and time-consuming.

Recently the off-line (OLP) technique based on computer simulation of the coater robot motion was developed and applied to the thermal spray processes. The OLP technique enabled robot programming operations in the real spray booth to be replaced by simulation within a virtual software environment. As discussed in Chapter 2.4, application of these software tools accelerates the process of spray program development and at the same time avoids blockage of the production booth to perform programming operations. Furthermore, the coating programs developed with OLP are more transparent, flexible for further modifications, and enable more accurate and precise robot motion control.

An important functionality of advanced OLP software packages, such as RobCad from Siemens Industry Software, in addition to robot motion programming is an ability to calculate numerically an accumulation of the coating thickness on the component surface. This functionality enables a closed spray path development process including programming of robot motion, analysis of simulated thickness result and subsequent spray path improvement within the virtual OLP environment. Furthermore, simulation results in the form of thickness mapping allow coating features to be investigated at any point on the component surface. This, in addition to the conventional thickness verification methods based on metallographic evaluation of a limited number of cross sections of the component, provides a much higher level of confidence that thickness requirements are fulfilled at any point on the component. To provide an accurate simulation of the coating thickness distribution on the real turbine components, an accurate deposition process model which describes dynamic changes of the

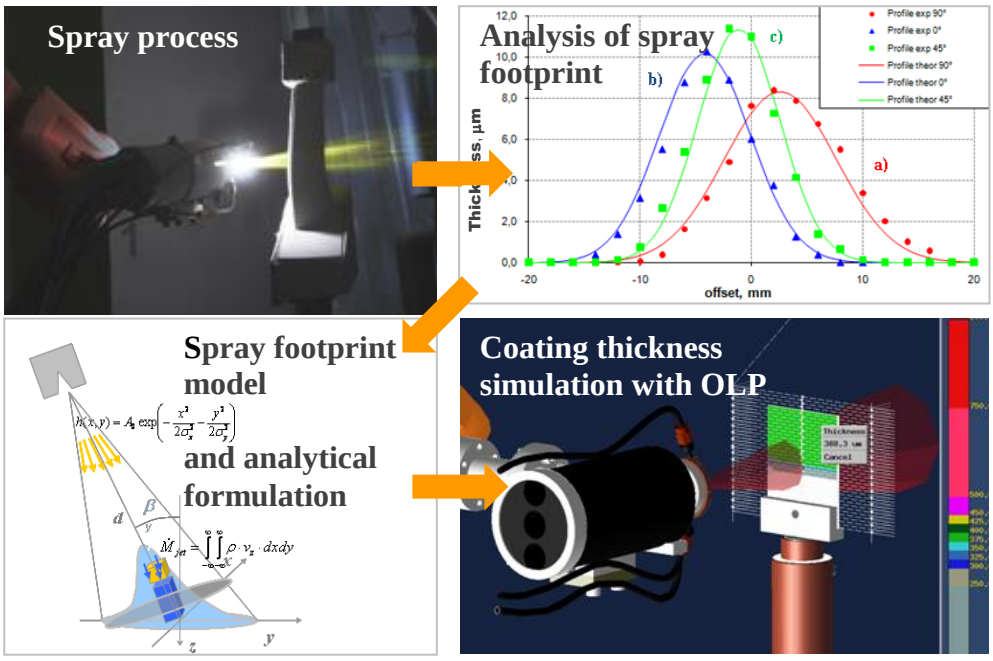

Figure 1.1: Concept of realistic coating thickness simulation with application of off-line programming and robotic simulation.

spray footprint has to be developed. An input of the basic footprint together with the model describing footprint change with the process conditions is necessary for calculation of thickness distribution generated by an arbitrary motion of the spray gun on the component. This simulation concept is illustrated in Figure 1.1. Here, dependences of spray gun settings, geometry conditions at the substrate and cinematic parameters of the spray gun motion over the surface of a particular component have to be reflected by the simulation model to provide a realistic coating layer simulation within the OLP environment.

As pointed out in Chapters 2.3 and 2.4, most of the known thermal spray models and corresponding simulation tools developed to describe coating process are predominantly focused on some selected coating aspects or sub-processes. Thus, an interaction of feedstock powder with plasma or flame jet defines in-flight properties of particles prior to the impact onto the substrate surface and has a high influence on coating characteristics. These in-flight characteristics are commonly expressed by radial and axial distributions of particles' velocities, temperatures and sizes. On the other hand, complex thermo-mechanical interactions during a single particle impact, spreading and solidification on the substrate and previously deposited particles define the final coating morphology and physical properties. The surface geometry of a particular component in combination with cinematic and geometric characteristics of the spray gun motion defines the distribution of macroscopic properties in the coating pattern. Despite a lot of theoretical and experimental efforts, the relationships between the spray gun settings, in-flight properties, substrate conditions, gun motion characteristics and final properties of the coating layer such as thicknesses, porosity, interface roughness, and elastic and thermal properties are not established well enough to provide a reliable prediction of properties of the final coating layer on a particular component.

A need to predict thickness distribution in a coating layer motivated development of several simplified semi-empirical coating deposition models. These models are based on simulation of a basic coating footprint. In the case of an immovable spray gun this footprint represents a spray spot with a bell-like shape. Following the motion of the spray gun along the particular trajectory, the spray spot moves on the substrate surface and, as a result, produces the final coating layer. Thickness distribution in the spray spots and corresponding spray profiles, produced by a linear motion of the gun, are usually described by Gaussian functions. In multiple models, discussed in Chapter 2.3, the distribution functions were static and symmetrical around the spray spot centre. This simplification leads to the resulting spray profile, produced by gun motion, being independent of the motion characteristics. The assumption of the spray spot symmetry simplifies mathematical formulations for numerical calculation of the coating layer thickness but leads to a loss of model accuracy. Furthermore the parameters which define the spray spot were represented by empirical characteristics

calculated by data fitting from the direct measurement of actual spray patterns and do not have a relation to the physical processes involved in the deposition process. These limitations make it difficult to use the available models to predict coating layer thickness for variety of spraying conditions such as variable gun speed, spray distance and spray angle.

The final goal of the deposition process modeling is to discover peculiarities of coating layer formation under technically important process conditions on a particular component. This goal can be achieved by direct calculations for relatively simple components. In general, an implementation of the model into the OLP simulation software is necessary to predict coating thickness on the real turbine components with complex 3D geometry. The software implementation requires analytical understanding and mathematical formulation of the relationship between resulting thickness and deposition characteristics. Development of an accurate analytical model of deposition process with application for atmospheric plasma spraying of the TBC coating is the aim of this study.

1.2 Structure of the thesis

In this research a new coating simulation model which describes realistic cases of the asymmetrical spray patterns taking into account dependences of the thickness distribution on the practical process parameters and spray conditions has been developed. In Chapter 3.1 the general assumption and definitions of the models of the plasma and powder jets are discussed. In Chapter 3.2 a mass conservation principle was applied to connect the distributions of the powder flux and resulting coating thickness distribution in an asymmetrical elliptic spray spot, which is described by a 2D Gaussian function. Furthermore, the amplitude and standard deviations of this Gaussian function were linked to each other and to the process parameters governing the total deposition mass, such as feed rate and deposition efficiency. The analytical solutions for the thickness distribution in the spray spot, taking into account changes of spray distance and inclination of the substrate in an arbitrary direction, were developed in Chapter 3.3 by application of the multi-directional transformation of rotation and shift. These transformations ensure conservation of powder mass approaching the surface for the substrates with arbitrary inclination in relation to the major axes of the elliptic spray spot. A corresponding analytical solution was applied in Chapter 3.4 to the realistic practical conditions, when the spray distances are much larger than the dimensions on the spray spot. In this case it is shown that the spray spot conserves the elliptic shape. Some modeling aspects for strongly asymmetrical spots, produced by spraying with double, triple and multiple injectors, are discussed in Chapter 3.5. In Chapter 4.1, based on the spray spot model, an analytical solution for thickness distribution in the spray profile is developed.

Important aspects of thickness dependence on the direction of the gun motion and further process parameters are discussed. An analytical calculation of the layer thickness was accomplished in Chapters 4.2 and 4.3 for the substrates with flat and cylindrical geometry. In particular, an influence of the substrate geometry and spray process parameters on the thickness and surface morphology is investigated and discussed. Some aspects of numerical simulation for free-form surfaces are discussed in Chapter 4.4. In Chapter 5 an experimental input of the necessary spray spot characteristics is introduced and discussed. Furthermore, an experimental verification of the model with comparison of the measured and predicted profile and complete coating layer results obtained for various process conditions is done and discussed. Chapter 6 describes substantial aspects and results of the model implementation into the RobCad simulation software. A change of parameters of the spray process, such as spray distance, direction of the gun tilt to the substrate, and local substrate curvature during the run time, is considered by the presented simulation approach. A realistic prediction and examination of the coating thickness is shown on an example of a turbine blade, coated with a program developed by RobCad software. The further perspectives to combine the spray process model, off-line simulation and on-line monitoring techniques are outlined in Chapter 7 to achieve more accurate and predictable coating simulation.

2 State of the art in thermal spraying

2.1 High temperature coatings for gas turbines

2.1.1 Gas turbine conditions

Structural materials and components of gas turbine engines for aircraft and power generation applications operate under very aggressive conditions characterized by high temperature and mechanical load in an oxidizing and corrosive atmosphere. The inlet temperatures in stationary gas turbines are about 1400-1500°C [1] and tend to exceed 1600°C for very modern engines. Increasing demands for turbine performance and efficiency require an increase in inlet temperatures up to levels close to melting points of the typical structural materials. Rotating blades and stationary vanes are the most loaded parts of the turbine, which are working at very high temperature and thermo-mechanical stresses. Furthermore, the rotating blades are subject to extreme centrifugal forces, which they have to sustain at high temperature in an aggressive environment. The combustion chamber and hot section of the turbine consist of diverse components which provide structural integrity and at the same time the thermal and environmental protection of the turbine components. Some of

these components are presented in Figure 2.1. These components undergo specific types of thermal, mechanical and corrosive load depending on the position in the turbine and particular operating conditions.

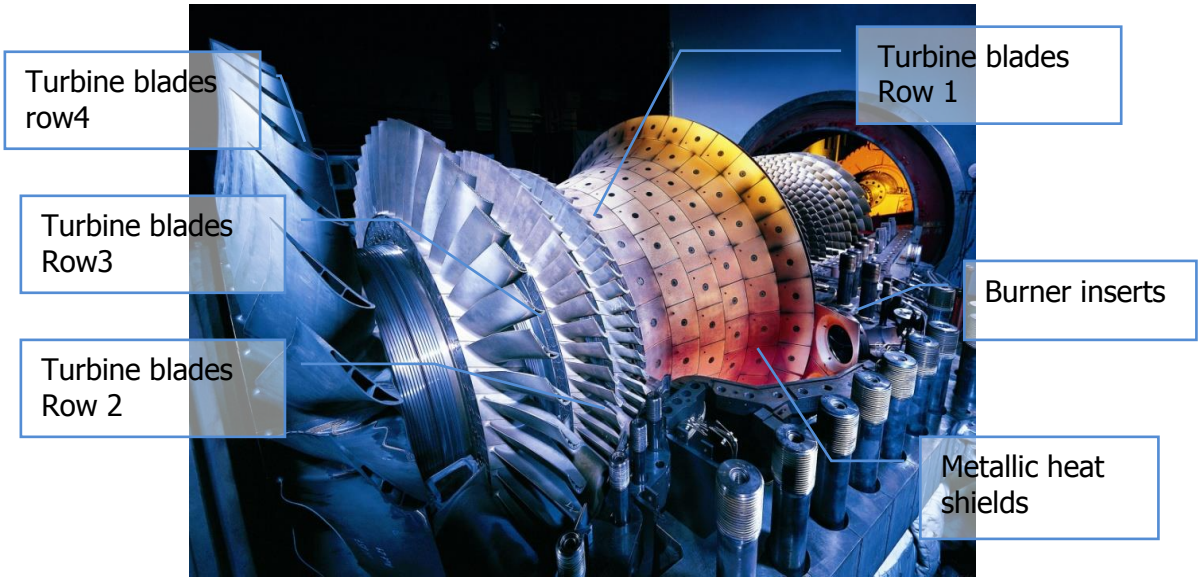

Figure 2.1: Hot gas section of gas turbine from Siemens.

Very complex manufacturing processes [1,2] and structural materials are involved in the production of these components to provide the needed functionality and sufficient lifetime.

2.1.2 Technology aspects of gas turbine components manufacturing

Technology improvements in materials in combination with development of manufacturing processes enable increasing turbine temperature demands to be achieved. Development of high temperature superalloys with advances in casting processes to produce components with directionally solidified and single crystal structures allowed a substantial increase in operation temperature. The superalloys have been developed as alloys on nickel or cobalt basis to achieve high mechanical strength and creep sustainability in combination with good oxidation and corrosion resistance at high temperatures. Improvement of high temperature mechanical properties of superalloys is typically compromised by a decrease in their environmental resistance at high temperatures. Hence, further substantial increase of the inlet temperature was achieved by introduction of the cooled blades and vanes. The air from the compressor is used to cool the most thermally loaded blades and vanes by passing the air through the internal channels of these components. This internal cooling requires production of complex internal cooling channels, which required development of advanced casting processes. The next generation of the cooled parts has film cooling, produced by

multiple rows of the narrow cooling holes, which provide a continuous cooling air film over the outer component surface. Due to the internal and outer film cooling, the temperatures on the functional surfaces of hot turbine parts could be substantially reduced, enabling a simultaneous increase in the gas temperatures. It should be mentioned that use of the air from the compressor for cooling purposes causes a substantial loss of the overall turbine efficiency. Hence other thermal protection mechanisms have to be used to provide further thermal protection of the turbine parts without reducing the engine efficiency.

The need to protect components from environmental degradation at elevated gas temperatures and at the same time not compromising their mechanical properties motivated development of protective coatings [3,4]. A type, application area and parameters of coatings depend on requested operational lifetime of a component during which the environmental protection has to be guaranteed. In general, overall lifetime of the component is defined by the turbine service conditions and is limited by mechanical properties of the superalloy and by functional lifetime of the protective coating. Figure 2.2 presents an overview of advances in the manufacturing technologies to produce modern turbine blades and vanes, including casting, cooling and coating processes.

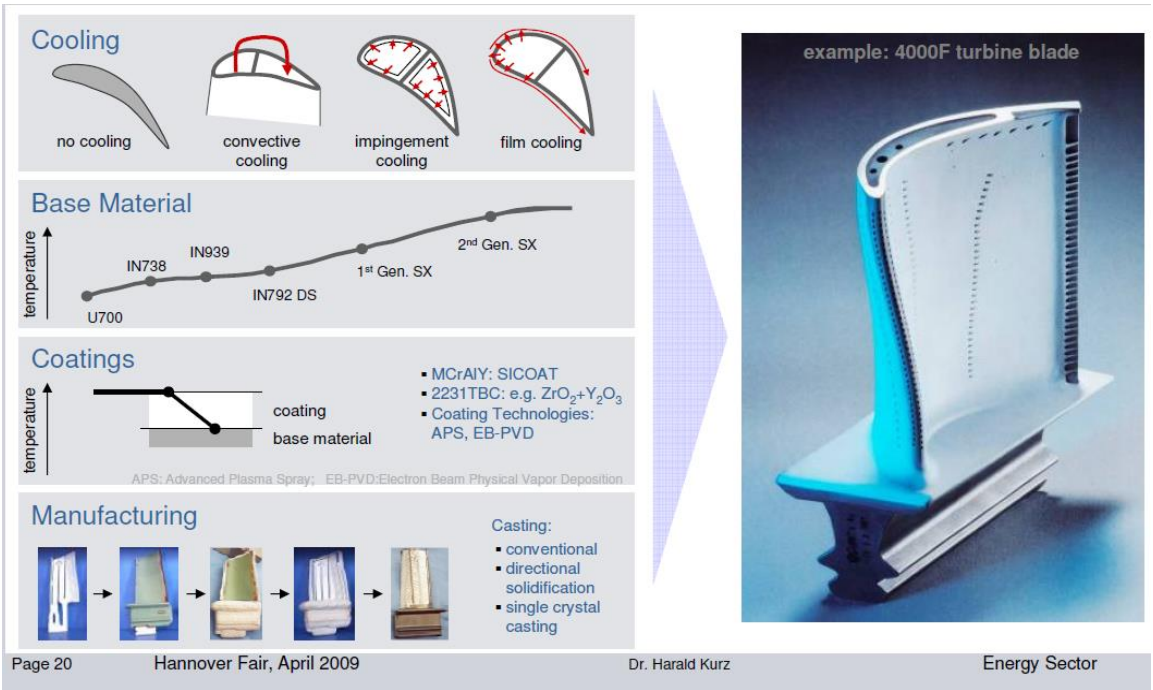

Figure 2.2: Turbine blade manufacturing progress, TBC coated blade from Siemens [2].

2.1.3 Oxidation and corrosion protective MCrAlY coatings

The most critical components of a gas turbine including rotating blades and stationary vanes have to be coated to enable oxidation and corrosion resistance. Two types of coatings

are most widely used for oxidation and corrosion protection: diffusion aluminide coatings based on nickel aluminides (NiAl) and overlay MCrAlY (typically M = nickel or cobalt) coatings [5,6]. The diffusion coatings are produced mostly by chemical vapor deposition (CVD), pack cementation or slurry fusion processes. Applied to nickel based substrates these coatings represent NiAl intermetallic phase produced by aluminium diffusion from the gas phase into the nickel alloy. The MCrAlYs are mostly deposited with thermal spray processes such as Low Pressure Plasma Spraying (LPPS) and High Velocity Oxy-Fuel Splaying (HVOF). The NiAl type of coatings has good oxidation resistance but lower thermo-mechanical properties at high temperatures in comparison with MCrAlY coatings. Hence for the high mechanically loaded parts of the gas turbine engines the trend is to use thermal sprayed MCrAlY coatings. The function of both NiAl and MCrAlY coating types is to provide a surface reservoir of aluminum which interacting with oxygen from the environment at high temperature forms a protective and adherent oxide layer. This thermally grown oxide (TGO) layer increases in thickness during the operation lifetime of the component. The TGO is represented by a high adherent and slowly growing Al_2O_3 oxide, which prevents or slows down further diffusion of oxygen into the coating. The aluminum, which is found generally in NiAl phase, is consumed by both TGO formation at the outer coating interface and by interdiffusion with the substrate at the inner coating surface. Due to aluminum consumption at both interfaces the coating becomes depleted producing aluminum depletion zones which increase in thickness with time and temperature. When aluminum from NiAl phase is completely consumed and the concentration reaches a critical minimum level, other non-protective oxides like Cr_2O_3 and/or spinels may form besides the protective TGO, leading to internal oxidation [3-6]. The lifetime of the MCrAlY is limited by depletion rate of aluminum and initial aluminum reservoir in the coating. The depletion rate is mostly defined by chemistry of the coating and the substrate material at selected service temperature. On the other hand, the initial amount of the aluminum reservoir is defined by coating thickness. The thicker coatings provide longer oxidation protection due to a larger amount of aluminum in the coating. Typically coatings of about 100-300 μm are used for gas turbine components for service temperatures up to 900-1100°C [3-6] depending on coating type and expected lifetime. Controlling the coating thickness for MCrAlY is a necessary requirement to achieve the oxidation lifetime of the coated turbine component in service. The coating thickness distribution on a turbine component is one of the most critical production parameters defining the quality of the MCrAlY coating.

2.1.4 Thermal barrier TBC coatings

The temperature capability of MCrAlY coatings is currently approaching its physical limit and further improvement is becoming increasingly difficult. Due to this a lot of efforts were devoted to developing thermal barrier coatings (TBC). This class of coatings represents ceramic coating layers with low thermal conductivity. The TBC insulates an internally cooled component from the hot gas enabling much higher combustion temperatures (with an increase of 100-200°C) without any increase in the bond coat and base alloy temperatures [3-6]. Thermal barrier coatings are playing an increasingly significant role in gas turbine engines both for aero and industrial applications. The TBC is usually applied with electron beam physical deposition (EBPVD) and atmospheric plasma spraying (APS) processes.

Thermal barrier coatings are multilayer systems consisting of a diffusion aluminide or MCrAlY metallic bond coat layer and a low thermal conductivity ceramic top layer. The bond coat provides oxidation resistance and mechanical adherence of the ceramic top coat. An Yttrium Stabilized Zirconia (YSZ) with 7-8 wt% Y_2O_3-ZrO_2 is the commonly used ceramic material for a top coat layer, which provides sufficient thermal insulation in combination with mechanical compatibility with bond coat and chemical stability at high service temperatures up to 1200°C [3]. The properties of the ceramic layer can be controlled by chemical composition and physical structure. Currently there are a lot efforts dedicated to developing ceramics based on Zirconates, stabilized with Gd, Yb, La, Hf etc. which combine low thermal conductivity and high phase stability at elevated temperatures [6]. Furthermore, for the TBC coatings it is desirable to produce porous (with typical porosities of 10-20%) micro-cracked or vertically segmented structures. The coating porosity and micro-cracks reduce the thermal conductivity and in the same time improve mechanical properties which determine the TBC operating lifetime. The latter is generally limited by delamination of the ceramic top coat layer [5,6]. The delamination is caused by occurrence and growth of interface cracks between the top and bond coat layers due to thermo-mechanical stresses and TGO growth. These stresses appear due to the mismatch of coefficients of thermal expansion (CTE) between bond and top coating layers. Usually in service conditions the TGO, which is growing with time at the bond coat interface, serves as a crack nucleation region. The TGO has very low ductility and very high elastic modulus and undergoes high thermo-mechanical stress due to a large mismatch of CTE between the bond and top coat layers. This leads to TGO cracking and delamination as its thickness achieves a certain level of about 8-10 micrometers [5]. Improvement of strain tolerance of the ceramic TBC layer is required to achieve sufficient spallation lifetime. A better bonding of the APS deposited ceramic layer is achieved by rough

bond coat surfaces increasing spallation life time due to better mechanical interlocking of top and bond coat layers enabling higher stresses to be withstood without coating delamination.

Increase of operating temperatures requires applying of thicker TBC coatings to achieve necessary thermal insulation of the components. Increase of ceramic layer thickness leads to higher temperature differences between bond and top coat surfaces. This causes higher mechanical stresses within TBC layer and corresponding stored strain energy which represents a driving force for crack propagation [7]. Hence for a given TBC the thickness is an important factor affecting not only overall thermal protection but also expected lifetime of the coating. Due to these reasons, in order to achieve sufficient thermal protection of the component during requested service lifetime, an optimal TBC coating thickness has to be established and strictly controlled in the coating production process.

2.2 Deposition of TBC system with thermal spray processes

2.2.1 General aspects of thermal spray processes

Thermal spraying represents coating deposition processes in which a feedstock material injected into the flame or plasma torch becomes molten or semi-molten, and is accelerated and sprayed onto a substrate surface. There are several processes used to apply thermal sprayed coating such as conventional flame spray, electric arc wire spray, detonation spraying, high velocity oxy-fuel (HVOF) spray, and atmospheric and low pressure plasma spray (APS and LPPS) processes [8-12]. Furthermore the cold spray process [12] can be added to conventional thermal spray process due to similar process features. The feedstock material can be provided in the form of wire or more usually as powder of micrometer size. All thermally sprayed coatings represent overlay coatings produced by coating material build-up on the substrate surface. Thermally sprayed coatings can vary in thickness range from several tens of micrometers up to several millimeters depending on process and area of applicability. A variety of materials such as metals, ceramics, plastics and composites can be deposited with thermal spray processes.

Thermal sprayed coatings are built path by path and layer by layer according to the continuous motion of the spray gun over the substrate surface. The coating properties depend on the particular process settings, which will be discussed in detail for APS process in the next chapters. Furthermore, the kinematic and geometry parameters related to the spray gun motion substantially affect characteristics of the final coating layer on a particular component. The kinematic parameters, such as surface speed of the gun, spray distance and angle relative to the substrate surface, influence deposition temperature and mass

distribution within a coating layer. These parameters are controlled by the motion of the spray gun typically attached and driven by the industrial robot (IR). The robot motion program has to be optimized in order to control the kinematic parameters during deposition, and thus obtaining coatings with the desirable thickness distribution and properties. Coating trials are carried out varying the kinematic motion parameters in order to optimize the robot path and optimize coating thickness and properties distribution on a particular component.

2.2.2 Deposition of TBC with atmospheric plasma spray

Atmospheric Plasma Spraying (APS) is widely used for deposition of ceramic TBC coatings. In the APS process an arc with a high power density is generated by the spray gun under the atmospheric conditions between a rod-shaped, centrically arranged tungsten cathode and a ring-like copper nozzle representing anode [8,9]. The principal schematic of the spray gun is shown in Figure 2.3.

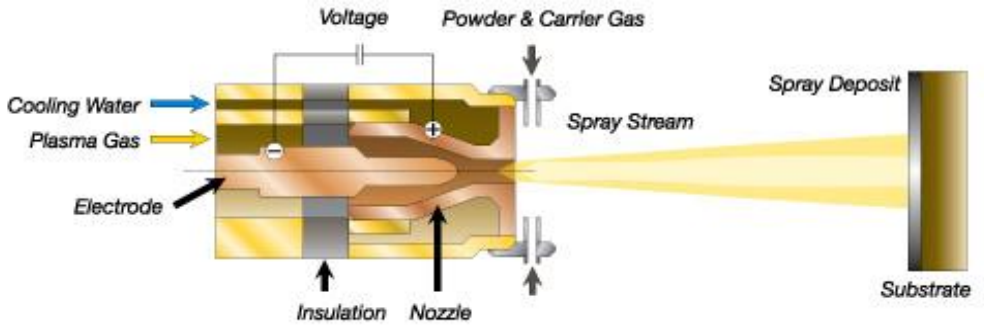

Figure 2.3: Schematic of atmospheric plasma spray process (Sulzer Metco).

The plasma jet operating principle lies in the transfer of energy from an electric arc discharge, generated between cathode and anode, to the process gas flowing between them. Argon is usually used as the primary process gas with the addition of secondary gases such as hydrogen, helium or nitrogen [10]. The process gas is ionized by an electrical discharge sustained by DC power [9]. The ionized gas creates high-pressure electrically neutral plasma which leaves the nozzle at high speed and temperature. Coating powder is usually fed by injectors into the plasma jet either from outside of the gun or directly in the diverging exit region of the nozzle (external and internal powder injection). The powder is fed by injectors with the help of carrier gas, which is usually argon. The powder particles are heated up by the plasma and accelerated towards the substrate to be coated. The particle velocities typically vary between 100 and 500 m/s depending on the process. The particles interacting

in flight with the plasma jet achieve a molten or semi-molten state and have velocities sufficient to enable spreading on the interface of the substrate or previously deposited coating layer. As a result of continuous motion of the spray gun over the substrate, typically following a meander-like pattern, a uniform coating thickness and structure can be achieved. The properties of the final coating layer such as thickness, porosity, and thermal and mechanical properties are controlled by deposition process parameters [10,11].

As commonly accepted, one of the most important groups of process parameters is in-flight particle properties, which include particle temperature, velocity and size distribution in the plasma jet prior to impact. From one side they are determined by plasma gas properties such as gas constitution, temperature, velocity, viscosity and particles' dwell time in plasma. From another side, the feedstock powder properties such as chemistry, size distribution, density, morphology and production method have a substantial effect on their in-flight and final coating characteristics. The plasma properties are governed for a particular process by spray gun settings, which are commonly expressed in terms of arc current, power, primary and secondary gas flow rates. The distribution of particles in the plasma jet is mostly controlled by injection parameters such as powder feed rate and carrier gas flow. Thus, low injection velocity caused by low carrier gas flow rate leads to penetration of particles only into the relatively cold periphery of the spray jet, resulting in insufficient melting and acceleration. On the other hand, excessive velocity of the particles can lead to crossing through the central hot zone of the plasma jet into the colder periphery on the other side.

Coating adhesion and bonding depends on the substrate surface conditions and in particular on the surface roughness and interface purity. The spraying conditions and substrate geometry influence the coating bonding and structure as well. Improved bonding is achieved by a rough bond coat interface enabling a sufficient mechanical interlocking. The substrate temperature affects the coating structure and deposition stress generated in the coating as the molten droplets continually impact the substrate. In practice, during coating the substrate can be cooled to control the deposition temperature. In general the correlation between plasma parameters, particle in-flight properties and deposited coating characteristics is complex due to complex process interactions that take place. Detailed discussion of the peculiarities of TBC coating formation will be done in the Chapter 2.4.

2.2.3 Deposition of bond coat MCrAlY

The APS TBC coatings are sprayed as a top layer above the metallic bond coat layer. The MCrAlY bond coat is usually deposited by Low Pressure (LPPS) or Vacuum Plasma Spraying (VPS) processes. In these processes, analogously to the APS process, the

feedstock material in the form of powder is melted and accelerated by DS plasma discharge. Here the spraying is done in a vacuum seal chamber in an inert atmosphere under low pressure conditions. Usually, the chamber is pumped down to a pressure of 0.001 Pa and then filled with Argon to prevent oxidation of sprayed particles by oxygen from the environment [9]. Because of the low process pressure, the plasma gas stream temperature and velocity profiles are extended to greater distances in comparison with APS spraying.

Currently in many cases High Velocity Oxy-Fuel combustion spraying (HVOF) is used to apply the MCrAlY coatings due to the ability to produce a coating layer with sufficient structure and lower production costs in comparison with LPPS. In HVOF spraying, the thermal and kinetic energy of the flame is used to melt and accelerate the coating powder. A fuel together with oxygen is fed into a chamber in which combustion occurs. Liquid (such as kerosene) or gas fuel (typically hydrogen) can be used in the HVOF process. The combustion products expand through the nozzle, achieving supersonic velocities [9,12]. Feedstock powder particles are injected mostly internally into the combustion chamber where they melt and become accelerated during the flight through the nozzle. The expanded supersonic gas flow at the nozzle exit undergoes a series of substantial expansions and compressions. They lead to the appearance of typical gas flow inhomogeneities - so called shock diamonds - which disappear with distance downstream from the nozzle. In this process very high particle velocities up to 500 m/s are achieved with relatively low particle temperatures. Very high kinetic energy of the particles impacting the substrate ensures a good mechanical bonding even if the particles are not completely molten. For thermal spray coatings, especially with the HVOF process, it is very important to prepare the substrate properly to ensure sufficient bonding. Thus, degreasing and roughening by grit blasting has to be done prior to deposition. High particle velocities and short dwell time in the flame enable very dense homogeneous layers to be produced, preventing oxidation of particles during flight, which is highly desirable for MCrAlY coatings.

2.2.4 Structure of thermal sprayed coatings

The most important characteristics of thermal sprayed coatings used as production control are thickness, porosity, and roughness distribution on a particular component. These characteristics define corresponding physical properties such as temperature difference within TBC, thermal conductivity, elastic modulus and bonding strength. Metallography is a commonly used method to evaluate coating properties and to provide quality control in the production conditions. The evaluation is performed on cross sections of coated samples [9,13,14]. The sections of appropriate size are usually prepared from larger pieces of coated

material by cutting with an abrasive cutting saw [13]. The cross sections of ceramic coatings are usually mounted into the epoxy resin under vacuum conditions. After removal of ambient air the liquid epoxy penetrates the cracks and pores of ceramic TBC ceramic layer. After hardening of the epoxy, the mounts have to be grinded on rotating discs. The grinding represents a multi-stage process done with series of abrasive SiC or Al_2O_3 papers of subsequently decreasing grit size. Ultrasonic washing has to be done at each grinding step to remove contamination. The finishing of the mounts is done by polishing with polishing cloth with the addition of very fine diamond pastes [13]. Use of correct cutting, grinding and polishing parameters is extremely important to avoid pullouts, cracks and other artificial effects caused by preparation procedure. Usually parameters of each preparation step are specified to obtain consistent data on coating structure. In order to investigate a grain structure of metallic coatings an additional etching step is required. The microstructure investigation is done on the mounts with the help of an optical microscope or preferably with a scanning electron microscope (SEM). Usually the analysis and quantification of the structural properties is accomplished by post processing of metallographic images with the help of various software tools [14]. Typical structure of multilayer TBC with ceramic top and metallic bond coat on a superalloy substrate is presented in Figure 2.4. From metallography most information about coating thickness, porosity, roughness, interface purity and quality of the coating can be obtained and analyzed. The metallography samples can be used for extended evaluation of chemical composition and indentation hardness of the coating. Porosity of the coating is evaluated by analysis of contrast differences on the metallography images. Usually the apparent porosity is defined as the ratio of dark to light areas on the images (see Figure 2.4) representing areas of voids and ceramic material respectively. Further properties such as interface purity and coating roughness are typically studied by optical metallography. The ceramic layer thickness is evaluated by measuring the distance between top and bond coat interfaces, the metallic bond coat thickness is defined similarly. Due to natural roughness of coating layers, the thickness usually is measured at multiple locations and an average value is calculated.

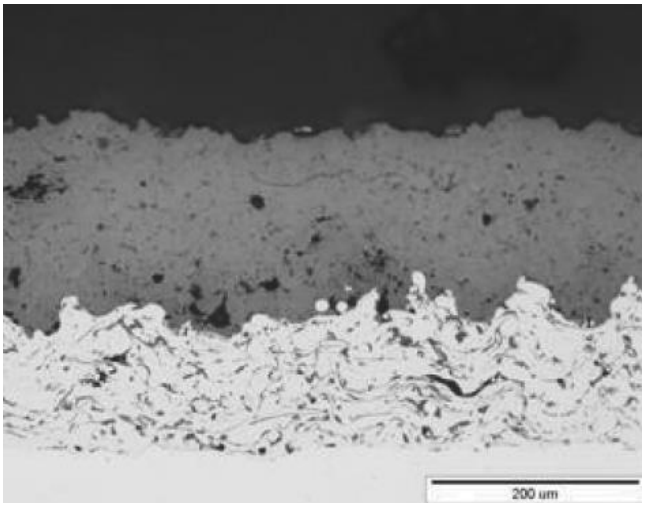

Figure 2.4: Typical metallography image of APS sprayed TBC system [13].

2.2.5 Process stability control and on-line monitoring techniques

The most important characteristics of the coating production process are process stability and reproducibility. During spraying the fluctuations and drifts of process parameters take place [15-17]. One of the main sources of the process drift is wearing of the spray gun cathode. This wearing is caused by high thermal load and erosion of cathode material with time. Cathode erosion leads to continuous reduction of the ark discharge voltage and power, consequently leading to a decrease in plasma particle velocity and temperature. This decrease already becomes substantial after several hours. Typical lifetimes of the cathode in production conditions are about 30-60 hours [15]. Another source of the fluctuations is a permanent motion of the discharge arc root on the surface of the anode with changes regarding its attachment point. This motion causes fluctuations of electrode voltage with characteristic times of milliseconds. In addition to the plasma fluctuations, the fluctuations of the feed rate caused by the powder feeder take place with characteristic times of several seconds [15]. These drifts and fluctuations influence the powder particle in-flight properties and result in spatial and temporal variations of critical characteristics such as particle melting state, velocities, trajectory and temperature values and distributions. Stability of these in-flight characteristics defines the particle conditions prior to impact and, together with substrate surface conditions, define final coating properties.

The monitoring of the in-flight particle characteristics can be performed with various methods. In particular, the measurement of particle velocity can be performed by laser Doppler anemometry or by timing of a particle passage between two selected positions with a high speed video camera. The temperature evaluation is typically done by the pyrometer technique. The characteristics of individual particles or their ensembles can be captured to monitor their actual and average values. Recently, in order to control stability of these in-flight characteristics, various commercially available sensors such as Tecnar Accuraspray, Tecnar DPV2000, Oseir Spraywatch, Inflight Particle Pyrometer, and Stratonics Thermaviz [16] are utilized for the on-line monitoring of the coating production process in the spray booth. These sensors enable on-line monitoring of the spray process and detecting the drifts and fluctuation of particle in-flight parameters which can harm the homogeneity and reproducibility of the final coating properties. The real-time monitoring of particle parameters and taking of corrective actions in case of drift detection can improve the traditional approach of setting of process variables after post-process examination of final coating characteristics [17]. Linking the plasma parameters to the particle state through a design of experiments can be done for understanding of coating properties [18]. Development of on-line monitoring techniques enables a comprehensive relationship between coating properties and deposition

process settings to be established for the assessment and improvement of manufacturing reliability.

2.3 Thermal spray evaluation and modeling

2.3.1 Characterization of particles in-flight properties

In theoretical investigation of thermal spraying, the deposition process is typically divided into sub-processes. The most important of these are the generation of a free plasma jet and the interaction of the injected powder particles with the plasma. The resulting temperature, velocity and particle mass distribution represent in-flight particle properties. Several theoretical approaches were outlined to describe behavior of the free plasma jet. A comprehensive review of the available approaches for particle characterization and modeling is done in [19]. A three-dimensional theoretical model was employed to predict the plasma velocity, plasma temperature fields in frames of continuous medium theory [20]. Equations of mass flow continuity and conservation of momentum and total energy were used here as governing equations. The plasma was assumed to stay in a steady state and local thermodynamic equilibrium state characterized by an equal temperature of the gas atoms, ions and electrons at each point. In addition, a negligible energy loss by radiation and the absence of chemical reactions in the gas phase were assumed. Computation showed that the plasma jet expands due to heat and mass exchange between plasma and ambient air, leading to a decay of velocity and temperature in radial and axial directions. Hence the width of the plasma jet becomes larger with an increase in distance downstream from the nozzle. In the overview [21], the behavior of the free atmospheric plasma spray jet has been experimentally investigated. Obtained results indicate that a Gaussian error function can represent the radial distributions of the mean axial velocity and temperature of plasma gas. A hyperbolic relationship was used to describe mean plasma gas velocity and temperature decay with axial distance. The experimental and theoretical dependences of powder particle velocities on the distance were studied as well. It was shown that powder particles, accelerated by the drag force created by the plasma gas, can reach the plasma velocity at a certain distance, and due to inertia can exceed it beyond these distances. The size of powder particles had a strong influence on their trajectory and velocity distribution. The plasma perturbations by the carrier gas flow and powder particles were investigated theoretically in [22] in frames of a three-dimensional computational model, based on solution of energy and mass transport equations. As shown in particular in Figure 2.5, the injection of carrier gas results in deflection of the plasma jet. This deflection is aggravated with

increasing carrier gas flow. The temperature and particle velocity contour become non-symmetrical about the axis of the jet and shift from the center line. This shift increases with distance downstream of the plasma jet. The radial distribution of temperature, axial velocity and powder density had a bell-like shape. Furthermore, the maximum particle density distribution decreases and the characteristic width of powder density distribution increases with an increase in carrier gas flow rate. The simulation results for particle speed and temperature distribution were compared with corresponding experimental data for NiCrAlY and 8YSZ powders. A stochastic nature of the injection process has been studied theoretically in [23]. Calculation of trajectories and temperatures were done for Al_2O_3 particles with a solution of dynamics equation taking into account plasma viscous drag and gravitation forces in combination with thermal transfer. The paper [24] reviews experimental and analytical techniques that examine effects related to various types of external and internal injection of powder on APS spray jet parameters. Particle trajectories and distributions in the powder jets produced with single injectors with varying carrier gas flow and powder size distributions were observed experimentally. As an important effect related to external powder injection, a by-passing of the particles which do not penetrate the core of the plasma jet was investigated. For a given carrier gas flow rate, the particle velocity at the injector exit is nearly independent of particle size; therefore, the finer particles may have insufficient momentum to penetrate the plasma jet and thus bypass the jet. The observed radial distribution of powder particles exhibited a Gaussian shape with a shift towards to the injection direction, as expected from the theoretical models discussed above. This shift increased linearly with an increase in carrier gas flow rate.

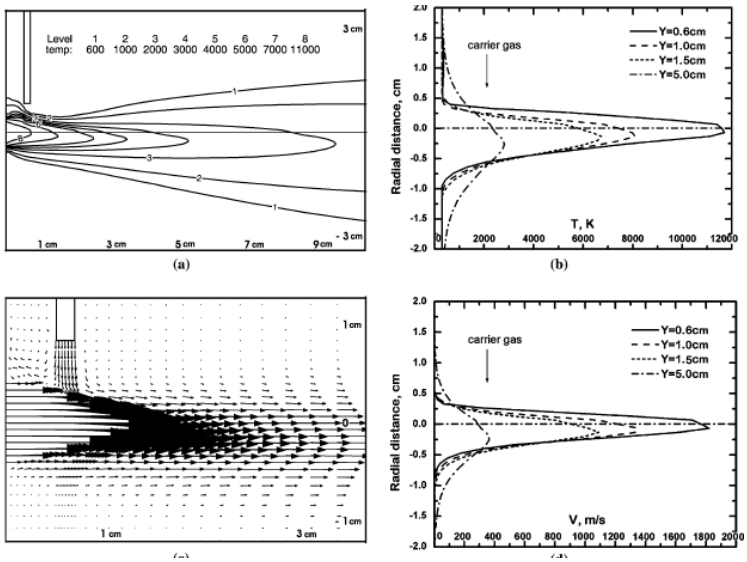

Figure 2.5: Spatial distribution of particle temperature and speed [22].

In the production conditions, multiple injectors are usually used to feed the powder. One- and two-port powder injection schemes applied to the APS process were experimentally investigated in [25]. Radial distributions of mean particle velocities, and diameter and volume flux were measured and evaluated under different combinations of

plasma and carrier gas flow rates at a certain nominal stand-off distance. An effect of carrier gas flow and powder size distribution on the particle in-flight characteristics and trajectories was investigated. The optimum trajectory was found for the particles which have a mechanical moment that is not too low to be deflected by the plasma but not too high to fly through the jet. The particles have to penetrate inside the plasma jet and travel along the hottest zone of the plasma jet. In this case, the maximum amount of particles reached the highest surface temperature, which resulted in the highest deposition efficiency. The results for the single injector spraying are in agreement with results reported by previous authors. For the spraying from two injectors it was found that as a result of the interaction between the powder and gas flows, both the mean particle velocity and mean diameter distribution were more symmetrical about the centre line of the plasma torch in comparison with single injection. Furthermore, with increasing of the carrier gas flow rate, the radial distributions of the powder particle sizes, concentration, velocities and, as a result, the particle flux changed from a single bell-like to a double bell-like shape. The evaluated powder flux distributions were compared with the actually sprayed stationary spray spot deposit. A correlation between the shape of the deposit and the powder flux density was found. Hereby, the total value of the measured flux was found to be almost twice as high as the value resulting from the deposit measurements. This phenomenon is explained by deboning of a portion of particles detected in flux measurement which were not sufficiently melted, especially on the fringe of the plasma jet. These particles were likely to have bounced off and could not adhere to the substrate upon impact; however, they were still included in the volume flux distribution calculation. The ratio of the deposited volume to measured particle volume indicated the approximate deposition efficiency.

The effect of deposition efficiency and particle bonding together with particle in-flight properties plays an important role for the characterization and modeling of the overall coating process and will be addressed in detail in the next paragraph.

2.3.2 Peculiarities of particles impact and deposition

Deposition of thermally sprayed particles can be considered as a continuous splat quenching and rapid solidification process [26]. It was observed that the substrate temperature and interface conditions have a strong impact on morphology of the impacted droplets, splat formation and consequently on the microstructure and properties of the deposit. The impact of these factors on coating adhesion and cohesion, in particular for ceramic Al_2O_3 coating, were studied in the paper [27]. Thus, the adhesion and cohesion increases almost linearly with the substrate roughness. For the preheated substrates,

typically by plasma jet prior to starting powder injection, the adhesion increases as well even for the substrates with lower roughness. In the paper [28], the substrate temperature effect on single splat formation has been studied. The results show that there is a threshold transition for the substrate temperature at which the splat structure changes from a fragmented splash to a disk-shaped morphology. In the case of zirconia particles this temperature was found in the range of 250–300°C. It has been observed that the splat–substrate and inter-splat contact at higher substrate temperatures increases leading to reduced porosity, and higher thermal conductivity and bond strength. These results are in good agreement with a study performed in [29], showing that for smooth stainless steel substrates, ZrO_2 exhibits almost perfect disk-shaped splats on hot substrates with a temperature of about 300 °C and fingered splats on cold substrates below 100 °C. The obtained results showed a strong influence of the particle impact velocity on splat thicknesses and degree of flattening. It was found that the splat thickness varied substantially from about 1 μm to more than 2 μm for particles with 22-45 μm initial size when the velocity decreased from 200 to 60 m/s caused by a reduction of degree of flattening with a reduction of particle velocities. The preheating of the substrate up to 300 °C led to adhesion-cohesion values up to three times higher than those obtained for coatings deposited onto non-preheated substrates for various spraying conditions. The adhesion-cohesion values decreased with larger particles which were not as well molten as the smaller particles. On the other hand, it was shown that the adhesion was strongly dependent on the oxidation rate of the substrate caused by preheating and decreased when the oxide layer became too thick.

The effect of inclined substrate on the shape and morphology of the splats was studied further in [30], [31]. Splats were obtained by APS spraying of 8YSZ powder on flat inclined substrates in front of a plasma torch. It was shown that impact on the inclined substrate produces features such as fingering, ridging, splashing and overlapping of elliptical shaped splats. Circular splats with a point of impact coinciding with the geometrical center of the splat are obtained from 0° and 10° inclination angles. The particles impacting at higher angles produced elliptical shaped splats with the impact points situated close to one of the two geometric foci of the ellipse. Furthermore, with increase of inclination angle, the spallation of splats from the substrate was to be more prevalent. The partial or complete peeling of splats was found to be common at substrate inclination angles over 60°. This was attributed to a decrease of bonding strength caused by a reduction of particle normal velocity and momentum which is needed to provide sufficient bonding. The effects of spraying conditions, and in particular, the effect of spray angle on the morphology of thermally sprayed particles of metallic nickel-based alloy particles sprayed using the LPPS technique have been studied with the application of several statistical tools in [32]. A strong effect of

spray angle on the elongation factor of the splat shape for metallic splats was shown. In [33] a theoretical stochastic approach was developed to model a shape of individual splat and formation of an inter-splat porosity and surface roughness of the coating buildup. The effect of in-flight particle properties and the surface temperature and inclination angle on the individual splats and complete 8YSZ coating layer were studied and summarized in [34]. In particular, it was confirmed that the morphology of the splats changes from a disk-like to a fragmented fingered shape with an increase in particle size. The corresponding coating layer exhibits increased porosity due to an increase in the degree of particle fragmentation. Coatings sprayed on inclined substrate had predominant crack orientation in line with the off-angle spray direction, with higher porosity in comparison with normally sprayed coatings. Furthermore, higher substrate temperatures and low particle velocity lead to lower porosity and improved inter-splat contact.

2.3.3 Macroscopic characterization and modeling of deposit profile

The spray parameters and substrate conditions determine the microstructure, physical properties and adhesion of the coating. On the other hand, the amount and distribution of the coating material in the spray pattern is determined by the distribution and in-flight characteristics of the powder in the plasma jet. The thermal and environmental protection provided by the continuous coating layer very much depends not only on microstructure but also on the macroscopic coating distribution and interface morphology of the coating footprint. Some aspects of the practical development of the spray parameters to optimize coating properties and geometrical footprint characteristics were presented in [35]. In particular, an influence of the gun parameters and operating conditions on the shape of the stationary spray spot pattern was presented. In [36] an effect of standoff distance on the torch diameter, heat transfer to the substrate and deposition efficiency for APS and HVOF processes was experimentally investigated. It was found that the dependence between the jet width and standoff distance is close to linear for APS processes with F4 (Sulzer Metco) and PlazJet (Praxair) spray guns. The heat flux towards the substrate and the torch efficiency decreased with a hyperbolic trend with an increasing in the standoff distance. Furthermore, based on the experimental results, a Gaussian distribution was applied to describe the radial distribution of the heat flux to the substrate. In study [37] a diversity of coating profiles was obtained for Al_2O_3-13%wt. TiO_2 coating applied by APS process with F4 gun from Sulzer Metco was investigated for different sets of coating parameters and operating conditions. The deposit profiles were produced by a linear relative motion between the spray gun and the substrate. It was confirmed that thickness distributions in the spray

profiles can be fitted by Gaussian functions. An influence of arc current, total plasma gas flow and hydrogen fraction, carrier gas flow and injector diameter on the deposit characteristics such as profile height and Gaussian standard deviation was experimentally investigated and some empirical fitting dependence of these parameters was proposed. The arc current and the plasma gas flow rate, based on the results, are the major factors which affect the velocity and temperature of the powder particles and consequently determine the deposition efficiency and coating pattern characteristics. The interface of the coating pattern can be characterized in the macro and micro scale, which enables coating waviness and roughness to be evaluated correspondingly. In paper [38] the thickness distribution and interface morphology of the APS profiles of Al_2O_3-TiO_2 powder on the flat steel substrates were examined experimentally. The profile waviness was investigated by two non-destructive methods with a coordinate measuring machine (CMM) and a laser profilometer. The deposit roughness was measured by stylus and laser profilometry. Furthermore, the morphology and geometry of the deposit profiles were examined with optical microscopy. It was detected that all measured profiles could be fitted by Gaussian functions with about the same parameters irrespective of the measuring method. The profile thickness characterized by maximal height and area under the profile were found to be linearly dependent on the number of spray passes. On the other hand, the coating roughness appeared not to be dependent on the number of passes. In a further paper [39] an influence of geometrical processing parameters such as spray distance, spray angle, and positioning of the powder injector on the spray profiles were studied. The net deposit profiles were measured and then fitted by Gaussian distribution functions: $f(x) = \frac{1}{\sqrt{2\pi}\sigma} \exp\left(-\frac{(x-\mu)^2}{2\sigma^2}\right)$. Here σ represented a standard deviation of thickness distribution and μ is a displacement of the profile maximum from the plasma torch position. Examples of the spray profiles are shown in Figure 2.6. The spray distance and deposition angle were identified as the main variables influencing the deposit geometry. The profile geometry was characterized by the maximum height, profile width, degree of symmetry and

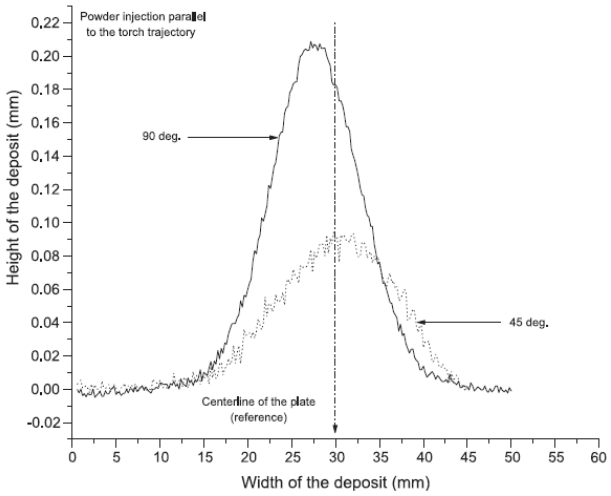

Figure 2.6: Measured thickness distribution in APS sprayed 8YSZ spray profiles [39].

position of the profile maximum. In particular, it was found that changing the spray angle sharply influenced the deposition efficiency, the deposit height, the offset of its centre of mass, its width at its half maximum height, as well as its skewness. Furthermore, it was pointed out that geometry of the deposit depends on the orientation of the injector relative to the torch trajectory, which leads to different profiles deposited if powder injection is oriented parallel and perpendicular to the torch motion direction. The effect of spray angle on the properties of plasma spray deposits of NiAl and Cr_3C_2-NiCr materials was investigated in [40]. It was found that coating porosity increased as the spray angle deviated from normal to the substrate orientation. The surface roughness of the Cr_3C_2-NiCr deposit was not sensitive to the spray angle, whereas NiAl exhibited an increase as the spray angle decreased. Microhardness, tensile adhesion strength, and interfacial fracture toughness decreased with spray angle. The reasons for variation of these properties with spray angle were discussed in connection to morphology of splats, change of the local spray angle and change of momentum of particles impacting on the substrate and previously deposited particles. An approximate mathematical model was proposed to describe the deviation of the spray profile from Gaussian form caused by spray angle for 1D symmetrical spray profile.

2.3.4 Prediction and simulation of coating layer properties

The various analytical approaches were developed to predict geometry and morphology of coating pattern applied to real substrates. Thus, in paper [41] a finite element method (FEM) was applied to simulate a deposition process of 8YSZ coating onto a turbine blade. In particular the deposition temperature and mechanical properties such as strain and stress in the coating were simulated on a realistic 3D model of the turbine blade. A general approach to simulate a coating pattern thickness based on application of flow rate functions for an arbitrary motion of the spray gun was proposed in [42]. These functions, introduced in a generalized form, described relative distribution of the powder mass flow in dependence on coordinates on the substrate, orientation of the gun and spray distance. The portion of the sprayed material lost due to particles splashing on impact was introduced as a deposition efficiency factor. This model was used to determine the optimal path for a spraying application and showed how various raster patterns can be combined to provide the necessary continuous path over the surface. In paper [43] this generalized model was applied to simulation of the coating pattern on the free geometry substrates and used for the creation of the gun trajectory to achieve desired thickness distribution using mathematical optimization methods. In paper [44] a two dimensional (2D) finite difference (FD) simulation model was developed to predict the thickness of coatings by numerical integration of the

deposit rate function for a selected robot trajectory over the component. The deposit rate functions were described analytically by a symmetrical two-dimensional (2D) Gaussian distribution. A basic analytical expression for the thickness in a spray profile and in a coating layer deposited onto a rotating disc was derived. The input parameters of the deposit rate functions were the Gaussian pre-exponential parameter, describing a thickness amplitude factor and the standard deviation, defining a width of the spray spot. The Gaussian standard deviation was considered as independent of directions on the substrate, thus describing a case of a round symmetrical spray spot. Both parameters were considered as unknown functions of the stand-off distance and determined experimentally by measurement of the actual thickness distribution in the spray profiles. It was pointed out that the idealized behavior, related to symmetry of the spray spot, results in differences between the measured and predicted shape and thickness of the coating profile. In paper [45] a mathematical model was presented to calculate the thickness of a coating sprayed onto a rotating disc in the case of a time-dependent powder feed rate. A further mathematical model for spray deposition on a rotating large object with a smooth, rotationally symmetrical, curved surface which allowed varying spray distance and direction was developed in [46]. In particular, the simplified spray deposition model was presented to make possible a method to approximate a deposit rate from the results of layer thickness measurements. Here also, a symmetrical deposition rate function was used to link explicitly the thickness growth rate with the total volume flow rate. Here, the volume flow rate was assumed to be constant with the Gaussian standard deviation, linearly dependant on the distance from the spray gun to the substrate. An influence of the deviations of the spray profile from the Gaussian shape and the uniformity of thickness in the coating layer caused by an off-normal spray angle were discussed in [47]. In this paper, an arc deposition technique was evaluated for fabricating net shape turbine blades by incremental coating material deposition. The spraying result on flat substrates was numerically simulated deposition of Zn coating with meander-like spray patterns, applied with different scanning steps and spray angles. An influence of the spray angle on profile thickness distribution was considered by a rotation transformation of coordinates on the tilted substrate plane. It was found that coating uniformity increases with a decrease of the scanning step. On the other hand, with a smaller scanning step the coating become thicker with an increase in deposition temperature. For electric arc spraying application, it was observed that the coating uniformity can be achieved a scanning step equal to one standard deviation of the Gaussian thickness distribution in the spray profile. With its increase above one standard deviation the coating layer became wavy in a macroscopic range.

2.4 Off-line programming and deposition process modeling

2.4.1 On-line robot programming

Nowadays the use of robots for the application of the thermal spray coatings is becoming a standard technique in the gas turbine industry. Industrial robots enable human operators to be replaced, and achieve a high level of process accuracy and reproducibility for diverse processes such as machining [48-49], arc welding [50] and finally for thermal spray coating. Furthermore, the use of robots for the coating processes enables operation in vacuum or hazardous environments of production spray booths. Typically, coating process development involves mostly on-line operations such as robot programming, performing spray trials and verification of the spray result directly in the spray booth. The on-line programming of the robots is typically carried out by a skilled operator. The operator guides the robot through a desired path, which is usually marked directly on a surface of a set-up component. For example, for a simple geometry, the spray gun trajectory represents a meander-like pattern, created by application of parallel paths with a constant distance between them and with a constant gun speed. The robot motion in the teach-in method is controlled manually by a teach pendant which causes the naming of this technique. The programming involves manually jogging the robot between selected locations which are placed on the marked path. These locations have to be recorded in the robot controller memory to be later utilized for a continuous motion of the robot. During robot motion, it is typically desired to keep the distance between the spray gun and substrate constant and equal to the nominal spray distance. Furthermore, it is advantageous to keep the normal orientation of the spray gun in relation to the substrate surface, holding the spray angle as close as possible to 90° to the surface. In order to provide a control of the spray distance and spray angle, different tools and methods were developed. Typically, robot teaching is provided with the help of pointing tools attached to the spray gun. They have to be able to control or measure distance and orientation vector of the spray gun. It is usual to attach to the spray gun a rod-like tool with a fixed length, which is selected to be equal to the desired nominal spray distance. The coordinates of the tool tip represent the tool center point (TCP) frame. The coordinates of this frame at selected positions of the gun while moving along the desired path can be used for robot programming. As summarized in [50], more complex devices equipped with force torque sensors or visual control sensors can be used. These tools can provide semi-automatic generation of the robot path according to the path, marked on the substrate, and improve accuracy of programming. It should be mentioned that, even with these controls, guiding the robot along the desired path accurately and not allowing

collisions of the gun or robot parts with the substrate usually represents a very difficult and time-consuming task, especially for the substrates with a complex geometry.

The final robot motion program is a text file in a specific programming language with a sequence of motion instructions. In order to complete the program, the specific robot attributes such as TCP speed, motion type, and location approaching accuracy have to be set at robot locations. The program typically includes loop commands to enable programming of motions with repetitions, for example to apply multiple coating layers. After the setting of the tool, and in particular defining a position of TCP in coordinate system connected to the robot, the robot controller is able to calculate necessary robot joint configurations and motion parameters to perform robot motion along the programmed path with defined speed and motion attributes. No manual programming of motion of each robot joint is needed, due to the ability of robot controllers to work with inverse kinematics. After the completion of the programming code, the motion program can be compiled to the robot language and loaded into the robot controller. Despite improvements in conventional on-line programming methods, they still have considerable drawbacks caused by the manual nature of the programming operations. First of all, the spray program created manually is strongly dependent on the skill and experience of the coating operator. Thus the motion program generated using the “teach-in” method lacks accuracy due to sub-optimal spray gun positioning and definition of the initial spray path contour. These on-line programs lack flexibility and reusability needed for further adjustment and optimization. Another disadvantage related to industrial utilization of the method is a blockage of the production booth during robot programming, which is usually connected with considerable development time and costs.

2.4.2 Off-line programming technique

The main specific feature of the off-line programming (OLP) methods is the performing of program development operations not in the production booth but in a test environment with subsequent transfer of the program to the robot. The off-line environment can be represented by another test booth used only for the programming efforts, or by a virtual copy of the production booth created with simulation software. The hardware-based off-line methods avoid blockage of the production booth but have the same technical drawbacks as conventional on-line methods discussed above, caused by using on the same teach-in approach to generate the robot program. These methods are widely used in the automation industry for robotic systems and overall production lines for example for car part

painting and welding, machining and milling [49] processes. Recently, the off-line method was successfully applied in production of thermal spray coatings [51]. An implementation of the OLP in the production environment is becoming possible due to the development of the realistic robot simulation (RRS) interface [52]. This standardized interface is being developed to integrate the motion software used by the robot controller, which actually defines the precise motion of the real robot, into OLP simulation software. This enables the robot programs and configuration files to be created and updated by OLP software and provides data transfer between virtual and real controllers, translating the programs to the native controller language.

The OLP software enables the robot program to be generated within the virtual cell based on the CAD data of a component to be coated, with subsequent simulation of the robot motion. The virtual work cell includes geometrical and kinematic models of the robot and auxiliary tools included in the booth. The user can test the reachability of the robot locations and tune kinematic and geometric properties of the robot motion in combination with the other kinematic devices such as, for example, turntables, without use of the real spray booth.

There are various software tools such as RobCad from Siemens PLM Software, RobotStudio from ABB, Delimia from Dassault Systems etc. [50], IGRIP from Deneb Robotics, etc. which were developed for off-line programming. One of the widely used commercially available software packages is RobCad [53]. The software enables the design, simulation, optimization, analysis and off-line programming of multi-device robotic and automated manufacturing processes. It includes an accurate off-line teaching feature for a real robot with an extensive library of standard robot models and robot controller configurations. RobCad is a work cell based simulation tool that allows various multi-device robotic and automated manufacturing processes to be developed, simulated and optimized. The software enables the automation tools for robot placement, equipment selection, path planning and optimization, program generation and collision detection. RobCad integrates core technologies and process-specific applications addressing a wide range of manufacturing processes including spot welding, arc welding, laser and water-jet cutting, painting and material handling [54].

In general, the OLP technique based, for example, on the RobCad software package has evident technical advantages in comparison with conventional teach-in methods. The programming procedure is performed within a virtual software environment and does not need a real robot and hardware, which avoids blockage of a production booth. The programs developed with OLP are more transparent, flexible for further modifications, and enable more accurate and precise robot motion control.

2.4.3 Thermal spray modeling and smart process planning

Recently, different OLP approaches and tools were applied to generate CAD based robot paths for thermally sprayed coating to achieve a required level of coating uniformity. The simulation package based on IGRIP software was developed to calculate thickness and porosity distribution of plasma sprayed coatings [58]. The physical module was developed to predict properties of the coating spot pattern. The pattern data which correspond to various spray parameters are stored in a data table which can be downloaded by the software to be used as a “paintbrush” to calculate final coating properties. This calculation is done by the CAD robot programming software. A subsequent calibration of the pattern data is used to adjust the simulation result to the experimental data for selected simplified substrate shapes, which include critical elements for coating deposition. After the generation of the coating cell with the CATIA software package, the simulation of the coating thickness on the turbine parts was performed. The calculation results were compared with experimental data for turbine parts. Furthermore, advantages of the use of off-line programming for coating production for turbine parts were discussed. In [46] the deposition rate functions were applied to simulate coating layer thickness on free form surfaces. Furthermore, a mathematical approach was outlined to optimize the gun trajectory with respect to gun speeds and spray angle to achieve optimal thickness distribution. The results of numerical computation with MATLAB software were presented for various free-form surfaces. An approach to solve the trajectory planning task is outlined in [43]. The problem was set to find a finite set of spray gun configurations, which minimizes the error between a target coating and the coating induced by these configurations. A suitable objective function for gun configuration was defined, and algorithmic solutions for the optimization problem were presented. The calculations were performed including graphics hardware. In [56] a new tool which can be used as an external module for the commercially available off-line software RobotStudio from ABB was discussed. This tool was developed to generate a robot trajectory directly on components with complex geometry to adjust the TCP speed automatically according to thermal spray operating parameters. Some examples of robot trajectory optimization for a workpiece with sharp edge geometry were discussed. In particular, the kinematic constraints of robot motion when the torch follows a trajectory that contains a large change of torch orientation by crossing the sharp edge, a reduction of TCP speed was observed. The gun speed drop led to a local increase of the coating thickness. The optimization of the motion parameters when crossing the sharp edge area was done by a gradual change of the gun orientation from orientation at the left and right sides of the corner. This led to reduction of the gun speed drop and improvement of thickness uniformity. Furthermore, the ways of analyzing heat transfer and

the calculation of residual stress in the coating were to be integrated in the offline programming tools to provide a complete simulation before on site spray manipulation.

The methods for process modeling in thermal spray have similar features to the painting process applied in the automobile industry. Thus in [57] an analytic deposition model was presented for electrostatic rotating bell atomizers, which are used in the automotive painting industry. The developed spray model captures the complexity of asymmetric deposition patterns generated by atomizers and takes into account both the surface curvature and the deposition pattern of atomizers, enabling planning tools to optimize trajectories to meet several measures of quality including coating uniformity. In particular the asymmetric spray pattern is modeled as a sum of 2D Gaussian functions with maximums shifted by certain offsets, resulting in a volcano-like shape of the spray pattern. The planar deposition model was extended to arbitrary surfaces, located at varying offset distances and orientations, by projecting the deposition flux from the deposition model plane onto the surface in a way that preserves the total paint volume. It was assumed that a planar deposition pattern is known at a reference plane placed normally to the paint jet at a fixed stand-off distance. Time integration of the deposit pattern characterized by a 2D Gaussian functions enable a deposition profile referenced as 1D collapse pattern to be calculated. This 1D collapse pattern was used to gain experimentally the 2D pattern characteristics such as displacements and standard deviations of the Gaussian functions. Corresponding experimental results were used to evaluate the process models and verify the interaction between the deposition pattern, trajectory, and surface curvature for planar and curvature surfaces. In [58] this model was applied to develop automatic concepts for robot path planning for car parts with non-planar surface geometry. The global optimization procedures that attempt to determine all coverage variables simultaneously were found computationally expensive and not practical. The optimization of coverage variables was done by decomposing the coverage problem into three relatively independent sub-problems: selection of a “seed” pass termed the start curve on the surface, selection of the speed profile along a given pass, and selection of the optimum index spacing between a given pass and its adjacent pass (path offset). As the best choice for the starting curve, the geodesic lines with a minimal Gaussian curvature were used. The next paths were generated by offsetting of the curve from the previous one along the indexing curve, which is placed on the surface and is orthogonal to the current curve. The generation of the next candidate path and index width between the current path and the candidate path was done with the requirement that the resultant paint deposit on the optimization profile is acceptably uniform. This optimization required knowledge of the spray pattern to calculate the resulting thickness distribution for the generation of the next paths.

3 Analytical model of thermally deposited spray spot pattern

Definition of the coating thickness distribution on an arbitrary substrate surface requires an exact model of the basic coating pattern such as a spray spot. The parameters of the real spray spot depend both on the spray parameters and on the local geometry of the substrate. The analytic or numerical description of all interactions related to the spray gun parameters and substrate geometry is a very complex task which needs knowledge of a large number of input process parameters, which are in most cases unknown or not studied extensively enough for a self-consistent model to have been developed.

In this work a spray process model is developed, which uses a limited number of model parameters to describe the deposit pattern. Experimental data are used to gain nominal parameters which accomplish the model definition. These nominal parameters are defined in a reference experiment by the spraying of a basic coating pattern with nominal parameters on a flat substrate. The flat substrate in this test is placed at a nominal distance from the spray gun with a normal orientation to the substrate surface. With the application of basic physical and geometrical principles, the parameters of the spray spot captured on the reference substrate can be applied for spraying onto an arbitrary substrate surface with various positions and orientations in relation to the spray gun. The model describes the most important characteristics of real thermal spray patterns related to their asymmetry and the complexity of coating thickness distribution. An accurate description of these characteristics allows analytical solutions to be obtained for coating thickness distribution on substrates with basic flat and cylindrical geometries. On the other hand, the model is not too complex for effective application in CAD based software tools to simulate the coating deposition process on arbitrary components with a complex 3D geometry, in particular on gas turbine parts.

3.1 Model of the spray jet

Based on the results of the experimental and theoretical investigations discussed in the previous section, the properties of the coating deposit strongly depend on the distribution and physical conditions of the powder particles in the plasma or flame jet. The sprayed powder forms by itself a jet with a specific spatial distribution of the particles' mass, velocities and temperature. As experimentally and theoretically investigated, the radial distribution of these properties in the perpendicular cross section of the spray jet can be described with a high accuracy by Gaussian functions. The axial dependence of the mean particles' temperature and velocity on the distance downstream from the nozzle is typically described by hyperbolic dependences. The divergent form of the spray jet can be typically

approximated by a conical shape with the angle of divergence which depends on the specific spraying process. It should be mentioned that the plasma and powder jets can be displaced from each other, which is a result of the side injection of feedstock particles into the plasma.

In order to model the dependences within the plasma and powder jets let us consider an orthogonal coordinate system $\{x_m, y_m, z_m\}$, connected to the spay gun, with axis z_m aligned with the central axis of the particle jet. Axes x_m and y_m lie perpendicular to the jet plane. In the case of placing the substrate at a distance z_m in front of the spray gun the value z_m defines the spray distance d. The spray distance is determined as a distance from the spray gun to the point of intersection of the plasma jet's central axis with the substrate surface.

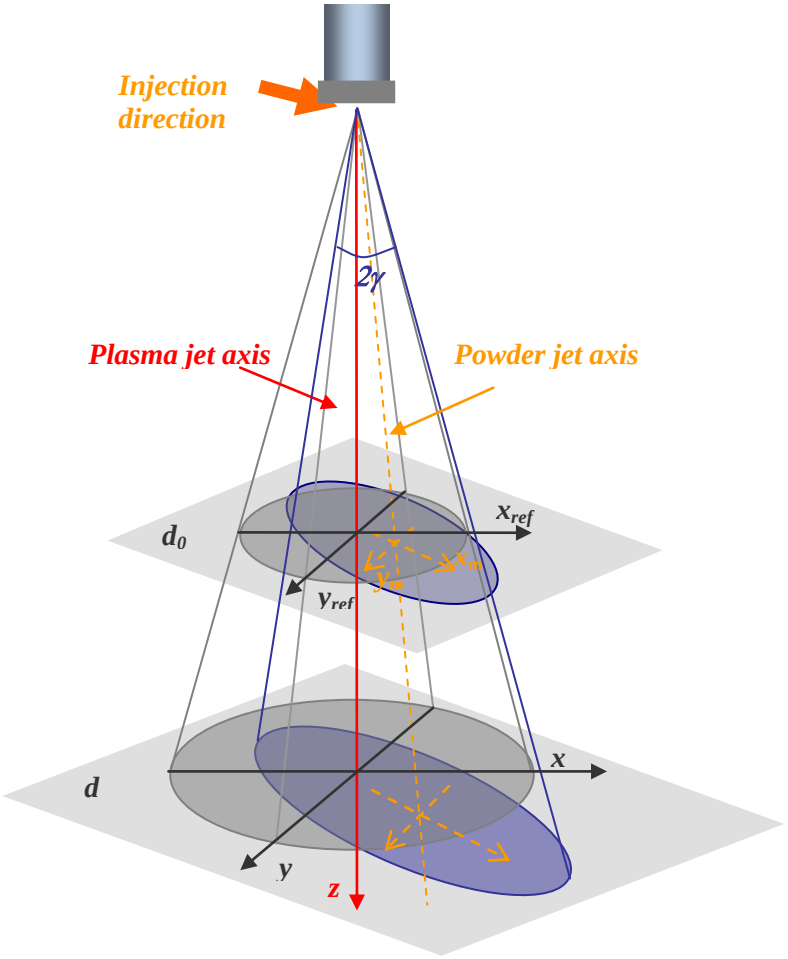

Figure 3.1: Geometric model of the plasma and powder jet.

In the chosen coordinate system, the Gaussian distribution of the spray jet characteristics can be written in the following form:

$$f(x_m, y_m, z_m) = f_0 \exp\left(-\frac{x_m^2}{2\sigma_x^2(z_m)} - \frac{y_m^2}{2\sigma_y^2(z_m)}\right). \qquad (3.1)$$

Here, f_0 is a pre-exponential factor. The σ_x and σ_y are Gaussian standard deviations. It should be pointed out that the standard deviations are functions of the spray distance $\sigma = \sigma(z_m)$. The lines of constant values of the function (3.1) have a form of ellipses in the normal to the spray jet plane and have a mountain-like Gaussian shape in any section perpendicular to this plane. The x_m and y_m axes coincide with the major and minor axes of

these ellipses. Hence the chosen coordinate system $\{x_m, y_m, z_m\}$ coincides with the main coordinate system related to the mass distribution function. Physically, the pre-exponential factor defines a magnitude or intensity of the corresponding property. The standard deviations σ_x and σ_y define the rates of spreading of the distribution curve in two perpendicular directions. The fact that both standard deviations in general are not equal causes an asymmetry of the radial distribution of the powder particles' properties. This asymmetry is caused by the nature of the spraying process. Thus, most of the APS spray guns utilize external injection of the powder particles into the plasma jet from the side by one or multiple radial positioned injectors. The powder, accelerated by the carrier gas, penetrates the core of the plasma jet, which causes a broadening of the distribution curve and an increase in the standard deviation in the direction of particle injection. The resulting asymmetry of the distribution can be controlled practically by carrier gas flow and depends on the relation between the kinetic energy of the injected particles, on the one hand, and the viscose and energetic properties of the plasma on the other hand. Furthermore, the powder mass, temperature and velocity distributions become not only asymmetrical but are also shifted from the centerline of the plasma jet. This effect causes non zero displacements x_0 and y_0 of the powder jet in respect to the free plasma jet (see Figure 3.1). In most practical cases, the mass, velocities and temperature distributions for radial powder injection are asymmetrical and show substantial shifts in the radial plane. In another case, when powder particles are injected into plasma or flame jet axially inside the spray gun the particles' property distributions are close to symmetrical with $\sigma_x = \sigma_y = \sigma$, and no measurable displacement $x_0 = y_0 = 0$ takes place. This type of injection is typically used for most HVOF and some APS spray guns. As discussed before, the standard deviations σ_x and σ_y together with the shifts x_0 and y_0 of the distribution functions increase with increasing distance z_m from the spray gun. This effect is caused by the divergent trajectories of the particles and expansion of the powder jet with increasing distance from the spray gun. It is common to assume that the powder jet having an expanding conical form has the particles' trajectories which are close to divergent straight lines. This assumption can be made for long enough distances from the spray gun, where no perturbations of the jet by carrier gas and injected powder occur. The dependence of the standard deviations and displacements on the distance from the spray gun can be written as:

$$\sigma_x(z_m) = \sigma_{x0} \cdot f(z_m),\ \sigma_y(z_m) = \sigma_{y0} \cdot f(z_m),$$
$$x_0(z_m) = x_0 \cdot f(z_m),\ y_0(z_m) = y_0 \cdot f(z_m). \qquad (3.2)$$

Here the function f denotes a shape factor and describes geometry of the spray jet. For the conical jet this function can be written in the linear form:

$$f(z_m) = 1 + tg\gamma \cdot \frac{z_m - d_0}{d_0}. \qquad (3.3)$$

Here d_0 represents a nominal distance at which the nominal values of the standard deviations σ_{x0}, σ_{y0} and displacements x_0, y_0 are measured and considered as known. The angle γ denotes an angle of the spray cone divergence. For example, as reported in the literature [24] the typical values of the divergence angle of the powder jets are $2\gamma < 15°$ for typical APS processes. Due to the dependence of the standard deviations on distance, the powder jet becomes wider with distance. An increase of the displacements with distance describes an increase of the shift between symmetry axes of the plasma and powder jets.

3.2 Model of the asymmetrical single injection spray spot

In this study, it is considered that the normal component distributions of the powder speed v_z, the powder mass density ρ and the resulting mass flux density ρv_z in any cross section of the powder jet can be described by the Gaussian law according to the relation (3.1). It is assumed that the coating process occurs in stationary conditions, thus no time dependent fluctuations of the in-flight particles' properties occur. Practically, it is assumed that the deposition process is sufficiently controlled to minimize fluctuations of plasma power, powder feed rate and flow rates of plasma and carrier gases. Furthermore, the wear state of the electrode is controlled to provide sufficient stability of the process parameters without causing significant changes in the coating pattern characteristics.

In the case of spraying from some fixed position of the spray gun with a single injector onto the flat substrate surface, the coating pattern represents a spot with an elliptical or round shape. The thickness distribution in this spot has a Gaussian distribution, reflecting the Gaussian distribution of the powder flux density. In order to predict coating pattern properties, knowledge of the in-flight particles' characteristics and of the mechanisms of the interaction at the substrate surface is necessary. It is practically very difficult to measure or compute the three-dimensional (3D) distribution of the particles' in-flight characteristics. Furthermore, the mechanisms of the particles' bonding by coating deposition are not well investigated and rely mostly on experimental data for particular processes. Due to these difficulties, let us connect unknown characteristics of the powder mass distribution in the jet to well measurable parameters of the coating deposit with the help of the following considerations.

The mass of powder with a local density ρ, crossing any infinitely small element of volume with an area $dx_m dy_m$ and thickness of dz_m can be defined as:

$$dm_{jet} = \rho(x_m, y_m, z_m) \cdot dx_m dy_m dz_m, \tag{3.4}$$

The particles' velocity distribution can be characterized in frames of continuous media theory by a velocity field $\vec{v}(x_m, y_m, z_m)$. The radial components of the particles' velocity v_x and v_y do not contribute to the mass transport to the substrate. Let us assume that only the axial component of the velocity v_z contributes to the average powder flux from the jet to the substrate. The powder particles, moving towards the substrate along the jet axis, cross in a time unit a layer with a thickness of:

$$dz_m = v_z dt\,. \tag{3.5}$$

Thus, the mass of powder particles moving towards the substrate in z direction can be calculated as:

$$dm_{jet} = \dot{m}_{jet} dx_m dy_m dt = \rho(x_m, y_m, z_m) v_z(x_m, y_m, z_m) dx_m dy_m dt\,. \tag{3.6}$$

Here, the average particles' velocity v_z and density ρ are the functions of the radial and axial distances. Assuming a Gaussian distribution (3.1) for velocity v_z and density ρ, the mass flux density of powder approaching the substrate in a time unit can be written in a form:

$$\dot{m}_{jet} = \rho_0 v_{z0} \exp\left(-\frac{x_m^2}{2\sigma_x^2} - \frac{y_m^2}{2\sigma_y^2} \right). \tag{3.7}$$

Relation (3.7) contains in-flight particle parameters such as maximal velocity v_0 and particles' density ρ_0. As mentioned before, definition of these parameters is a complex enough task which requires, for example, utilization of particle in-flight sensors. On the other hand, a relation between these parameters and total powder feed rate can be established mathematically by the application of the mass conservation principle for the powder particles approaching the substrate. Thus, the total amount of powder crossing the whole substrate area in a time unit dt according to the formula (3.7) can be calculated as:

$$\dot{M}_{jet} = \int d\dot{m}_{jet} = \int_{-\infty}^{\infty}\int_{-\infty}^{\infty} \rho \cdot v_z \cdot dx_m dy_m\,. \tag{3.8}$$

The last two-fold integral, taking into account (3.7), can be calculated in the explicit form according to the known relation $\int_{-\infty}^{\infty} \exp\left(-x^2/2\sigma^2\right) dx = \sqrt{2\pi}\sigma$ for the Gaussian functions. Thus, after the calculation of the integrals in (3.8) the total mass flux towards to the substrate can be written explicitly as:

$$\dot{M}_{jet} = 2\pi\sigma_x\sigma_y \cdot \rho_0 v_0 . \quad (3.9)$$

This equation connects unknown in-flight parameters $\rho_0 v_0$ with a total mass $\dot{M}_{jet}$ and distribution parameters σ_x and σ_y as follows:

$$\rho_0 v_0 = \frac{\dot{M}_{jet}}{2\pi\sigma_x\sigma_y} . \quad (3.10)$$

Let us introduce a powder feed rate $\dot{M}$ as an amount of powder injected into the plasma per time unit. The total amount of powder crossing each section of the jet, according to the mass conservation principle, has to be equal to the amount of powder injected into the plasma and exiting the spray gun. Thus we can write following relation:

$$\dot{M}_{jet} = \dot{M} . \quad (3.11)$$

According to (3.10), (3.11) and taking into account (3.7), we can rewrite the equation for the powder mass flux density excluding unknown in-flight parameters $\rho_0 v_0$:

$$\dot{m}_{jet} = \frac{\dot{M}}{2\pi\sigma_x\sigma_y} \exp\left(-\frac{x_m^2}{2\sigma_x^2} - \frac{y_m^2}{2\sigma_y^2} \right). \quad (3.12)$$

This is an important equation which defines the particles' mass distribution as a function of the known or practically measurable process parameters. Here, the total powder feed rate $\dot{M}$ is a known parameter. The standard deviations σ_x and σ_y are the variables which represent characteristics of a particular spray process. These parameters can be in general established experimentally with a help of particle in-flight sensors by capturing and analysis the particles' mass flux distribution. It should be mentioned that the practical procedure to determine these in-flight properties is quite complex and not developed enough to provide sufficient accuracy of measurements.

On the other hand, the particles' mass flux distribution $\dot{m}_{jet}$ determines a mass distribution $\dot{m}_{coat}$ in the deposited coating pattern. The standard deviations of the mass flux distributions in the incoming powder jet and the mass distribution in the coating pattern σ_x and σ_y can be assumed to be equal. Here, the distribution of the deposited powder can be evaluated with experimental methods that are developed well enough. In particular, an experimental evaluation of the stationary spray spot by scanning or metallography technique enables the standard deviations of the mass and thickness distributions to be established with high accuracy.

An example of a spray spot deposited with a single injector and a chosen coordinate system is presented in Figure 3.2. In order to describe the spray spot, it is advantageous to

use the coordinate system $\{x_m, y_m, z_m\}$ related to the main axes of the mass distribution function, and at the same time with the main axis of the spray spot ellipse to simplify mathematical formulations. On the other hand, the orientation of the main axes is variable and itself represents a characteristic of the deposition process. Furthermore, the spray spot is shifted in relation to the spray jet axis, and this shift represents a variable which has to be determined in the coordinate system related to the spray jet.

Let us introduce a rectangular reference coordinate system $\{x_{ref}, y_{ref}, z_{ref}\}$ which is connected to the spray gun and at the same time refers to the reference flat substrate. The axis z_{ref} of this coordinate system is aligned along the plasma jet axis. The x_{ref} and y_{ref} axes are placed in an imaginary reference plane which is placed perpendicular to the spray jet axis at a nominal distance d_0. This plane coincides with the flat substrate surface if the spraying is performed under the nominal conditions. In the reference test, used to determine characteristics of coating distribution, the x_{ref} and y_{ref} axes are aligned parallel to the width and height of the reference plate respectively. The z_{ref} axis coincides with the substrate normal. The zero of the coordinate system is placed at the spray jet axis, which is directed into the geometrical centre of the substrate. In this case the coordinates related to the spray spot main axes and the reference coordinates are connected by the following relation:

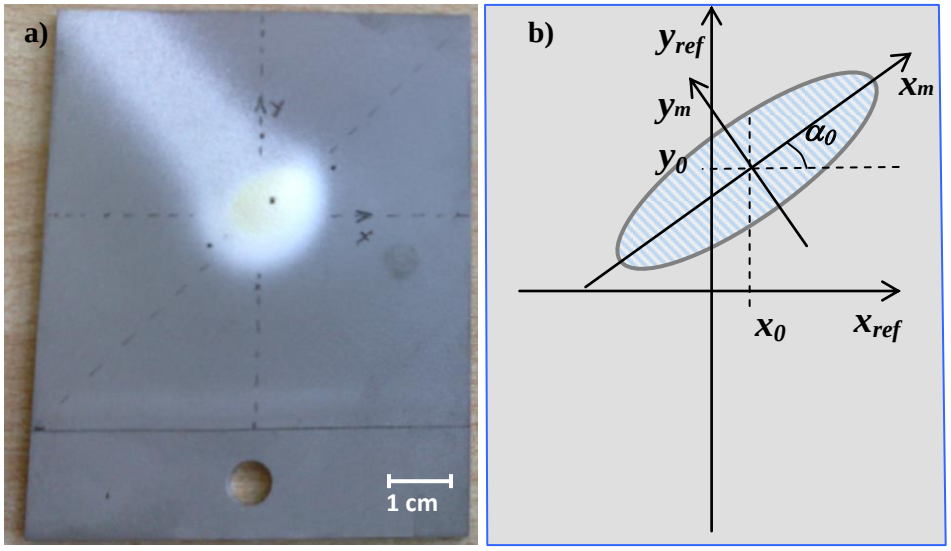

Figure 3.2: Spray spot modeling: a) real 8YSZ APS spray spot applied with a single injector; b) geometric model.

$$
\begin{aligned}
x_m &= \cos\alpha_0 (x_{ref} - x_0) + \sin\alpha_0 (y_{ref} - y_0), \\
x_m &= -\sin\alpha_0 (x_{ref} - x_0) + \cos\alpha_0 (y_{ref} - y_0), \\
z_m &= z_{ref}.
\end{aligned}
\tag{3.13}
$$

This relation represents a transformation of rotation by an angle α_0 in the plane (x_{ref}, y_{ref}) about the z_{ref} axis and shift on the vector (x_0, y_0) in the reference plane.

The angle α_0 describes an orientation of the main axes of the spray spot ellipse. One of the main axes of the spray spot ellipse, along which the standard deviation is maximal, is aligned parallel to the direction of the powder injection, but in general case can differ from this direction. The angle of rotation can be defined as an angle between the main axis x_m of the spot and x_{ref} axis of the chosen coordinate system on the substrate.

It should be mentioned that the transformation (3.13) of rotation and shift does not change the elementary area elements which are used to calculate mass flux to the substrate:

$$dx_m dy_m = dx_{ref} dy_{ref} . \tag{3.14}$$

In the coordinate system $\{x_{ref}, y_{ref}, z_{ref}\}$ connected to the reference plane, taking into account (3.13) and (3.14), the powder mass flux crossing a unit area element $dx_{ref} dy_{ref}$ can be written explicitly in the following form:

$$\dot{m}_{jet}(x_{ref}, y_{ref}, z_{ref}) = \frac{\dot{M}}{2\pi\sigma_x\sigma_y} \exp\left(- \frac{((x_{ref} - x_0)\cos\alpha_0 + (y_{ref} - y_0)\sin\alpha_0)^2}{2\sigma_x^2} \right.$$

$$\left. - \frac{(-(x_{ref} - x_0)\sin\alpha_0 + (y_{ref} - y_0)\cos\alpha_0)^2}{2\sigma_y^2} \right). \tag{3.15}$$

The total flux of the particles' mass in the spray jet $\dot{m}_{jet}$ is practically much higher than the mass $\dot{m}_{coat}$ of the corresponding coating deposit on the substrate. In general, not all powder particles which exit the spray gun and are accelerated by plasma jet can adhere to the substrate upon impact and contribute to the coating deposit formation. The amount of powder which contributes to the coating deposit depends on multiple factors and in particular on velocity, temperature, size distribution and melting state of powder particles, and furthermore on the temperature and geometry conditions at the substrate surface. The powder losses during the deposition process can be taken into account with the introduction of the deposition efficiency factor A. The deposition efficiency represents a ratio of deposited dm_{coat} and total sprayed dm_{jet} masses and can be introduced according to the following relation:

$$dm_{coat} = A dm_{jet} . \tag{3.16}$$

The deposition efficiency A refers to the spraying onto the flat infinite substrate with a certain spray distance, orientation of the gun and fixed substrate temperature and surface morphology. Let us introduce nominal deposition efficiency A_0, defined by spraying at the

nominal distance d_0 with a spray gun orientation normal to the substrate. The nominal efficiency A_0 represents a characteristic of a particular deposition process. The dependence of the deposition efficiency A on the spray angle φ_n and distance z_{ref} can be approximated for most practical cases by the following relation:

$$A(\varphi_n, z_{ref}) = A_0\left(1 - q\frac{z_{ref} - d_0}{z_{ref}}\right)\cos^m \varphi_n . \tag{3.17}$$

Here φ_n is an angle between the normal vector $\vec{n}$ to the substrate surface and the ray connecting the spray gun tip and the measurement point. The efficiency has a maximum value A_0 with the normal orientation of the gun $\varphi_n = 0$ and decreases with the spray angle down to zero at $\varphi_n = 90°$. The rate of efficiency decrease with the spray angle is controlled by the parameter m. The dependence on the spray distance is described by the parameter q. These parameters have to be obtained experimentally. The influence of the spraying conditions such as spray angle and spray distance will be studied in Chapter 5.

Assuming that the density of the deposited coating ρ_{coat} is known, it is easy to define the coating thickness dh_{spot} deposited per time unit dt onto the element of the substrate surface with an area $dx_{ref}\,dy_{ref}$ by definition of the coating mass increase:

$$\rho_{coat} dh_{spot} dx_{ref}\, dy_{ref} = dm_{coat} . \tag{3.18}$$

According to this relation and taking into account (3.6), (3.14) and (3.16), the thickness of coating deposited onto the element $dx_{ref}\,dy_{ref}$ can be calculated according to the expression:

$$dh_{spot} = \frac{A}{\rho_{coat}}\dot{m}_{jet}(x_{ref}, y_{ref}, z_{ref})dt . \tag{3.19}$$

Here, the mass distribution function in the spray jet is described by the expression (3.15). The time integration in (3.19) can be performed, assuming an independence of the feed rate and coating characteristics on time. In the coordinate system related to the substrate surface, taking into account (3.15), the equation for thickness distribution in the spray spot takes following form:

$$\Delta h_{spot} = \frac{A\dot{M}\cdot\Delta t}{2\pi\sigma_x\sigma_y\rho_{coat}}\exp\left(-\frac{((x_{ref} - x_0(z_{ref}))\cos\alpha_0 + (y_{ref} - y_0(z_{ref}))\sin\alpha_0)^2}{2\sigma_x^2(z_{ref})}\right.$$
$$\left. - \frac{(-(x_{ref} - x_0(z_{ref}))\sin\alpha_0 + (y_{ref} - y_0(z_{ref}))\cos\alpha_0)^2}{2\sigma_y^2(z_{ref})}\right). \tag{3.20}$$

Here Δt refers to the spraying time. It should be mentioned that, due to the divergent character of the powder jet, the standard deviations σ_x, σ_y and displacements x_0, y_0

increase with the distance z_{eff} from the spray gun. The dependence of the standard deviations and displacements on the spray distance is described by relation (3.2). The equation (3.20) enables the maximum thickness of the spot pattern for a particular spray process to be calculated. The maximum is found at the position with $x_{ref} = x_0$ and $y_{ref} = y_0$:

$$\Delta h_{spot}^{\max} = \frac{A\dot{M} \cdot \Delta t}{2\pi\sigma_x\sigma_y\rho_{coat}}. \tag{3.21}$$

The maximum thickness increases linearly with the deposition efficiency A, feed rate $\dot{M}$ and spraying time Δt. On the other hand, it decreases with an increase of the standard deviations σ_x and σ_y, which describe the spray spot widths along the main axes of the ellipse. The maximum thickness together with the Gaussian standard deviation and spot rotational angle are the generic characteristics of a single spray spot shape.

The total coating volume corresponding to the spray spot can be calculated based on (3.20) similarly to (3.8) by an integration of the Gaussian function over the whole substrate surface:

$$V_{spot} = \int_{-\infty}^{\infty}\int_{-\infty}^{\infty} \Delta h_{spot}(x_{ref}, y_{ref})dx_{ref}dy_{ref} = \frac{A\dot{M} \cdot \Delta t}{\rho_{coat}}. \tag{3.22}$$

It can be seen that the volume does not depend on the thickness distribution in the spray spot, defined by σ_x and σ_y, and is defined only by the deposition efficiency A, feed rate $\dot{M}$, coating density ρ and spray time Δt.

In order to demonstrate a numerical result for the thickness distribution in the spray spot pattern let us use an example of the process parameters as presented in Table 3.1.

Table 3.1: Example characteristics of the 8YSZ spray spot from a single injector

Nominal deposition efficiency:	A=45%
Powder feed rate:	$\dot{M}$ =50 g/min
Spraying time:	Δt =2 sec
Nominal spray distance:	150 mm
Nominal standard deviations:	σ_x =4 mm, σ_y =3 mm
Nominal spot displacements:	Δx_0 =4 mm, Δy_0 =2 mm
Nominal angle of spot rotation:	α_0 =30°
Angle of jet divergence	γ =15°
Coating density:	ρ_{coat}=5,5 g/cm^3
Spray angle efficiency factor:	m =0,5
Distance efficiency factor:	q =0,5

These characteristics are typical for atmospheric plasma spraying of 8YSZ coating. According to the equation (3.20) the dependence of thickness on the coordinates related to the substrate plane can be plotted as presented in the Figure 3.3. A detailed comparison of the simulation with corresponding experimental result and the procedure for gaining the model parameters is done and discussed in Chapter 5.1.

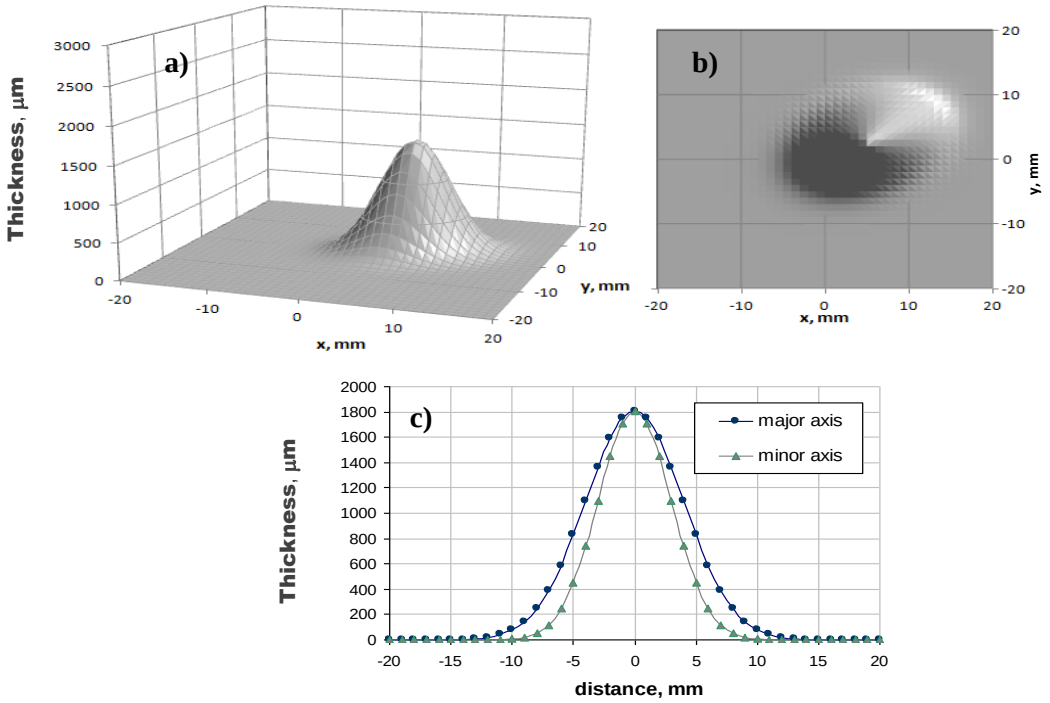

Figure 3.3: Thickness distributions in the spray spot deposited with a single injector: a) 3D plot, b) view from top of substrate, c) perpendicular cross sections along major and minor axes of spot ellipse.

3.3 Influence of spray angle on spray spot pattern

The thickness distribution in the spray spot pattern deposited onto the flat substrate and placed normally to the spray gun at a constant distance d_0 can be found according to the equation (3.20). Complex geometry of the components to be coated mean it is not possible to maintain a constant spray distance and spray angle for all component surface points. Hence, for a realistic simulation of coating thickness, a dependence of the spray pattern on the spray distance and spray angle must be reflected in the model.

As mentioned above, the thickness distribution in a coating pattern is defined by the distribution of the axial component of the powder mass flux in the powder jet in the immediate vicinity of the substrate. In general, the equation (3.15) enables the mass flux

density $\dot{m}(x_{ref}, y_{ref}, z_{ref})$ distribution at any point of the spray jet cone to be calculated. Knowledge of the powder mass flux distribution in combination with an input of the deposition efficiency A and coating density ρ_{coat} enable the thickness distribution on the substrate to be calculated according to the expression (3.19). Let us consider that the nominal deposition efficiency A_0 and the coating density ρ_{coat} are known for spraying onto the nominal substrate plane, placed the distance d_0 normally to the plasma jet. In addition, let us consider that the parameters defining a geometry of the spray pattern, such as nominal standard deviations σ_{x0}, σ_{y0} and spot displacements x_0, y_0, are measured in the selected reference coordinate system. As introduced in Chapter 3.1, the process and geometry parameters in general are functions of the spray distance and spray angle. In particular, the standard deviations and displacements increase with distance downstream from the nozzle according to the relations (3.2) and (3.3). The dependence of the deposition efficiency on the distance and spray angle can be described according to the relation (3.17) and must be evaluated experimentally for the particular deposition process. In general, the coating density ρ_{coat} depends on the angle and distance as well. But for the practical coating processes, coating density is mostly determined by the bulk density of the sprayed material. The variation in coating porosity caused by spray angle and distance, which typically have to stay within 10-20% range for 8YSZ or within several percent for metallic coatings, causes just a weak influence on the coating density and can be neglected for the future considerations. Hence, let us take for the further calculations a constant coating density $\rho_{coat}(\varphi, d) = \rho_0$, which is measured at the reference substrate. For a typical APS spray process to apply 8YSZ powder, the nominal density can be assumed as shown in Table 3.1.

Let us consider a case of coating deposition by spraying at a certain spray angle onto a flat substrate placed at a variable distance from the spray gun. The tilting of the spray gun in respect to the substrate surface can be described by two angles. The first one is the angle φ, which is measured between the symmetry axis of the plasma jet and the substrate surface normal $\vec{n}$. This angle represents a spray angle which defines an inclination of the gun to the substrate surface. The second one θ describes the orientation of spray jet inclination, measured between the gun inclination plane and axis x_{ref} of the chosen reference coordinate system. For the further considerations, let us define a rectangular coordinate system $\{x, y, z\}$ connected to the surface of the substrate with a zero point placed at the intersection of the symmetry axis of the plasma jet z_{ref} and the substrate surface at variable distance d from the spray gun as presented in Figure 3.4.

According to the relation (3.19) the powder mass flux through a unit surface element of the reference plane is defined and considered as known in the reference coordinate system $\{x_{ref}, y_{ref}, z_{ref}\}$. In order to model the coating pattern deposited onto the inclined substrate placed at a variable distance from the spray gun tip, let us describe the powder mass flux and coating thickness distribution in the coordinate system related to the substrate $\{x, y, z\}$.

We chose the rectangular axes x and y which lay in the substrate plane and represent a result of the rotation of coordinate axes x_{ref} and y_{ref} connected to the spray gun. The z axis is aligned with the substrate surface normal $\vec{n}$. The substrate surface is described in this coordinate system by a simple relation $z = 0$. The coordinates $\{x, y, z\}$ can be obtained from $\{x_{ref}, y_{ref}, z_{ref}\}$ by three subsequent rotations by an angle θ in the plane $\{x_{ref}, y_{ref}\}$, then by an angle φ in the plane $\{x, z\}$ and finally turn by an angle $-\theta$ in the plane $\{x, y\}$. In matrix notation, these transformations can be written as:

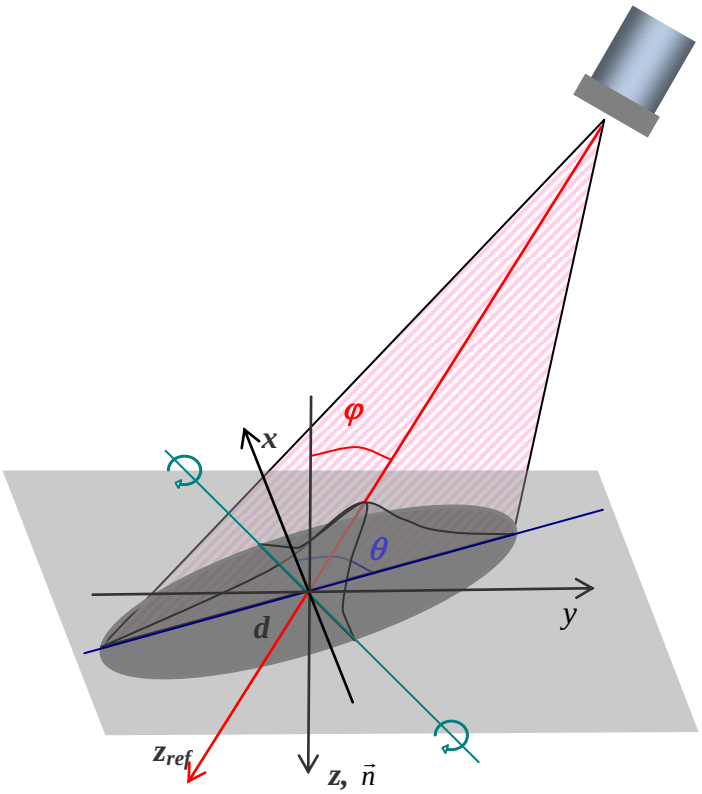

Figure 3.4: Description of the spray gun tilting.

$$x_{refi} = x_{di}(d) + \tau_{ij}^{\theta}(\theta) \cdot \tau_{jk}^{\varphi}(\varphi) \cdot \tau_{kl}^{-\theta}(\theta) \cdot x_l \,. \qquad (3.23)$$

In this expression, a summation of vector components is performed for all repeated indexes. Here we used the following definitions of components $\{x_i\} = \{x, y, z\}$ and $\{x_{refi}\} = \{x_{ref}, y_{ref}, z_{ref}\}$. Corresponding rotation matrixes and the shift vector can be defined as:

$$x_{di} = \begin{pmatrix} 0 \\ 0 \\ d \end{pmatrix}, \; \tau_{ij}^{\theta} = \begin{pmatrix} \cos\theta & -\sin\theta & 0 \\ \sin\theta & \cos\theta & 0 \\ 0 & 0 & 1 \end{pmatrix},$$

$$\tau_{ij}^{\varphi} = \begin{pmatrix} \cos\varphi & 0 & -\sin\varphi \\ 0 & 1 & 0 \\ \sin\varphi & 0 & \cos\varphi \end{pmatrix}, \; \tau_{ij}^{-\theta} = \begin{pmatrix} \cos\theta & \sin\theta & 0 \\ -\sin\theta & \cos\theta & 0 \\ 0 & 0 & 1 \end{pmatrix}. \qquad (3.24)$$

The shift vector x_d defines the spray distance by displacement of the substrate plane in relation to the reference coordinate system, connected to the spray gun tip. The product of the rotation matrixes $T = \tau^{\theta}\tau^{\varphi}\tau^{-\theta}$ determines the orientation of the coordinate system on the substrate in relation to the axes of the reference system. This transformation of coordinates after the multiplication of the matrixes in (3.23) can be finally written in the following form:

$$x_{refi} = x_{di}(d) + T_{ij}(\varphi,\theta)\cdot x_i \,. \tag{3.25}$$

Here a summation of vector components is performed for repeated indexes. The matrix T, after algebraic transformations, considering (3.24), can be written in the following form:

$$T_{ij}(\varphi,\theta) = \begin{pmatrix} \sin^2\theta + \cos^2\theta\cos\varphi & -(1-\cos\varphi)\sin\theta\cos\theta & -\cos\theta\sin\varphi \\ -(1-\cos\varphi)\sin\theta\cos\theta & \cos^2\theta + \sin^2\theta\cos\varphi & -\sin\theta\sin\varphi \\ \cos\theta\sin\varphi & \sin\theta\sin\varphi & \cos\varphi \end{pmatrix}. \tag{3.26}$$

This equation connects the coordinates $\{x_{ref}, y_{ref}, z_{ref}\}$ related to the spray gun and coordinates $\{x, y, z\}$ connected to the substrate surface tilted by an angle of φ about the axis with a unit vector $\bar{e}_{\eta} = \sin\theta\cdot\bar{e}_x - \cos\theta\cdot\bar{e}_y$ aligned under the angle θ to the chosen direction (x axis) on the substrate. It is evident that, for the case of spraying with a normal gun orientation $\varphi = 0$, the coordinate system $\{x, y, z\}$ coincides with the coordinates $\{x_{ref}, y_{ref}, z_{ref}\}$, shifted by a distance d from the spray gun. The expression (3.25), taking into account (3.26), can be written in the explicit form:

$$\begin{aligned} x_{ref} &= \sin^2\theta + \cos\varphi\cos^2\theta x - (1-\cos\varphi)\sin\theta\cos\theta y - \cos\theta\sin\varphi z \,, \\ y_{ref} &= -(1-\cos\varphi)\sin\theta\cos\theta x + (\cos^2\theta + \cos\varphi\sin^2\theta) y - \sin\theta\sin\varphi z) \,, \\ z_{ref} &= d + \cos\theta\sin\varphi x + \sin\theta\sin\varphi y + \cos\varphi z \,. \end{aligned} \tag{3.27}$$

The relation (3.27) in combination with (3.15) enables a local distribution of the powder flux density to be defined at any point in the coordinate system chosen at the substrate surface. In order to calculate the thickness deposited onto the inclined surface element with area $dxdy$, let us calculate the amount of powder crossing the corresponding element of the reference surface $dx_{ref}\,dy_{ref}$. Similarly to equation (3.18), we can calculate the powder mass and consequently coating thickness deposited onto the element area $dxdy$ on the substrate:

$$dh_{spot}(x,y) = \frac{A}{\rho_{coat}}\,\dot{m}_{jet}(x_{ref}, y_{ref}, z_{ref})\,\frac{dx_{ref}\,dy_{ref}}{dxdy}\,dt \,. \tag{3.28}$$

For the simplification of further mathematical formulations, let us align axes $\{x_{ref}, y_{ref}\}$ along the spray spot's minor and major axes $\{x_m, y_m\}$. In the coordinate system chosen this way we have $\alpha_0 = 0$ and can conclude an explicit relation for the coating thickness. Thus, taking into account expressions (3.2), (3.27) and (3.28), we can write the final expression for the spray spot thickness distribution:

$$dh_{spot}(x,y) = \frac{A(\varphi,d)\cdot \dot{M} dt}{2\pi\rho_{coat}\sigma_{x0}\sigma_{y0} f^2(x,y,d)} \frac{dx_{ref}\,dy_{ref}}{dxdy} \exp\left\{ \right.$$
$$\frac{\left(\sin^2\theta + \cos\varphi\cos^2\theta)x - (1-\cos\varphi)\sin\theta\cos\theta y - x_0 f(x,y,d)\right)^2}{2\sigma_{x0}^2 f^2(x,y,d)} + \qquad (3.29)$$
$$+ \frac{\left(-(1-\cos\varphi)\sin\theta\cos\theta x + (\cos^2\theta + \cos\varphi\sin^2\theta)y - y_0 f(x,y,d)\right)^2}{2\sigma_{y0}^2 f^2(x,y,d)} \left. \right\}.$$

Here the geometry factor f is calculated according to the expression (3.3) as:

$$f(x,y,d) = 1 + tg\gamma(d - d_0 + \cos\theta\sin\varphi x + \sin\theta\sin\varphi y)/d_0 . \qquad (3.30)$$

Here we took into account that the flat substrate surface is defined as $z = 0$ (see Figure 3.4). The ratio of the elementary areas $dx_{ref}\,dy_{ref}\,/\,dxdy$ in the expression (3.29) represents the Jacobian determinant for the transformation of the coordinates (x_{ref}, y_{ref}) to the coordinates (x, y), which can be calculated according to the following relation:

$$\frac{dx_{ref}\,dy_{ref}}{dxy} = \begin{bmatrix} \frac{\partial x_{ref}}{\partial x} & \frac{\partial y_{ref}}{\partial x} \\ \frac{\partial x_{ref}}{\partial y} & \frac{\partial y_{ref}}{\partial y} \end{bmatrix} = \frac{\partial x_{ref}}{\partial x}\frac{\partial y_{ref}}{\partial y} - \frac{\partial y_{ref}}{\partial x}\frac{\partial x_{ref}}{\partial y} . \qquad (3.31)$$

The equation (3.29), taking into account (3.30) and (3.31), defines a change in the geometry of the spot coating pattern in dependence on the spray distance and orientation of the spray gun in the case of flat substrate. It can be seen that for spraying with a non-zero spray angle $\varphi \neq 0$, the spray spot on the substrate does not have a strictly Gaussian form. The deviation from a Gaussian distribution is caused by the geometry factor f, defined by the equation (3.30). A numerical investigation of the spray spot features will be done in the next chapter.

3.4 Analytical solution for practical case of spray spots

From the geometry standpoint (see Figure 3.4), the local spray angle at any point (x, y) on the flat substrate for any orientation of the gun characterized by the angles φ and θ can be calculated according to the following relation:

$$\cos\varphi_n(x,y)=\frac{d\cos\varphi}{\sqrt{(d\cos\theta\sin\varphi-x)^2+(d\sin\theta\sin\varphi-y)^2+d\cos^2\varphi}}. \qquad (3.32)$$

Let us consider a case of spraying with a relatively long spray distance, which is important for practical application. This means that the distance is much longer than characteristic dimensions of the spray spot pattern, $\Delta x << d$ and $\Delta y << d$. These characteristic dimensions can be estimated with a 6σ rule. This rule points out that the coating thickness, distributed with Gaussian law, at the distances of $\Delta x = \pm 3\sigma_x$ and $\Delta y = \pm 3\sigma_y$ achieves values of approximately 1/100 of the maximum thickness calculated by (3.20) in the middle of the spray spot. The coating thickness can be considered as negligible outside of the region with a 6σ width. This requirement $\Delta x << d$ and $\Delta y << d$ is safely fulfilled for known APS and HVOF spray processes, performed with relatively high spray distances. Thus for the parameters set from Table 3.1 , taken as an example, $\Delta x = \pm 9$ mm and $\Delta y = \pm 12$ mm, which are much smaller in comparison with the nominal distance d_0=150 mm. Consideration of these requirements for practical conditions enable the relations (3.27), (3.30) and (3.17) to be simplified by neglecting the terms of next order of magnitude in respect to $\Delta x / d$ and $\Delta y / d$:

$$z_{ref}=d; \qquad f(x,y,d)=f(d)=1+tg\gamma(d-d_0)/d_0,$$

$$\cos\varphi_n=\cos\varphi; \quad A(\varphi,d)=A_0\left(1-q\frac{d-d_0}{d}\right)\cos^m\varphi. \qquad (3.33)$$

The Jacobian of transformation (3.34) for a flat surface with constant spray and orientation angles can be calculated explicitly:

$$\frac{\partial(x_m,y_m)}{\partial(x,y)}=\begin{bmatrix}\sin^2\theta+\cos^2\theta\cos\varphi & -(1-\cos\varphi)\sin\theta\cos\theta\\ -(1-\cos\varphi)\sin\theta\cos\theta & \cos^2\theta+\sin^2\theta\cos\varphi\end{bmatrix}=\cos\varphi. \qquad (3.34)$$

Taking into account (3.33) in combination with (3.34) and after obvious trigonometric transformations, the expression (3.29) can be written in the following form:

$$dh_{spot}(x,y)=\frac{A\dot{M}\cos\varphi\cdot dt}{2\pi\rho_{coat}\sigma_x\sigma_y}\exp\left\{\right.$$

$$\frac{1}{2\sigma_x^2}\left(\sin^2\theta+\cos\varphi\cos^2\theta)x-(1-\cos\varphi)\sin\theta\cos\theta y-x_0\right)^2+$$

$$+\frac{1}{2\sigma_y^2}\left(-(1-\cos\varphi)\sin\theta\cos\theta x+(\cos^2\theta+\cos\varphi\sin^2\theta)y-y_0\right)^2\left.\right\}. \qquad (3.35)$$

Here the standard deviations and displacements represent functions of the spray distance according to (3.2) and taking into account (3.33). The equation (3.35) defines a spray spot geometry in dependence on the spray distance d and tilting of the gun to the substrate

plane φ with an arbitrary orientation θ. It can be seen that the expression under the exponent in (3.35) after the multiplication of the corresponding terms is a quadratic form. This expression can be written in a basic form as a quadratic dependence on the coordinates:

$$f(x,y) = a_{11}x^2 + 2a_{12}xy + a_{22}y^2 + 2a_{13}x + 2a_{23}y + a_{33}. \qquad (3.36)$$

By simple algebraic transformations of the expression (3.36) it can be shown that the coefficients of the corresponding quadratic form can be calculated as:

$$a_{11} = \frac{1}{\sigma_x^2}(\sin^2\theta + \cos\varphi\cos^2\theta)^2 + \frac{1}{\sigma_y^2}(1-\cos\varphi)^2\sin^2\theta\cos^2\theta,$$

$$a_{12} = -\left[\frac{1}{\sigma_x^2}(\sin^2\theta + \cos\varphi\cos^2\theta) + \frac{1}{\sigma_y^2}(\cos^2\theta + \cos\varphi\sin^2\theta)\right](1-\cos\varphi)\sin\theta\cos\theta,$$

$$a_{22} = \frac{1}{\sigma_x^2}(1-\cos\varphi)^2\sin^2\theta\cos^2\theta + \frac{1}{\sigma_y^2}(\cos^2\theta + \cos\varphi\sin^2\theta)^2,$$

$$a_{13} = -\left[\frac{1}{\sigma_x^2}(\sin^2\theta + \cos\varphi\cos^2\theta)x_0 - \frac{1}{\sigma_y^2}(1-\cos\varphi)\sin\theta\cos\theta y_0\right],$$

$$a_{23} = -\left[-\frac{1}{\sigma_x^2}(1-\cos\varphi)\sin\theta\cos\theta x_0 + \frac{1}{\sigma_y^2}(\cos^2\theta + \cos\varphi\sin^2\theta)y_0\right],$$

$$a_{33} = \frac{x_0^2}{\sigma_x^2} + \frac{y_0^2}{\sigma_y^2}. \qquad (3.37)$$

The coating pattern shape described by quadratic form (3.36) has an elliptic form at the substrate plane. Using known methods of linear algebra, by transformation of rotation and shift this quadratic form can be brought to the canonical form. Let us introduce coordinates $\{x', y'\}$ on the substrate plane which represent new main axes of the spray spot ellipse. These coordinates are obtained by the requirement to bring the quadratic form under the exponent in (3.36) to the main axes. This transformation defines the coordinate shift and rotation which can be described by en equation:

$$\begin{pmatrix} x'_m \\ y'_m \end{pmatrix} = \begin{pmatrix} \cos\omega & \sin\omega \\ -\sin\omega & \cos\omega \end{pmatrix}\begin{pmatrix} x - x'_0 \\ y - x'_0 \end{pmatrix}. \qquad (3.38)$$

An angle ω defines an additional angle of spot rotation caused by spraying onto the inclined substrate surface in dependence on the gun orientation. The angle ω and the shifts x'_0 and y'_0 can be found by the requirement of absence of the free term and cross term of the quadratic form, obtained by substitution of (3.38) in (3.36). In accordance with this requirement, the angle and shift are defined by the following expression:

$$tg\,2\omega = 2a_{12}/(a_{11}-a_{22}),$$

$$x_0' = \frac{a_{13}a_{22}-a_{23}a_{12}}{a_{12}^2-a_{11}a_{22}},$$

$$y_0' = \frac{a_{23}a_{11}-a_{13}a_{12}}{a_{12}^2-a_{11}a_{22}}. \qquad (3.39)$$

It can be shown that performing the transformation (3.38) in the coordinate system connected to the main axes of the ellipse, the quadratic form (3.36) can be written in the following simple form:

$$f(x',y') = a_{11}'x_m'^2 + a_{22}'y_m'^2 + a_{33}'. \qquad (3.40)$$

Here the parameters a_{11}', a_{22}' and a_{33}' of the transformed quadratic form are calculated as:

$$a_{11}' = a_{12}\sin 2\omega + \frac{1}{2}(a_{11}-a_{22})\cos 2\omega + \frac{1}{2}(a_{11}+a_{22}),$$

$$a_{22}' = -a_{12}\sin 2\omega - \frac{1}{2}(a_{11}-a_{22})\cos 2\omega + \frac{1}{2}(a_{11}+a_{22}),$$

$$a_{33}' = a_{33} + a_{13}x_0' + a_{23}y_0'. \qquad (3.41)$$

Taking into account the transformation to the main axes of the spray spot ellipse, the thickness distribution can be finally written in the coordinate system related to the substrate in the following form:

$$dh_{spot}(x',y') = \frac{A\dot{M}dt\cdot\cos\varphi}{2\pi\rho_{coat}\sigma_x\sigma_y}\exp\left(-\frac{((x-x_0')\cos\omega+(y-y_0')\sin\omega)^2}{2\sigma_x'^2}\right.$$
$$\left.-\frac{(-(x-x_0')\sin\omega+(y-y_0')\cos\omega)^2}{2\sigma_y'^2}\right). \qquad (3.42)$$

Here σ_x' and σ_x' are the effective standard deviations, caused by off-normal spraying from arbitrary spray distance which can be calculated by the following relations:

$$\sigma_x'^2(\varphi,\theta) = 1/a_{11}',$$

$$\sigma_y'^2(\varphi,\theta) = 1/a_{22}'. \qquad (3.43)$$

This equation, which describes thickness distribution in a spray spot on an inclined surface, has the same form as the equation (3.20) for the spot sprayed under the nominal conditions. It can be shown analytically that, in the case of absence of nominal displacement $x_0 = y_0 = 0$, the displacement on the inclined substrate is absent as well $x_0' = y_0' = 0$ and hence the factor $q = 0$ is equal to zero. Furthermore, if the nominal standard deviations of the spray spot are equal $\sigma_{x0} = \sigma_{y0}$ the rotation angle of the spray spot ellipse is equal to the

orientation angle of the spray spot tilting $\omega = \theta$. In the case of no substrate tilting $\varphi = 0$ the equation (3.42) coincides with the equation (3.20). In a general case, the geometry of the spray spot, which is defined by the standard deviations σ'_x, σ'_y, displacements x'_0, y'_0 and positioning factor q', depends on the magnitude φ and direction θ of the spray gun tilt to the substrate plane. The dependence of the thickness distribution in the spray spot produced by tilting of the spray gun from normal orientation with $\varphi = 0°$ up to $\varphi = 75°$ based on the equation (3.46) for the initially symmetrical spray spot with $\sigma_{x0} = \sigma_{y0} = 4\,\text{mm}$ and further parameters set according to the table 3.1 is presented in Figure 3.5.

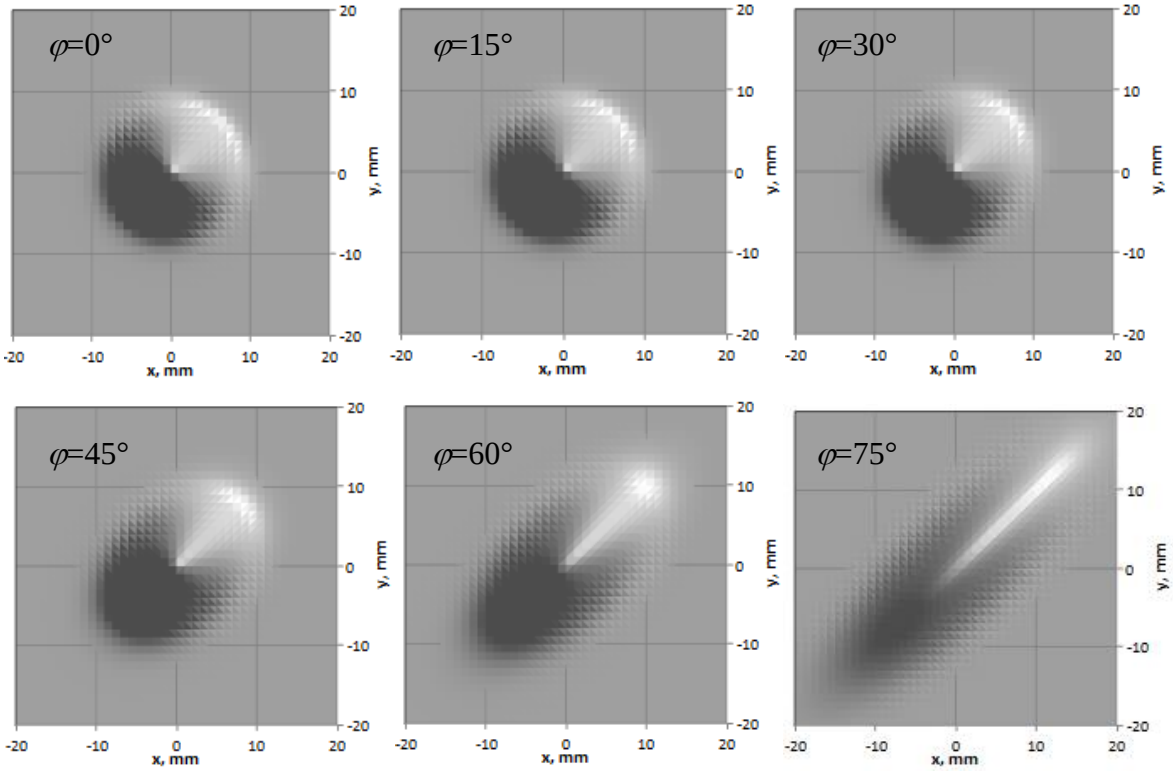

Figure 3.5: Calculation result for evolution of an initially round spray spot with increase of the spray angle φ in the direction $\theta = 45°$.

The calculation results for thickness distribution in the horizontal cross section of the spray spots, performed in the direction of the spray gun tilt, are presented in Figure 3.6 for various tilting angles. As can be seen from these both graphs, the spray spot becomes broader in the direction of the gun tilt. The maximum height of the thickness curve decreases monotonously with deviation of the spray angle from normal orientation. The total area under the curve decreases with the spray angle as a result of reduction of deposition efficiency with an increase in the spray angle. This effect follows from the dependence (3.33) of the deposition efficiency on the spray angle. Broadening of the spot in the direction of the spray gun tilting is

a result of increase of corresponding standard deviation of thickness distribution, which is a function of the spray angle φ. This effect is governed by the implicit dependence (3.43). This dependence of the standard deviation on the spray angle is presented in Figure 3.7. It can be shown analytically and can also be seen from Figure 3.7 that in the case of tilting of the gun only in the direction of the major axis, the corresponding standard deviation changes according to the relation $\sigma_x' = \sigma_x / \cos\theta$. The standard deviation in the direction of the minor axis does not change in this case $\sigma_y' = \sigma_y$. In a general case both standard deviations represent a complex function of their nominal values σ_x, σ_y and angles of tilting φ and orientation θ. Furthermore, as can be seen from Figure 3.6, the spot becomes shifted in the direction of the gun tilt which is a result of a shift of the center of mass of the spray jet on the inclined surface. Exact values of the spot center shift can be calculated according to the relation (3.39). The increase in the shift follows a similar trend as discussed before for the standard deviations in the case of tilting along one of the main axes of the spray spot.

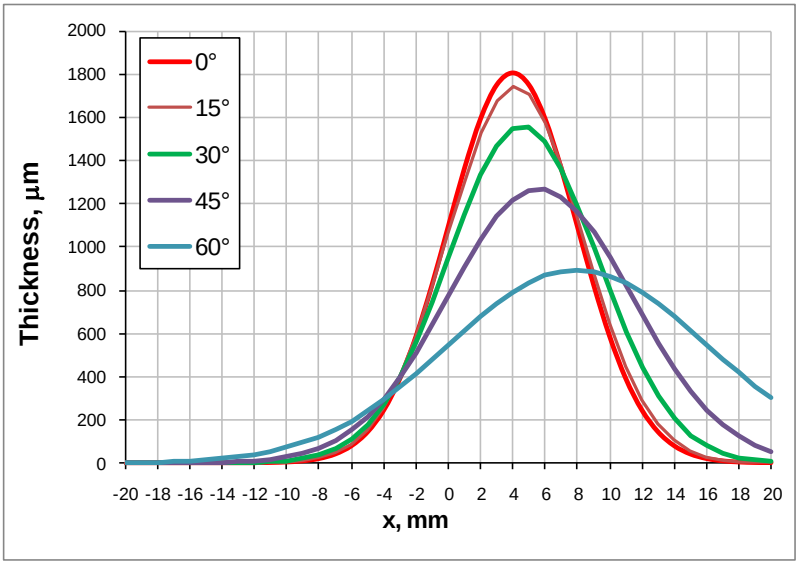

Figure 3.6: Calculation result for thickness distribution in a cross section of the spray spots produced by varying the spray angle φ in the direction of the main axis $\theta = \alpha_0$.

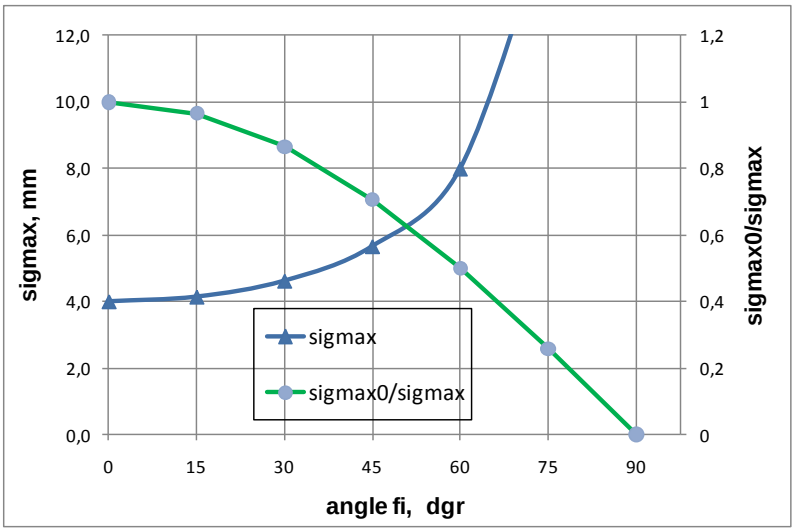

Figure 3.7: Dependence of the standard deviation measured in the tilting direction $\theta = \alpha_0$ on the angle φ.

3.5 Model of spray spot from double and multiple injectors

The coating pattern produced by spraying with multiple injectors can be represented as a superposition of the multiple spots produced by single injectors. Typically a double and triple injection is used for APS spray processes. In the case of double injection the coating powder is fed from two external injectors placed at the opposite positions of one diameter line on the spray gun. This placement makes possible a symmetrical distribution of powder flow around the central axis of the jet, which consequently leads to a symmetrical spray spot. As experimentally investigated and discussed in Chapter 1.3.2, the distribution of mass flux is practically controlled by carrier gas flow. In particular, with an increase in carrier gas flow rate the radial distributions of the powder particles' sizes, concentration, velocities and, as a result, the particles' flux, changes from a single bell-like to a double bell-like shape. The shape of the spray spot produced by a double injection can be modeled based on the approach used for single injector spraying. As we showed in Chapter 3.3, a single spray spot can be modeled as an elliptic spot with a Gaussian thickness distribution even for spraying onto an inclined substrate surface. Let us assume that the thickness distribution in a single spot is known by definition of the basic process parameters summarized in Table 3.1. Typical spray spots produced with 8YSZ coating by the APS process are presented in Figure 3.8. In particular, the shape of the spot is defined by a maximal height calculated according to the relation (3.20), standard deviations σ_x, σ_y and the angle of rotation α_0. In the case of inclined substrate, as shown in Chapter 3.3, these parameters are functions of spray angle φ and

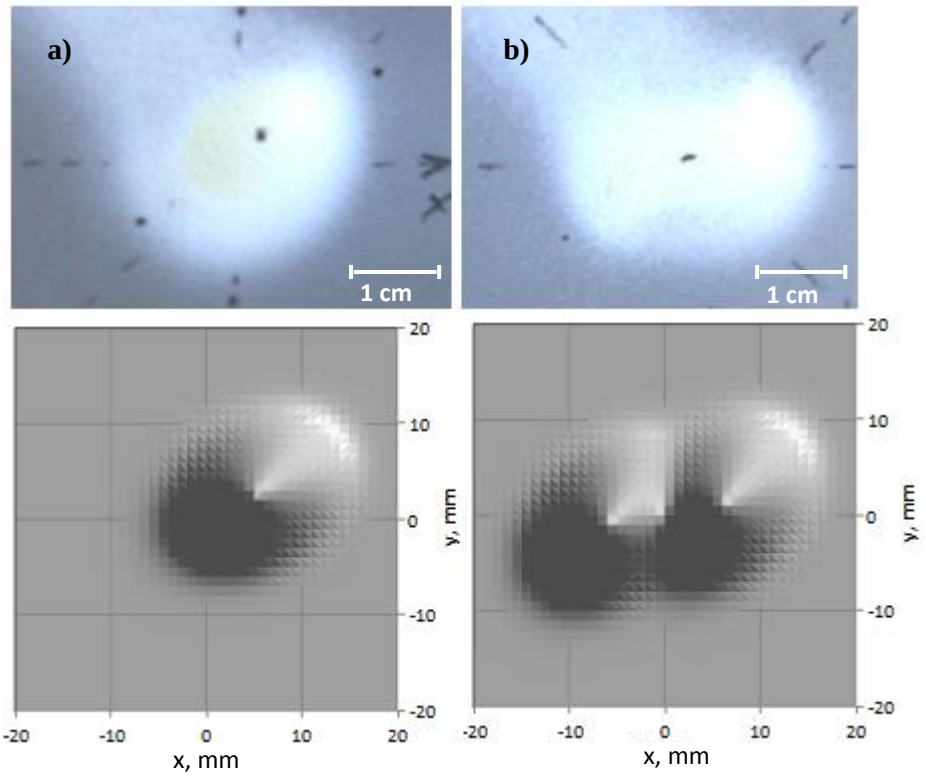

Figure 3.8: Optical photographs and models of APS 8YSZ spray spots produced with a) single and b) double injection process.

direction of the substrate inclination, defined by the angle θ. Let us assume that the displacements of the individual spots produced by one or two injectors are known and equal to $x_{10} = x_0$ and $y_{10} = y_0$. Assuming a symmetrical placement of the injectors, whose positions are offset angularly by 180°, the displacement of the second spot can be calculated as $x_{20} = -x_0$ and $y_{20} = -y_0$. The total coating thickness produced by these two injectors can be calculated as a sum of corresponding individual spots:

$$h_{spot}^{double}(x,y) = h_{spot}^{single}(x - x_0, y - y_0) + h_{spot}^{single}(x + x_0, y + y_0). \quad (3.44)$$

Here the thickness distribution in the individual spray spot is calculated according to the relation (3.20) in the case of normal spraying and by (3.42) in the general case.

Let us consider the case of spraying with more than two injectors. In practice, the triple and quarterly injections are used to spray coatings. The spot from multiple injections can be modeled, similarly to the double injection, as a superposition of multiple single spots, displaced by certain distances from each other. According to the equation (3.20), for each individual spot we can write following expression:

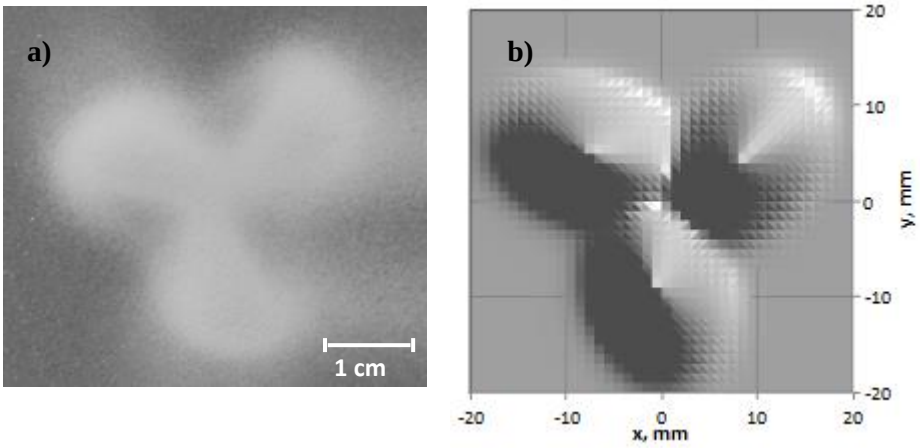

Figure 3.9: Spray spot produced with triple injection: a) photo of a real spot, b) model of the spray spot.

$$dh_{spot}(x,y) = \frac{A\dot{M}dt}{2\pi\rho_{coat}\sigma_x\sigma_y}\frac{1}{N}\sum_{i=1}^{N}\exp\left(-\frac{((x-x_{0i})\cos\alpha_{0i} + (y-y_{0i})\sin\alpha_{0i})^2}{2\sigma_x^2}\right.$$
$$\left. - \frac{(-(x-x_{0i})\sin\alpha_{0i} + (y-y_{0i})\cos\alpha_{0i})^2}{2\sigma_y^2}\right). \quad (3.45)$$

Assuming a symmetrical placement of injectors, the displacements can be calculated as:

$$\begin{pmatrix} x_{0i} \\ y_{0i} \end{pmatrix} = \begin{pmatrix} \cos\alpha_{0i} & \sin\alpha_{0i} \\ -\sin\alpha_{0i} & \cos\alpha_{0i} \end{pmatrix}\begin{pmatrix} x_0 \\ y_0 \end{pmatrix} \text{ and } \alpha_{0i} = \alpha_0 + \frac{2\pi}{N}. \quad (3.46)$$

Here i is a sequential number of one of the N of injectors. The x_{0i}, y_{0i} and α_{0i} are displacements and rotation angles of the spot with the number i. An example of the triple spot and corresponding model according to the equation (3.45) is shown in Figure 3.9.

From the theoretical point of view, it is important to analyze a contour of the multiple spot in dependence on the displacements of the individual spots. For example, let us perform analytical analysis for the simplest case of a double injection spot. It can be shown that a double spray spot has one of the basic configurations presented in Figure 3.10.

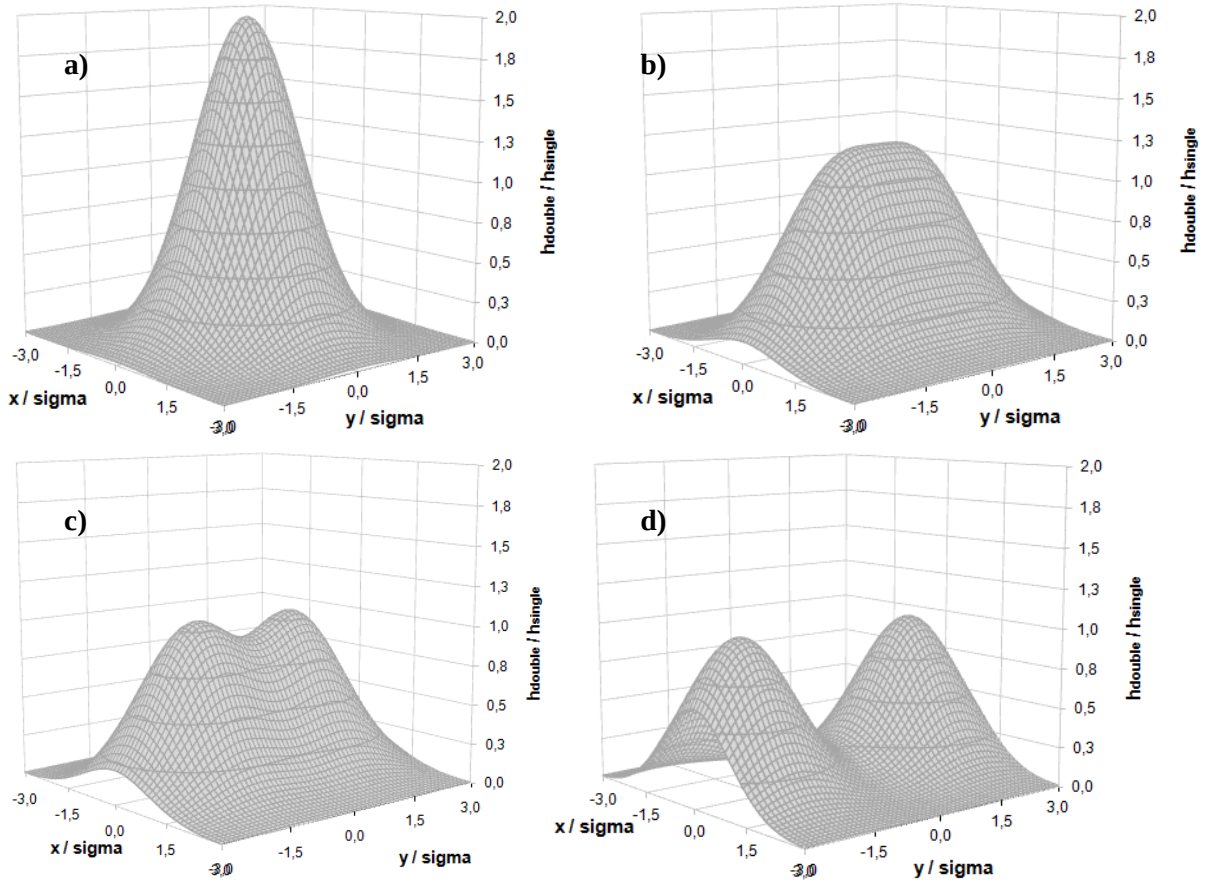

Figure 3.10: Basic configurations of thickness distribution in double injection spots: a) coinciding single spots, b) overlapping single spots with common maximum, c) overlapping double spot with two maximums, d) two displaced almost not interacting spots.

The configuration of the double spray spot is defined by a relative displacement of the single spray spots from each other. In order to investigate a spot configuration analytically, let us assume that each single spot is displaced along the x axis, furthermore that this axis coincides with the major axis of the spot ellipse. In this case, the coating thickness distribution in the cross section of the spot can be described by the following equation:

$$h(x, x_0) = \frac{h_0}{2}\left(e^{-\frac{(x-x_0)^2}{2\sigma_{eff}^2}} + e^{-\frac{(x+x_0)^2}{2\sigma_{eff}^2}}\right). \qquad (3.47)$$

As presented in Figure 3.10, the spray spot contour can vary from the configuration with one single peak in the middle to the configuration with two peaks corresponding to the

displacements of the spots. Let us find the position of the maximum of the spot. The local maximum position can be calculated using a requirement:

$$\frac{dh}{dx} = \frac{h_0}{2\sigma_{eff}^2}\{(x-x_0)e^{-\frac{(x-x_0)^2}{2\sigma_{eff}^2}} + (x+x_0)e^{-\frac{(x+x_0)^2}{2\sigma_{eff}^2}}\} = 0\,. \qquad (3.48)$$

The relation (3.48) is a non linear equation. The solution of this equation $x = x_{\max}$ which corresponds to the point where the maximum thickness $h = h_{\max}$ is achieved, can be found by numeric methods. Figure 3.10 shows a numerical solution of the equation (3.48) for the dependence of the maximum position $x_{\max}$ of the spray spot applied by double injection on the displacement $2x_0$ of the single spots. As can be seen from the graph, the spray profile can have three possible configurations according to the positions of the double spot maximums. The configuration of type 1 defines a spot with a single common maximum in the geometrical centre of the double spot, achieved due to a sufficient overlapping of two single spots. This configuration exists in the range of displacements with $x_0 < \sigma_{eff}$. Cases a) and b) from Figure 3.9 are examples of this configuration. An intermediate configuration of type 2 exists in the displacement range with $\sigma_{eff} < x_0 < 2\sigma_{eff}$, and defines a double spot produced by partial overlapping of two single spots with two maximums as in case c) from Figure 3.9. The configuration of type 3 is formed in the range of high displacements $x_0 > 2\sigma_{eff}$ and defines an extreme case of two non-interacting spray spots, with an example d) in Figure 3.9. For practical use, the configuration of type 1 with a single maximum in the middle of the spot is more preferable due to the high level of spot symmetry. The exact modeling of the spray spots of different configurations, taking into account variations of the process parameters and geometry relations, such as variation of spray distance and angle, are the necessary requirement for a realistic simulation of more complex coating patterns such as a spray profile and complete coating layer.

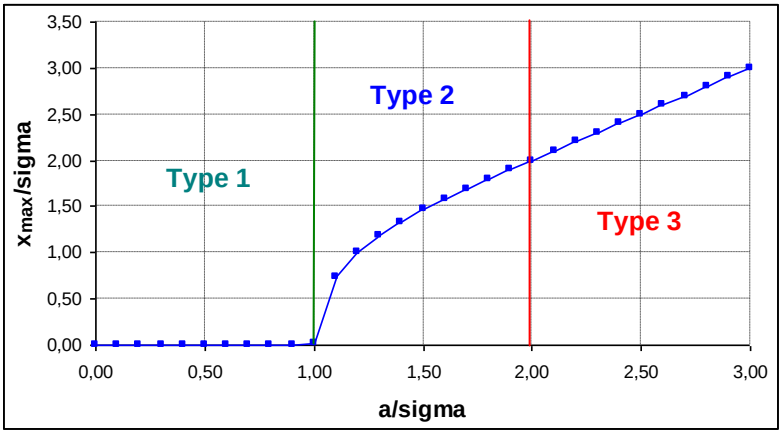

Figure 3.10: Dependence of the common maximum position of the double spray spot on the relative displacement of the single spots.

4 Model of the coating layer formation on substrate surface

4.1 Calculation of the thickness distribution in the linear spray profile

As was shown above, depending on the spray process and spraying conditions, the thickness distribution in the spray spot can vary in a wide range of sizes, orientations and configurations. The asymmetry of the thickness distribution in a static coating pattern, represented by a spray spot, leads to a dependence on the dynamic spray pattern, represented by spray profile, produced by a movement of the spray gun in the direction of motion.

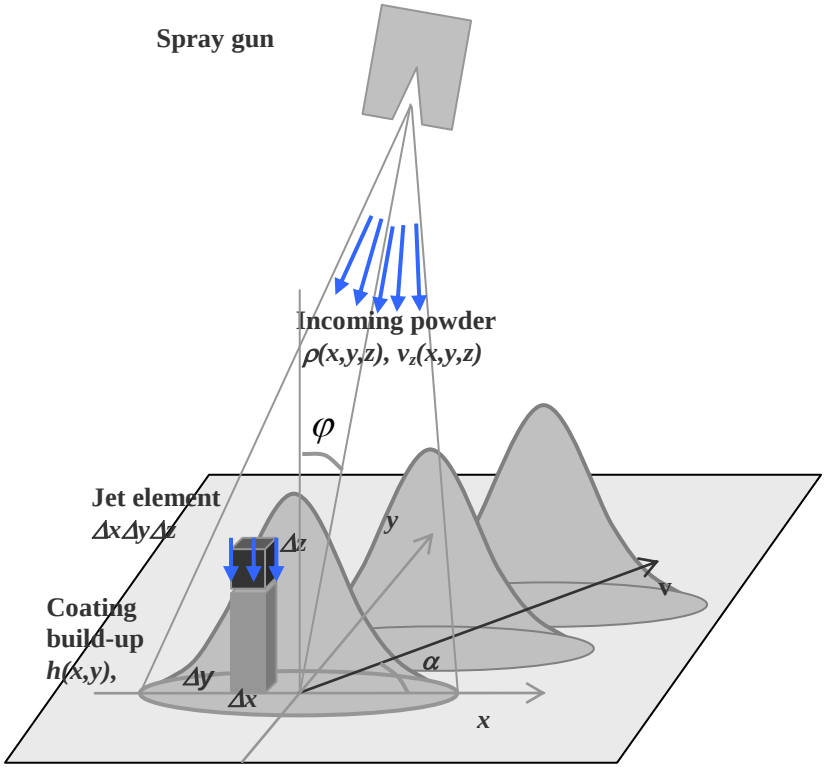

Figure 4.1: Modeling of the coating deposition process.

This dependence causes an asymmetry of the spray profile in respect to the gun motion direction. For example, an elliptical form of the single spray spot in accordance with mass conservation leads to a narrow and high profile when spraying with a gun motion along the spot's major axis and to a wide profile with lower thickness by spraying along the minor axis. Much more complex relations between the form of the spray spot and possible configurations of the spray profile take place in the case of multi-injector spraying. Ability to simulate a thickness distribution in a spray profile is a necessary requirement for simulating a final coating layer thickness.

Let us define a linear spray profile as a coating pattern produced by gun motion over a straight line on the substrate surface. In the case of linear motion at a constant speed, the gun trajectory $\vec{r} = \vec{r}_0(t)$ on the substrate surface is defined by the dependence of the gun coordinates x_0 and y_0 on time, and can be described by following simple cinematic relations:

$x_0(t) = x_0 + v\cos\alpha \cdot t$ and

$$y_0(t) = y_0 + v\sin\alpha \cdot t\,. \tag{4.1}$$

For the definition of the thickness distribution in the spray profile, continuous motion of the spray gun along a certain trajectory $\vec{r} = \vec{r}_0(t)$ can be subdivided into the sequence of the discrete positions $\vec{r}_{0i} = \vec{r}(t_i)$. The dwell time of the gun at each position $\vec{r}_i$ is to be assumed as $\Delta t_i = t_{i+1} - t_i$. Thus, the coating pattern sprayed at each small time interval represents a spray spot pattern produced by the gun situated at the position $\vec{r}_i$ during the time interval Δt_i. As presented in Figure 4.1, the result of this discrete motion can be defined as a sum of coating spots $h_i(x, y)$ sprayed at each time interval t_i from the corresponding position (x_{0i}, y_{0i}) of the gun according to the relation (3.20) or (3.42):

$$h_{profile}(x, y) = \sum_i \frac{A\dot{M}}{2\pi\sigma_x\sigma_y\rho_{coat}} \exp\left(-\frac{(x - x_{0i})^2}{2\sigma_x^2} - \frac{(y - y_{0i})^2}{2\sigma_y^2}\right)\Delta t_i\,. \tag{4.2}$$

In the extreme case of an infinitely small time interval, this expression can be written as:

$$h_{profile}(x, y) = \frac{1}{2\pi}\int \frac{A\dot{M}}{\sigma_x\sigma_y\rho_{coat}} \exp\left(-\frac{(x - x_0(t))^2}{2\sigma_x^2} - \frac{(y - y_0(t))^2}{2\sigma_y^2}\right)dt\,. \tag{4.3}$$

Here v is a gun speed and α is an angle between the direction of motion and x axis.

Taking into account (4.1) and assuming that the spray parameters such as the feed rate $\dot{M}$, deposition efficiency A and the characteristics of the spray spot do not change with time, (4.3) takes the following form:

$$h_{profile}(x, y) = \frac{A\dot{M}}{2\pi\sigma_x\sigma_y\rho_{coat}} \int_{t_0}^{t} \exp\left(-\frac{(x - x_0 - v\cos\alpha \cdot t)^2}{2\sigma_x^2} - \frac{(y - y_0 - v\sin\alpha \cdot t)^2}{2\sigma_y^2}\right)dt\,. \tag{4.4}$$

The expression under the integral in (4.4) can be transformed to one that is more appropriate for the integration form:

$$h_{profile}(x, y) = \frac{A\dot{M}}{2\pi\sigma_x\sigma_y\rho_{coat}} \exp\left(-\frac{\left((x - x_0)\sin\alpha - (y - y_0)\cos\alpha\right)^2}{2(\sigma_x^2\sin^2\alpha + \sigma_y^2\cos^2\alpha)}\right) \times$$
$$\times \int_{t_0}^{t} \exp\left(-\frac{1}{2}\frac{\sigma_x^2\sin^2\alpha + \sigma_y^2\cos^2\alpha}{\sigma_x^2\sigma_y^2}\left(vt - \frac{(x - x_0)\sigma_y^2\cos\alpha + (y - y_0)\sigma_x^2\sin\alpha}{\sigma_x^2\sin^2\alpha + \sigma_y^2\cos^2\alpha}\right)^2\right)dt\,. \tag{4.5}$$

The equation (4.5) enables the calculation of coating thickness distribution in the spray profile, produced by a finite motion of the gun along the linear segment of trajectory from some initial point corresponding to the moment of time t_0 to the time t. From the theoretical and practical point of view, it is important to analyze the case of a sufficiently long segment of the spray profile far away from the initial and final points of the gun trajectory. Mathematically,

it is equivalent to the infinite motion of the gun with $t_0 \to -\infty$ and $t \to \infty$. In this case, the Gaussian integral in (4.5) can be calculated analytically and written in the following form:

$$h_{profile}(x,y) = \frac{A\dot{M}}{\sqrt{2\pi}\rho_{coat}v\sqrt{\sigma_x^2 \sin^2\alpha + \sigma_y^2 \cos^2\alpha}} \exp\left(-\frac{((x-x_0)\sin\alpha - (y-y_0)\cos\alpha)^2}{2(\sigma_x^2 \sin^2\alpha + \sigma_y^2 \cos^2\alpha)}\right). \quad (4.6)$$

The equation (4.6) can be written in the simplest form in the orthogonal coordinate system $\{\xi,\eta\}$ where axis ξ is chosen to be parallel and axis η perpendicular to the direction of gun motion. Corresponding coordinate transformation can be written in the following form:

$$\xi(x,y) = (x-x_0)\cos\alpha + (y-y_0)\sin\alpha\,,$$
$$\eta(x,y) = -(x-x_0)\sin\alpha + (y-y_0)\cos\alpha\,. \quad (4.7)$$

In this coordinate system we can write the following equation for thickness in the linear spray profile in dependence on the coordinates related to the direction of gun motion:

$$h_{profile}(\xi,\eta) = \frac{A\dot{M}}{\sqrt{2\pi}\rho_{coat}v\sigma_{eff}} \exp\left(-\frac{\eta^2}{2\sigma_{eff}^2}\right). \quad (4.8)$$

Here η describes a distance from the spray gun trajectory to the observation point, measured perpendicular to the direction of gun motion. In Figure 4.2, a calculation result for the thickness distribution in the linear spray profile applied with the gun speed of 200 mm/s along the direction of 90° to the x axis on the flat substrate is presented. The process parameters from Table 3.1 were used for the calculations.

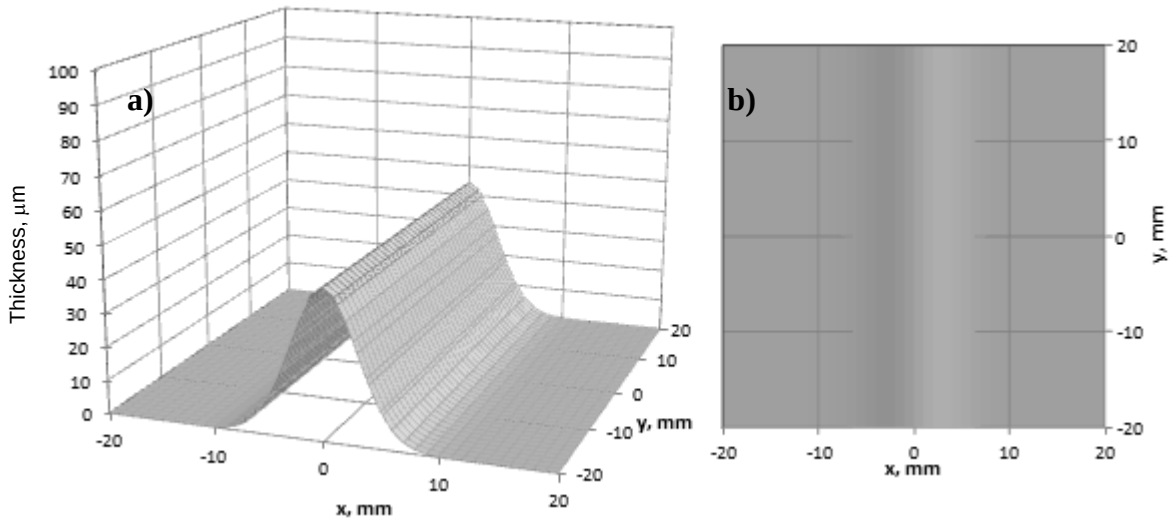

Figure 4.2: Thickness distribution in the spray profile deposited with single injector along the major axis x of the spray soot with $\alpha = 0°$: a) 3D plot, b) view from top of the substrate.

As could be expected, there is no dependence of thickness on the longitudinal coordinate ξ for an infinite spray profile. The parameter σ_{eff} characterizes a spreading of the Gaussian

curve along the transverse coordinate η, and represents an effective standard deviation of the thickness distribution in the profile, which is defined according to the following relation:

$$\sigma_{eff} = \sqrt{\sigma_x^2 \sin^2 \alpha + \sigma_y^2 \cos^2 \alpha}\,. \tag{4.9}$$

It should be mentioned that the effective standard deviation σ_{eff} depends on the direction of gun motion in respect to the main axis of the spray spot ellipse, characterized by the angle α, and on the values of the main standard deviations of the spray spot along σ_x and σ_y. Thus, if the direction of motion coincides with the main x axis of the spray spot with $\alpha = 0°$, the σ_{eff} equals to σ_y, for the motion of the gun along the main y axis of the spray spot with $\alpha = 90°$, σ_{eff} equals to σ_x. For any arbitrary orientation of the gun motion the standard deviation stays in the range $\sigma_x \le \sigma_{eff} \le \sigma_y$. The effective standard deviation defines practical profile width, which can be assumed to be a stripe of $6\sigma_{eff}$ width. The second parameter, defining the geometry of the spray profile, is a magnitude of thickness:

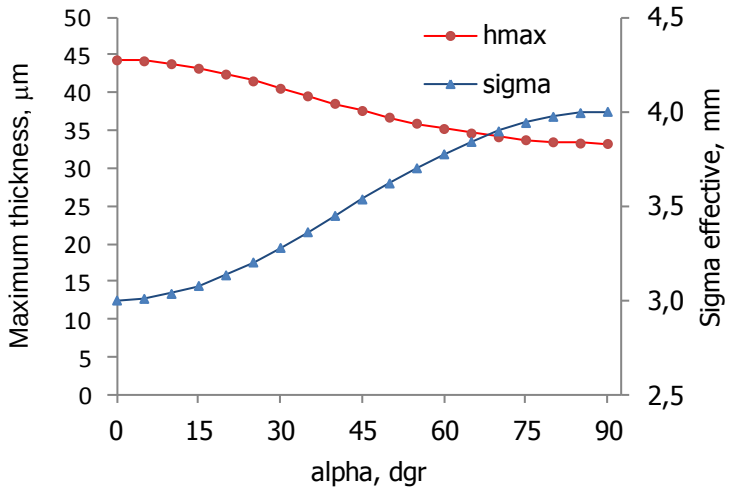

Figure 4.3: Dependence of maximal profile thickness and effective standard deviation on direction of gun motion.

$$h_{profile}^{\max} = \frac{A\dot{M}}{\sqrt{2\pi}\,\rho_{coat} v \sigma_{eff}}\,. \tag{4.10}$$

It can be seen from this expression that the maximum thickness of the spray profile is inversely proportional to gun speed v and the effective standard deviation σ_{eff}. The thickness in the cross section perpendicular to the gun trajectory follows the normalized Gaussian distribution with the standard deviation σ_{eff}. The dependence of the σ_{eff} and $h_{profile}^{\max}$ on the orientation of the gun motion α is presented in Figure 4.3 for the spray parameters from Table 3.1. The maximal thickness is achieved for the profile sprayed along the major axis of the spray spot with a minimal effective standard deviation. The minimal thickness appears for the profile with maximal standard deviation, corresponding to spraying

along the minor spot axis. As can be seen from Figure 4.4, the profile produced by gun motion along the direction of the spray spot major axis is lower but broader than the profile applied along the minor axis. This is a result of the mass conservation principle, which requires a constancy of the total deposited mass of the coating per time unit independently of the direction of gun motion. In general, the total mass deposited per time unit can be calculated as:

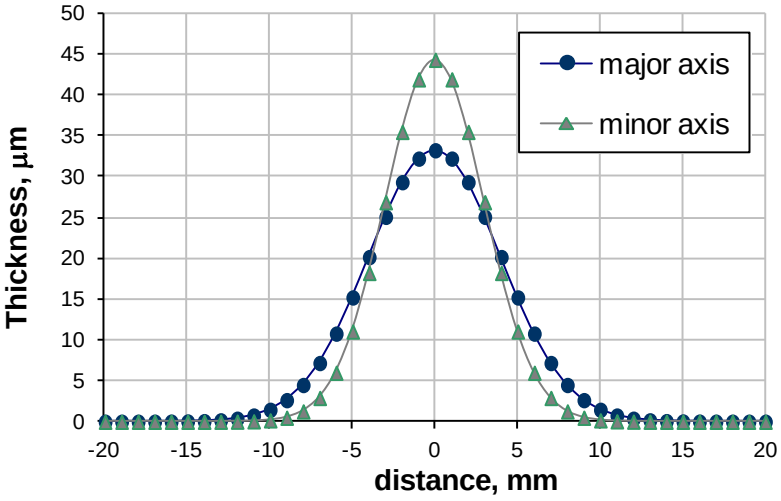

Figure 4.4: Thickness distributions in the spray profiles applied along minor and major axes of the spray spot.

$$dM = \int_{-\infty}^{\infty} \rho_{coat} v h(\eta) d\eta dt = \rho_{coat} v dt \int_{-\infty}^{\infty} h(\eta) d\eta \,. \tag{4.11}$$

The last integral represents an area under the curve of thickness distribution in the spray profile measured in the cross section perpendicular to the direction of the gun motion. Hence, despite the asymmetry of the spray profile in respect to the direction of gun motion, the requirement of mass conservation for coating deposition with constant gun speed v leads to the constancy of the area under the thickness distribution curves. The total mass of the profile segment deposited within a time interval Δt can be explicitly calculated as:

$$\Delta M = \frac{A\dot{M}\Delta t}{\sqrt{2\pi}\sigma_{eff}} \int_{-\infty}^{\infty} \exp\left(-\frac{\eta^2}{2\sigma_{eff}^2}\right) d\eta = A\dot{M}\Delta t \,. \tag{4.12}$$

According to (4.12) the mass is independent on the standard deviation σ_{eff} and subsequently on the direction of gun motion α and is defined only by the feed rate $\dot{M}$, deposition efficiency A and spraying time Δt. This equation is important for further consideration of the total mass of the profile, deposited onto the substrate with a certain finite length Δl, and for the experimental evaluation of the deposition efficiency. Thus, calculating the time Δt to spray a profile with the length $\Delta l = v\Delta t$, based on (4.12), we can get following expression for the deposition efficiency:

$$A = \frac{1}{\dot{M}} \frac{\Delta M}{\Delta t} = \frac{v}{\dot{M}} \frac{\Delta M}{\Delta l} \,. \tag{4.13}$$

This expression can be used to estimate the process deposition efficiency during spraying of the profile patterns.

4.2 Analytical solution for the coating layer thickness on a flat substrate

Typical robot programs to coat a flat substrate are designed to provide a raster movement of the spray gun applying the spray profiles displaced by a certain path offset on the substrate surface. In this case, the trajectory of the spray gun at the substrate surface represents a sequence of parallel or semi-parallel lines. The resulting thickness of the coating layer is accumulated by summation of the thicknesses of each individual profile. In the case of the coating deposition with constant gun speed v and a constant path offset p onto a flat substrate, the thickness of the coating layer can be calculated analytically. Let us consider the case of spraying with a number of the parallel paths. We define a path offset p as a distance between the centre lines of each neighboring spray profile. The coordinates of middle lines of each profile η_n can be defined as:

$$\eta_{0n} = p \cdot n\,. \tag{4.14}$$

Here index $n = -N...N$ denotes the number of the spray profile, $2N$ is the number of the profiles from the left and right sides of the central axis of the flat substrate.

Taking into account expressions (4.8) and (4.14) for the coating thickness distribution in a single spray profile, the thickness distribution in a coating layer can be calculated as:

$$h_{layer}(\eta, p, \sigma) = \frac{A\dot{M}}{\sqrt{2\pi}\rho_{coat} v \sigma_{eff}} \sum_{n=-N}^{N} \exp\left(-\frac{(\eta - p \cdot n)^2}{2\sigma_{eff}^2}\right). \tag{4.15}$$

Figure 4.5 visualizes an accumulation of the total thickness in the coating layer by the superposition of single spray profiles with a standard deviation of thickness σ_{eff} =3mm, displaced by variable path offset on the flat surface. As can be seen, a superposition of the smooth curves of thickness profiles, which follow Gaussian distributions displaced by a path offset from each other, results in an appearance of a continuous coating layer with a certain uniform thickness. The layer thickness depends strongly on the value of path offset. It should be mentioned that, analogously to the displacement of the double spray spot described in Chapter 3.4, the path offset should be small enough to achieve a smooth coating contour avoiding surface waviness by sufficient overlapping of the single spray profiles. In the case of a sufficiently large number of spray profiles $N \to \infty$ we can calculate a layer thickness and surface waviness analytically.

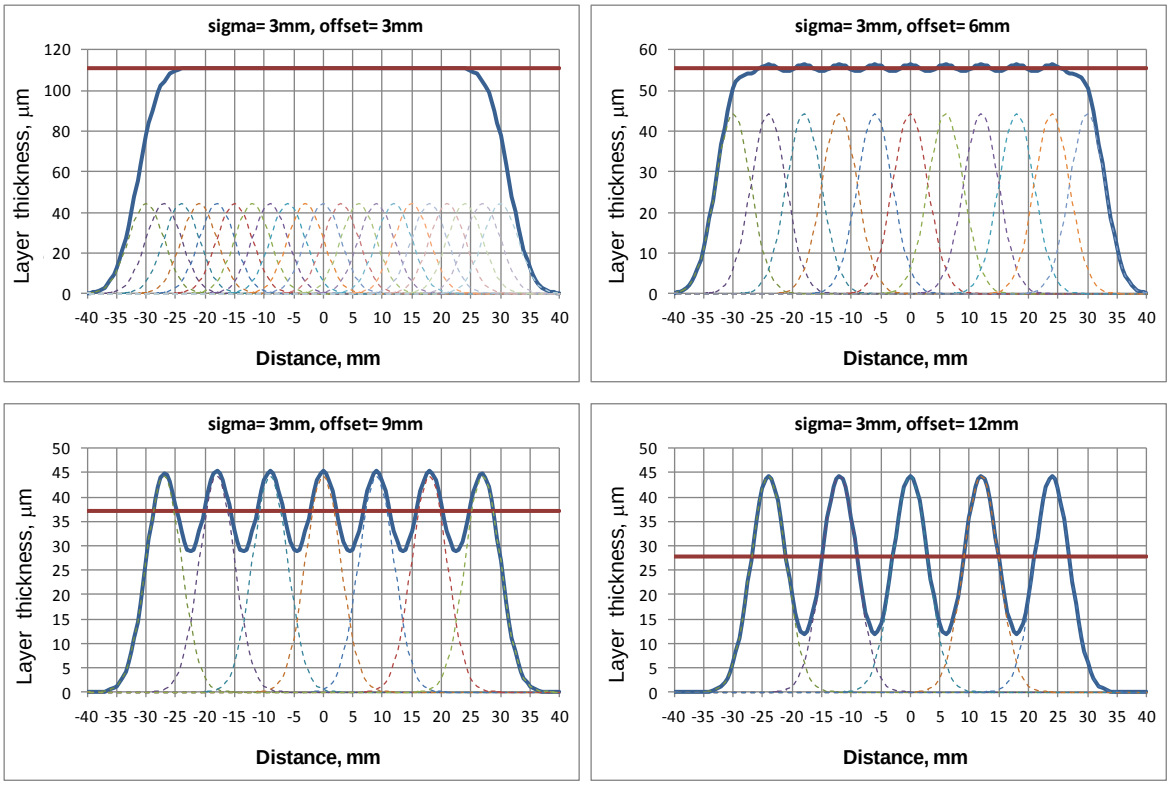

Figure 4.5: Accumulation of the total layer thickness of the coating by the application of single spray profiles with different path offsets.

The requirement $N \to \infty$ represents a good approximation of the real cases, when the width of meander spray pattern is large enough to avoid an influence of the profiles applied at the edges of the pattern on the coating thickness at the substrate. In this case the coating pattern can be represented by the periodical structure with a period p. Average value of thickness over the period p can be calculated as:

$$\bar{h}_{layer} = \frac{1}{p}\int_0^p h_{layer}(\eta, p, \sigma) = \frac{A\dot{M}}{\sqrt{2\pi}\rho_{coat} v \sigma_{eff}} \frac{1}{p} \sum_{n=-\infty}^{\infty} \int_0^p \exp\left(-\frac{(\eta - p\cdot n)^2}{2\sigma_{eff}^2}\right) d\eta . \qquad (4.16)$$

Due to the periodical behavior of the layer thickness distribution, we can perform the following transformation in the last integral:

$$\bar{h}_{layer} = \frac{A\dot{M}}{\sqrt{2\pi}\rho_{coat} v \sigma_{eff}} \frac{1}{p} \sum_{n=-\infty}^{\infty} \int_{(n-1)p}^{np} e^{-\frac{y^2}{2\sigma_{eff}^2}} dy = \frac{A\dot{M}}{\sqrt{2\pi}\rho_{coat} v \sigma_{eff}} \frac{1}{p} \int_{-\infty}^{\infty} e^{-\frac{y^2}{2\sigma_{eff}^2}} dy . \qquad (4.17)$$

The last expression represents the known Gaussian integral. Thus performing integration in (4.17) we have the following expression for the average layer thickness:

$$\bar{h}_{layer} = \frac{A\dot{M}}{\rho_{coat}} \frac{1}{vp} . \qquad (4.18)$$

The solution (4.18) shows that the layer thickness is inversely proportional to gun speed v and path offset p, and does not depend on the direction of gun motion α. Furthermore, the layer thickness is independent of the geometry and dimensions of the spray profile defined by σ_{eff} and consequently independent of the spray spot geometry characterized by standard deviations σ_x and σ_y. The layer thickness is defined for a coating with a given density ρ_{coat} only by coating mass transport parameters such as feed rate $\dot{M}$, deposition efficiency A and cinematic parameters defining the spray gun motion, such as gun speed v and path offset p. This is an important result, what makes possible an efficient method to predict coating thickness by a relatively simple calculation with an input of well determined spray process parameters.

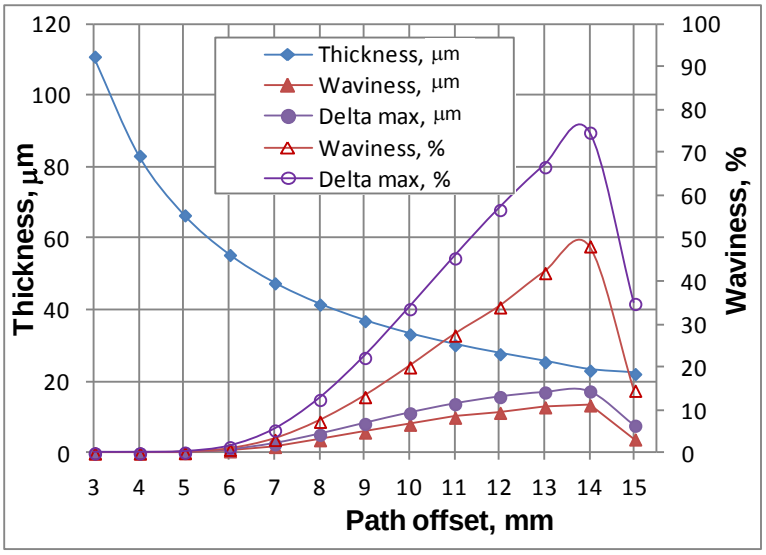

Figure 4.6: Dependence of layer thickness and waviness on the path offset.

Coating waviness Σ can be defined as averaged squares of differences between the actual h_{layer} and average thickness $\bar{h}_{layer}$ values as:

$$\Sigma^2(p,\sigma) = \frac{1}{p}\int_0^p (h_{layer} - \bar{h}_{layer})^2 d\eta \,. \qquad (4.19)$$

According to the relations (4.15) and (4.19), we can calculate coating surface waviness as:

$$\Sigma^2(p,\sigma) = \bar{h}_{layer}^2 \frac{1}{p}\int_0^p \left[\frac{p}{\sqrt{2\pi}\sigma_{eff}} \sum_{n=-\infty}^{\infty} \exp\left(-\frac{(\eta - p\cdot n)^2}{2\sigma_{eff}^2} \right) - 1 \right]^2 d\eta \,. \qquad (4.20)$$

Figure 4.6 shows the dependence of the layer thickness and macroscopic waviness on the path offset. The macroscopic waviness is nearly equal to zero up to a certain path offset value which is in the range $1\sigma_{eff} < p < 2\sigma_{eff}$. The relative waviness $\Sigma(p,\sigma)/\bar{h}_{layer}$ increases monotonously with increasing path offset up to a certain value. The average thickness decreases monotonously with the path offset even for quite large offset values. Practically a sufficiently small offset $p \approx \sigma_{eff}$ must be chosen to provide uniform layer thickness, avoiding the appearance of macroscopic coating waviness.

4.3 Calculation of coating thickness for cylindrical substrate

For practical application, in addition to the case of coating on a flat substrate, it is important to consider another principal case of coating deposited onto the cylindrical sample. In this case the coating can be applied with two strategies: deposition onto rotating cylinder from the gun placed in a fixed position and deposition by gun motion along the longitudinal axis of the cylinder. Let us find an analytical solution for the coating thickness distribution applied in the second case onto the fixed cylindrical substrate. In this case total thickness of the coating layer is accumulated by a superposition of the spray profiles produced by gun motion. Let us assume that a cylinder with a curvature radius R is coated by the selected number N of the gun paths, performed at a speed v and displaced with a path offset p. It should be mentioned that in order to produce a uniform or symmetrical thickness distribution on a cylinder, the paths must be symmetrically distributed along the cylinder circumference. In this case, the path offset and the number of paths cannot be chosen independently and must meet the following requirement:

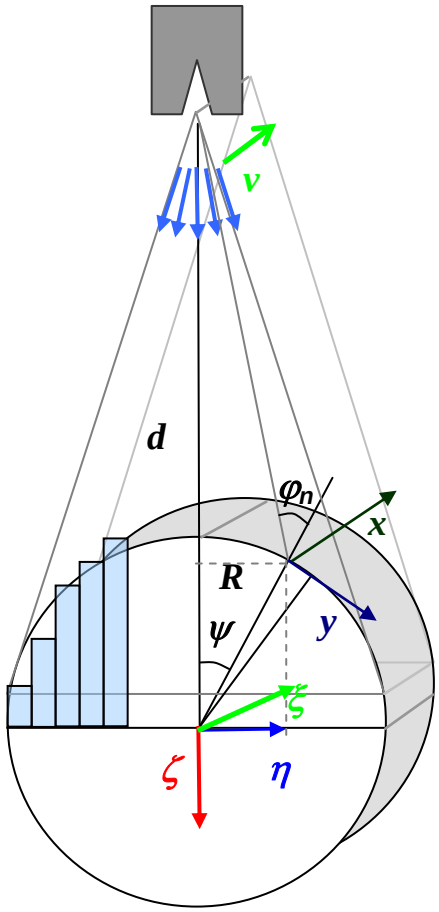

Figure 4.7: Geometry of the cylindrical sample.

$$N \cdot p = 2\pi R. \tag{4.21}$$

During spraying of a cylinder by contrast to a flat surface, the spray jet meets the surface with variable spray angles which vary in the range of $0° < \varphi < 90°$. Let us describe a linear motion of the spray gun along the symmetry axis of the cylinder which coincides with the ξ axis of the rectangular coordinate system $\{\xi, \eta, \zeta\}$. The η axis is aligned perpendicularly to the direction of gun motion and coincides with the diameter of the cylinder as shown in Figure 4.7. Furthermore, let us introduce a local coordinate system $\{x, y, z\}$, which is defined at each angular position ψ. Where the z axis is aligned with the surface normal, x is aligned along the symmetry axis of the cylinder and y is aligned along the tangent to the surface corresponding to the angular position ψ. In this coordinate system, each point on the

substrate surface can be described by an angular position with an angle ψ measured between the central axis of the spray fan and the surface normal. For each angular position ψ, a spray angle φ_n can be defined using geometric considerations in the following form:

$$\cos\varphi_n = -\frac{(1-\cos\psi)R^2 - dR\cos\psi}{R\sqrt{R^2 + (d+R)^2 - 2(d+R)R\cos\psi}}. \tag{4.22}$$

The angle ψ varies in the range of $-\psi_m < \psi < \psi_m$, where ψ_m denotes a critical angle corresponding to spraying along the tangential axis of the surface with zero spray angle. The critical angle can be calculated from the following relation:

$$\cos\psi_m = R/(d+R). \tag{4.23}$$

Let us consider a single spray path applied along the symmetry axis of the cylindrical substrate by a gun placed at a certain distance d from the cylinder surface. The thickness distribution in a spray profile is described by the equation (4.8) and can be written in the chosen coordinate system as:

$$h_{profile}(\varphi) = \frac{A(\varphi, d)\cdot\dot{M}}{\sqrt{2\pi}\rho_{coat}v\sigma_{eff}}\exp\left(-\frac{\eta(\varphi)^2}{2\sigma_{eff}^2}\right)\frac{d\xi d\eta}{dxdy}. \tag{4.24}$$

The term $d\xi d\eta / dxdy$, as in the case of description of the spray spot on the inclined surface by the expression (3.29), is included to consider the ratio of the area elements on the reference and substrate surfaces. Taking into account geometry relation $dy = Rd\psi$ and equality of x and ξ coordinates we can write:

$$d\xi = dx,$$
$$d\eta = dy\cos\psi. \tag{4.25}$$

Taking into account (4.25) and dependence of deposition efficiency on spray angle we have:

$$h_{profile} = \frac{A_0\dot{M}}{\sqrt{2\pi}\rho_{coat}v\sigma_{eff}}\cos^m\varphi\cdot\cos\psi\cdot\exp\left(-\frac{R^2\sin^2\psi}{2\sigma_{eff}^2}\right). \tag{4.26}$$

Let us consider spraying of a continuous coating layer onto the whole substrate surface by application of a number N of paths displaced by a path offset p. In this case the coating layer thickness can be calculated by a superposition of the spray profiles produced by corresponding spray paths:

$$h_{layer} = \frac{A_0\dot{M}}{\sqrt{2\pi}\rho_{coat}v\sigma_{eff}}\sum_{i=0}^{N-1}\cos^m\varphi_i(\psi_i)\cos(\psi_i - \psi_{i0})\cdot\exp\left(-\frac{R^2}{2\sigma_{eff}^2}\sin^2(\psi_i - \psi_{i0})\right). \tag{4.27}$$

where $\psi_{0i} = 2\pi\cdot i/N$ and $N = 2\pi R/p$.

The angle φ_i is calculated for each individual path i according to the equation (4.22). The result of numerical calculation of the coating thickness distribution on the cylindrical sample is presented in Figure 4.8. This result is obtained with the help of the corresponding Visual Basic programming routine and visualization with Excel tools.

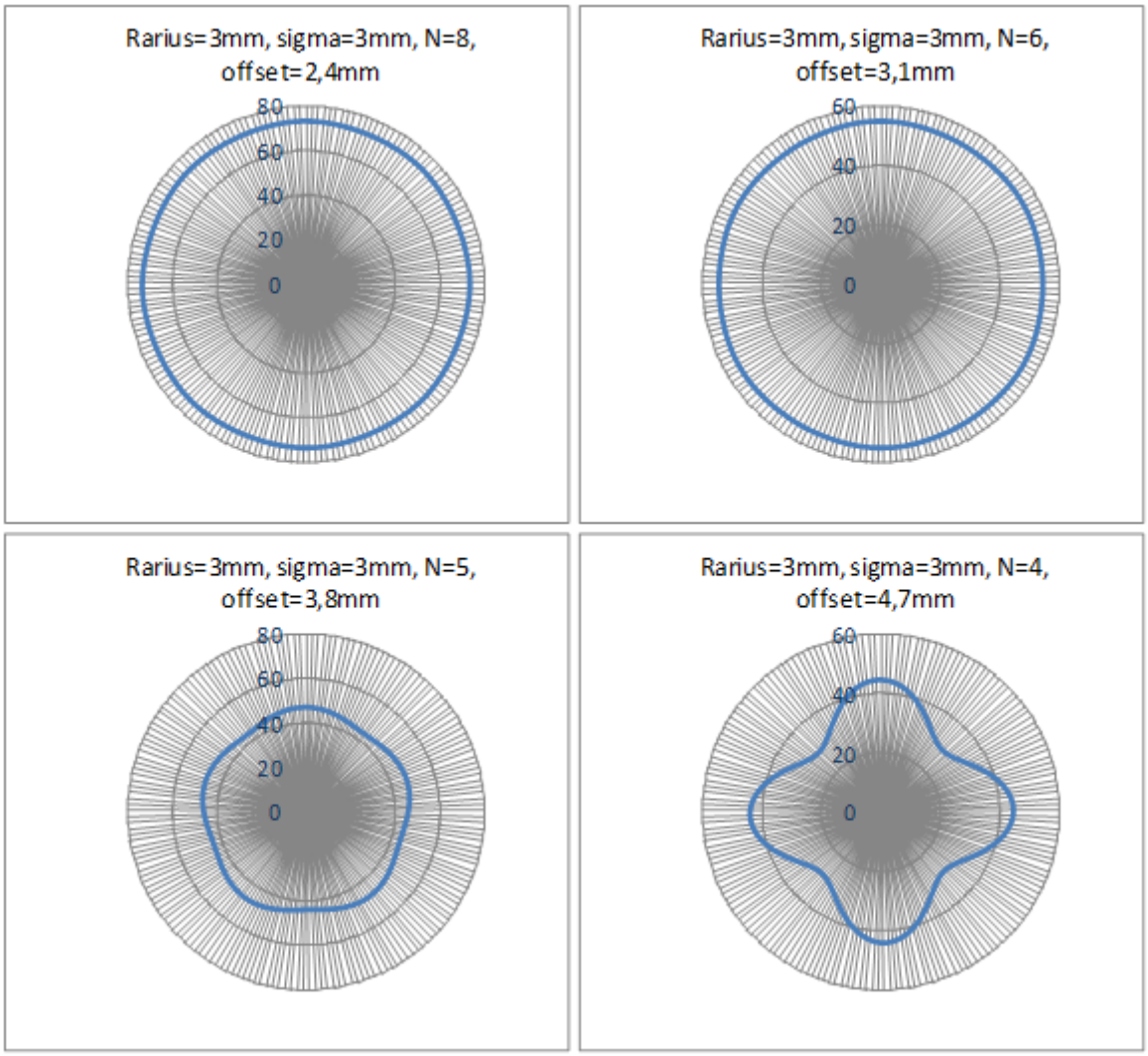

Figure 4.8: Accumulation of the total layer thickness of the coating by the application of single spray profiles with different paths offsets onto the cylinder sample.

As can be seen from this calculation, for a sufficiently small path offset and a sufficiently large number of spray paths, coating thickness distribution becomes uniform. With fewer paths and a corresponding increase in the path offset, coating waviness appears. It should be mentioned that the waviness level for the cylindrical substrate is higher than the corresponding waviness on the flat substrate for the same path offset (see Figure 4.5). Furthermore, the waviness appears at smaller offsets for the cylindrical substrate. This effect is a result of the substrate curvature. In order to quantify the effect of the spray path

parameters, path offset and curvature radius on the coating thickness on the cylindrical substrate, let us calculate analytically the average thickness for relatively small substrates.

Let us consider for the future a practical case where the curvature radius is much smaller than the spray distance *R<<d.* In this case, the relations (4.22) and (4.23) lead to the simple expressions for the inclination and critical angles:

$$\varphi = \psi \text{ and } \psi_m = \pi/2 . \tag{4.28}$$

The contribution of every single spray profile to the average thickness of the layer, taking into account (4.26), can be calculated as:

$$\bar{h}_{profile}^{cylinder} = \frac{A_0 \dot{M}}{\sqrt{2\pi}\rho_{coat} v \sigma_{eff}} \frac{1}{2\pi} \int_{-\pi/2}^{\pi/2} \cos^{m+1}\psi \cdot \exp\left(-\frac{R^2 \sin^2\psi}{2\sigma_{eff}^2}\right) d\psi . \tag{4.29}$$

For the selected number of spray paths we can calculate average layer thickness as a sum of the average thicknesses provided by each single spray path:

$$\bar{h}_{layer}^{cylinder} = \frac{A_0 \dot{M}}{\sqrt{2\pi}\rho_{coat} v \sigma_{eff}} \frac{1}{2\pi} N \int_{-\pi/2}^{\pi/2} \cos^{m+1}\psi \cdot \exp\left(-\frac{R^2 \sin^2\psi}{2\sigma_{eff}^2}\right) d\psi . \tag{4.30}$$

Taking into account the relation between number of paths and path offset (4.22), we have:

$$\bar{h}_{layer}^{cylinder} = \frac{A_0 \dot{M}}{\sqrt{2\pi}\rho_{coat} v \sigma_{eff}} \frac{R}{p} \int_{-\pi/2}^{\pi/2} \cos^{m+1}\psi \cdot \exp\left(-\frac{R^2 \sin^2\psi}{2\sigma_{eff}^2}\right) d\psi . \tag{4.31}$$

It should be mentioned that according to the relation (4.18), the first factor in the expression (4.31) refers to a coating thickness on the flat substrate. Hence we can finally write:

$$\bar{h}_{layer}^{cylinder} = \bar{h}_{layer}^{flat} \frac{1}{\sqrt{2\pi}} \frac{R}{\sigma_{eff}} \int_{-\pi/2}^{\pi/2} \cos^{m+1}\psi \cdot \exp\left(-\frac{R^2 \sin^2\psi}{2\sigma_{eff}^2}\right) d\psi . \tag{4.32}$$

It can be seen that the coating thickness on the cylindrical substrate depends only on the baseline thickness $\bar{h}_{layer}^{flat}$ on the flat substrate and on the dimensionless factor R/σ_{eff}, which defines a ratio of curvature radius to the profile standard deviation. Furthermore, the dependence on the factor m in this expression reflects the dependence of the deposition efficiency on the spray angle for a particular spray process.

Dependence of the layer thickness on the ratio of substrate radius to the effective standard deviation calculated according to the equation (4.32) is plotted in Figure 4.9.

As can be seen from the curve, the coating thickness on the cylindrical substrate increases from very low values for a small curvature radius up to the saturation value of the thickness on the flat substrate for enough high curvature radius R in comparison with the standard

deviation σ_{eff} . Physically, the effect of a reduction of the layer thickness with a decrease in the substrate radius is explained in the model by the decrease of the total amount of powder which is deposited onto the narrow substrate in comparison with corresponding virtually infinite flat substrate. Furthermore, a deviation of spray angle from 90° in the centre down to 0° at the edges of the substrate lowers thickness of the coating layer due to reduction of the effective deposition efficiency.

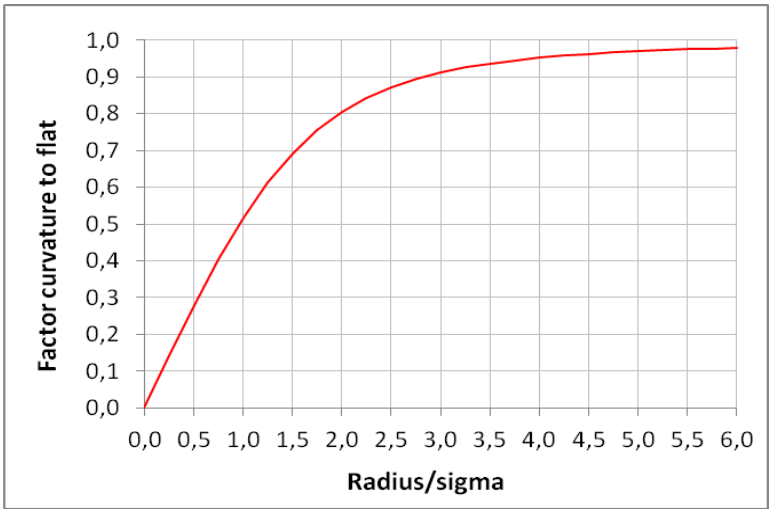

Figure 4.9: Dependence of the ratio of thicknesses on curvature and flat substrate on radius to sigma ratio.

4.4 Coating thickness simulation for arbitrary free-form surfaces

Simulation of the coating thickness distribution on a free-form substrate surface requires numerical computational methods. One of the most important tasks of this simulation is a realistic prediction of the resulting coating thickness on a substrate surface produced by a motion of the spray gun over a certain known trajectory at a known speed. The gun trajectory has to be developed to achieve a complete substrate surface coverage with a coating. A further task of the simulation is to provide guidelines for the subsequent optimization of the gun trajectory to achieve a uniform coating thickness distribution on the substrate. In order to be able to perform both these tasks, an accurate model of the spray spot pattern represents a necessary requirement. Any possible coating pattern produced by a motion of the spray gun is a result of the motion of the spray spot on the substrate surface. Analogously to painting, the spray spot acts as a paintbrush for thermal spraying. The equation (3.28) can be used to describe accurately the spray spot produced by a spray gun with a single injector. The equation (3.45) has to be considered to describe a spray process with multiple injectors by superposition of corresponding single spray spots produced by each injector. The coating pattern produced by the motion of the spray gun can be calculated as an integral along the trajectory of the spray spot at the surface:

$$h(\vec{r}) = \int_0^t \dot{h}(\vec{r} - \vec{r}_0(t))dt \cdot \qquad (4.33)$$

Here we introduce a local thickness growth rate function $\dot{h}_{spot} = \partial h_{spot} / \partial t$, defining an increase of thickness per time unit at the selected point. Based on the expression (3.28) and taking into account (3.15), this function can be written in the following form:

$$\dot{h}(x,y,z,t) = \frac{A(x_{ref}, y_{ref}, z_{ref}, t)\dot{M}}{2\pi\sigma_x\sigma_y\rho_{coat}} \exp\left(-\frac{((x_{ref} - x_0)\cos\alpha_0 + (y_{ref} - y_0)\sin\alpha_0)^2}{2\sigma_x^2(z_{ref})} \right.$$

$$\left. -\frac{(-(x_{ref} - x_0)\sin\alpha_0 + (y_{ref} - y_0)\cos\alpha_0)^2}{2\sigma_y^2(z_{ref})} \right) \frac{dx_{ref}\,dy_{ref}}{dxdy} . \qquad (4.34)$$

This function is defined and can be considered as known in the reference coordinate system $\{x_{ref}, y_{ref}, z_{ref}\}$, which is connected to the spray gun. Corresponding coordinates of the substrate surface points $(x_{ref}, y_{ref}, z_{ref})$ represent relative values in relation to the spray gun. It should be mentioned that the reference coordinate system continuously moves according to the motion of the spray gun. Definition of the absolute values of these coordinates requires defining of the spray gun's current position, and of the point of intersection of the spray jet and the surface at any moment in time. This definition can be done by the introduction of vectors $\vec{r}_{gun}$ and $\vec{r}_{sur}$. As follows from geometric considerations presented in Figure 4.10, the coordinates of the surface point in the reference coordinate system can be found from the following relation:

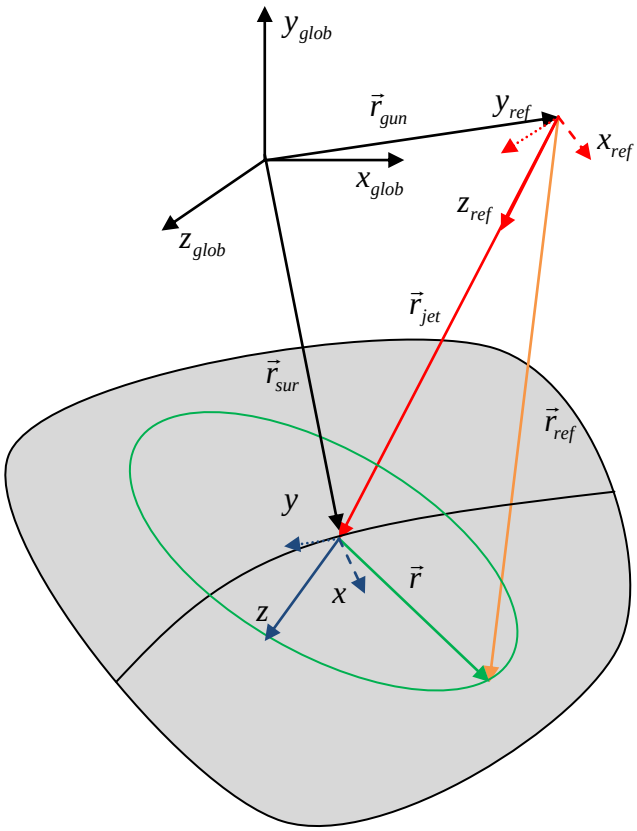

Figure 4.10: Definition of coordinates for arbitrary curvature surface.

$$\vec{r}_{ref} = \vec{r}_{sur} - \vec{r}_{gun} + \vec{r} = \vec{r}_{jet} + \vec{r} . \qquad (4.35)$$

It can be seen that the vector $\vec{r}_{sur} - \vec{r}_{gun} = \vec{r}_{jet}$ defines a radius vector of the spray jet which characterizes a distance from the substrate surface and spatial orientation of the spray jet. The vector $\vec{r}$ describes a distance from the center of the spray spot to the surface points. The motion of the spray gun and corresponding motion of the spray spot at the substrate

surface must be set as kinematic time dependences in any unmoved global coordinate system $\{x_{glob}, y_{glob}, z_{glob}\}$:

$$\vec{r}_{gun} = \vec{r}_{gun}(x_{glob}(t), y_{glob}(t), z_{glob}(t)) \text{ and}$$
$$\vec{r}_{sur} = \vec{r}_{sur}(x_{glob}(t), y_{glob}(t), z_{glob}(t)). \quad (4.36)$$

The dependence of the radius vector of the spray gun on time can be obtained by setting of the spray gun speed in a global coordinate system:

$$\dot{\vec{r}}_{gun} = \vec{v}_{gun}(t). \quad (4.37)$$

The coordinates of the center of the spray spot can be determined by setting the spray distance and orientation angles of the spray jet in the selected coordinate system. Similarly to the case of the flat tilted substrate surface in Chapter 3.3, let us introduce a local coordinate system $\{x, y, z\}$ related to the substrate surface with a center placed at the point of intersection of the spray jet axis with the substrate. The z axis is aligned along the inner normal to the surface, and the x and y axes lie in the tangent plane. Let us set at any point during the spray gun motion a value of the spray distance d:

$$\left|\vec{r}_{jet}\right| = d. \quad (4.38)$$

Furthermore, let us introduce a spray angle φ as an angle between the spray jet axis $\vec{r}_{jet}$ and the surface normal z:

$$\frac{\vec{r}_{jet}}{\left|\vec{r}_{jet}\right|} \cdot \vec{e}_z = \cos\varphi, \quad (4.39)$$

The orientation of the spray jet tilt can be set as an angle θ between the projection of the spray jet onto the tangent plane and the x axis of the selected coordinate system. This requirement can be written in the following vector form:

$$\frac{\vec{r}_{jet} - (\vec{r}_{jet} \cdot \vec{e}_z)\vec{e}_z}{\left|\vec{r}_{jet} - (\vec{r}_{jet} \cdot \vec{e}_z)\vec{e}_z\right|} \cdot \vec{e}_x = \cos\theta, \quad (4.40)$$

In the case of a flat substrate, these equations make it possible to obtain explicit relations which connect the coordinates at the surface and the reference coordinates in the form (3.27). In a general case, the position and orientation of the coordinate system $\{x, y, z\}$ depend on the local geometry of the substrate at the point of intersection with the spray jet axis and must be calculated for each position of the spray gun at any time moment. Solution of equations (4.38)-(4.40) in combination with (4.37), according to the relation (4.36), makes it possible to define coordinates of each affected point of the surface in the reference coordinate system $\{x_{ref}, y_{ref}, z_{ref}\}$ as a function of local coordinates $\{x, y, z\}$ at the surface at

any moment of time. Using these coordinates, the coating thickness growth rate can be determined explicitly using the relation (4.34). It should be mentioned that the Jacobian $dx_{ref}\,dy_{ref} / dxdy$ in (4.34) defines a rate of element areas of the substrate surface in relation to a corresponding elementary area of the reference plane. Their values are to be calculated at any point of the substrate surface affected by the spray cone. These values depend on the tilt of the spray jet axis to the local orientation of the surface normal and surface curvature. The deposition efficiency $A(\varphi_n(x,y,z,t), d(x,y,z,t))$ represents a local value which depends on local spray angle and distance, and must be calculated at any affected substrate surface point. Performing calculations (4.35)-(4.40) with subsequent calculation of thickness growth rate in (4.34) allows numerical integration to be performed and to calculate the total coating thickness distribution on the component surface.

An analytical solution is possible for the case of a flat substrate, which was discussed in Chapter 3.3. In a general case, numerical methods are needed to solve corresponding equations systems and perform calculations in (3.34). Use of the software tools which are able to perform numerical integration makes it possible to calculate the accumulation of the thickness on the substrate surface for particular components. In particular, continuous motion of the gun is modeled as a sequence of the gun positions captured at some selected time interval Δt. The substrate surface must be discretized. The finite element (FEM) approaches can be applied to the generation of the surface mesh with discrete nodes where the values of coating thickness are calculated. The thickness values between the nodes of the mesh can be interpolated by polynomial functions. An example of the surface mesh generated by RobCad software is presented in Figure 4.11. The time interval and the mesh spacing affect both the simulation of the motion and also the calculation of the coating thickness. They must be selected sufficiently small to simulate continuous deposition of coating but at the same time sufficiently large for numerical calculation to be performed within reasonable computing time.

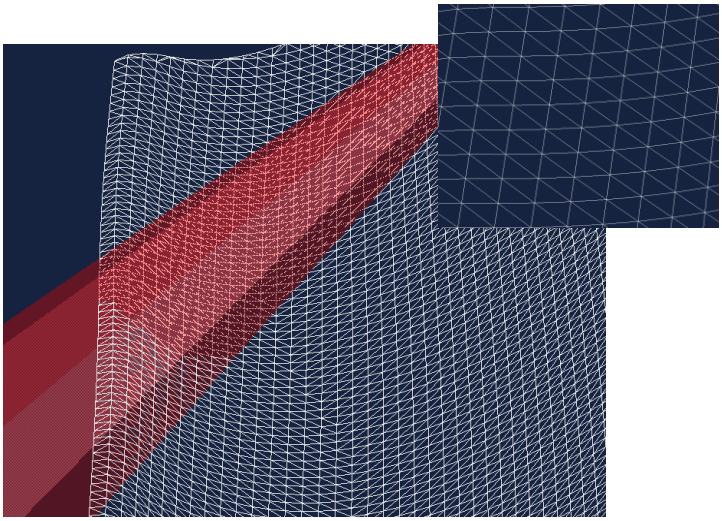

Figure 4.11: Example of surface discretization to simulate coating thickness in RobCad.

5 Experimental evaluation of process parameters and model verification

The considerations and equations presented in Chapters 3 and 4 represent a self-consistent model to simulate a thickness distribution in various coating patterns. In order to apply this model to a particular spray process, it is necessary to provide an input of the deposition efficiency and geometry parameters of the basic coating pattern. These parameters can be obtained by analysis of the spray spot or series of spray profiles.

Thickness distribution in the spray spot depends on a number of model parameters. The first group of these parameters is process variables. These are powder feed rate $\dot{M}$, spray distance d and orientation angles φ and θ, which are known variables of the process. The second group of these parameters characterizes geometry of the spray spot. These parameters are the nominal deposition efficiency A_0, standard deviations of thickness along the main axes σ_x and σ_y, displacements x_0, y_0 and angle of rotation of the single spray spot α_0 in the reference coordinate system. These characteristics represent unknown variables which will be determined by analysis of the spray spot or series of profiles deposited under nominal spraying conditions. The third group contains parameters m and p, which describe model dependences of the deposition efficiency on the spray angle and the spray distance respectively. An angle of the spray cone divergence γ belongs to this group. These parameters need either a geometric estimation or experimental input.

In this chapter, the methods to provide an input of these unknown parameters of the model will be discussed. Furthermore, model verification by comparison of the prediction results with corresponding experimental data for complete coating patterns will be done.

5.1 Experimental setup to deposit spray spot and profile

In order to investigate parameters of basic coating patterns, experiments to apply spray spots and profiles were performed at the Siemens TACR coating facility. In these experiments, the coating patterns produced by spraying ceramic 8YSZ powder using the APS process were studied and evaluated. The spraying was performed with an F4 spray gun from Sulzer Metco. The gun was attached to the six-axis industrial robot from ABB. The flat plates made of stainless steel with dimensions of 100x80mm and 2 mm thickness were used to deposit spray spots, profiles and complete coating layers. The test plates were grit blasted with silicon carbide grit prior to coating deposition to achieve sufficient coating bonding. The

coating deposition was performed under the nominal conditions, keeping constant values of process parameters. The spray gun settings: powder feed rates of single or double injector lines, flow rates of primary (Ar), secondary (H_2) gases and carrier (Ar) gases, torch current *I* and power *W* were maintained constant and equal to their nominal values during the whole experiment series. The 8%wt. Y_2O_3-ZrO_2 powder of 204NS type from Sulzer Metco was used as a feedstock coating material in the tests.

The spray spots were deposited from the stationary position of the spray gun placed at a nominal distance from the substrate with a perpendicular orientation of the spray gun to the substrate surface. The spray gun was moved by the robot manipulator from an initial position outside the substrate to the center point of the upper 80x80mm area of the substrate as shown in Figure 5.1. The spraying to produce a spray spot was performed during a time interval Δt of 2 seconds. After this, the spray gun was moved back to the initial position. Three spray profiles were deposited on the flat plates by the linear motion of the spray gun at a constant speed vertically, horizontally and tilted under 45°. The gun speed was set equal to the nominal value and was not changed during the tests. The number of spray program repetitions was set to achieve measurable thicknesses for all spray profiles. Deposition of the coating layers was done with a raster motion of the spray gun over the flat substrates with a constant distance between parallel paths characterized by the path offset. The return points for the spray gun were placed far enough away from the substrates to ensure constant gun speed during motion over the substrate. The programming of the robot and positioning of the spray gun was performed with OLP method, with Robcad Technomatics software from Siemens PLM. Substantial details of the corresponding robot programming with OLP are discussed in Chapter 6. The positioning of the spray gun tool central point (TCP) was checked in a dry run without plasma injection with a laser pointer attached to the spray gun. Two powder injectors were mounted onto the spray gun to evaluate single and double configurations of powder injection. The orientation of the gun and injectors used in the tests in relation to the flat substrate are shown in Figure 5.1. Depending on the type of injection only one top injector or both injectors were activated for powder feeding.

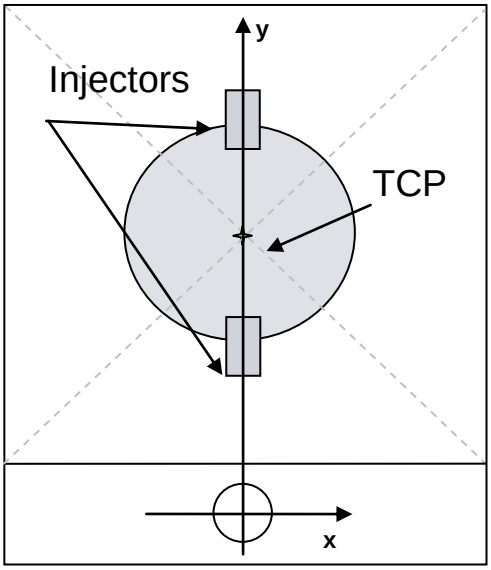

Figure 5.1: Orientation of spray gun in respect to test plate.

Table 5.1: Test plan for evaluation of spray pattern characteristics and model verification

Sample	Pattern	Injection	Total feedrate, g/s	Speed, mm/s	Distance, mm	Spray angle, dgr
s1	spot	single	nom		nom	90
s2	spot	double	2 × nom		nom	90
p1.1	4-profiles	single	nom	nom	nom	90
p1.2	4-profiles	single	nom	nom	nom	80
p1.3	4-profiles	single	nom	nom	nom	70
p1.4	4-profiles	single	nom	nom	nom	60
p1.5	4-profiles	single	nom	nom	nom	50
p1.6	4-profiles	single	nom	nom	nom	40
p1.7	4-profiles	single	nom	nom	nom	30
p1.8	4-profiles	single	nom	nom	nom-40	90
p1.9	4-profiles	single	nom	nom	nom-20	90
p1.10	4-profiles	single	nom	nom	nom+20	90
p1.11	4-profiles	single	nom	nom	nom+40	90
p2.1	4-profiles	double	2 × nom	nom	nom	90
l1	compl. layer	single	nom	nom	nom	90
l2	compl. layer	single	nom	nom	nom	70
l3	compl. layer	single	nom	nom	nom	50
l4	compl. layer	single	nom	nom	nom	30
l5	compl. layer	single	nom	nom	nom-40	90
l6	compl. layer	single	nom	nom	nom+40	90
c1	cylinder d1=10mm	single	nom	nom	nom	90
c2	cylinder d2=15mm	single	nom	nom	nom	90
c3	cylinder d3=30mm	single	nom	nom	nom	90

For the visualization of sprayed coating patterns the photos of the spray spot, profiles and complete coated layer (s1, p.1.1 and l1) from Table 5.1 are presented in Figure 5.2. Here the positions to evaluate thickness distributions are shown by the marker.

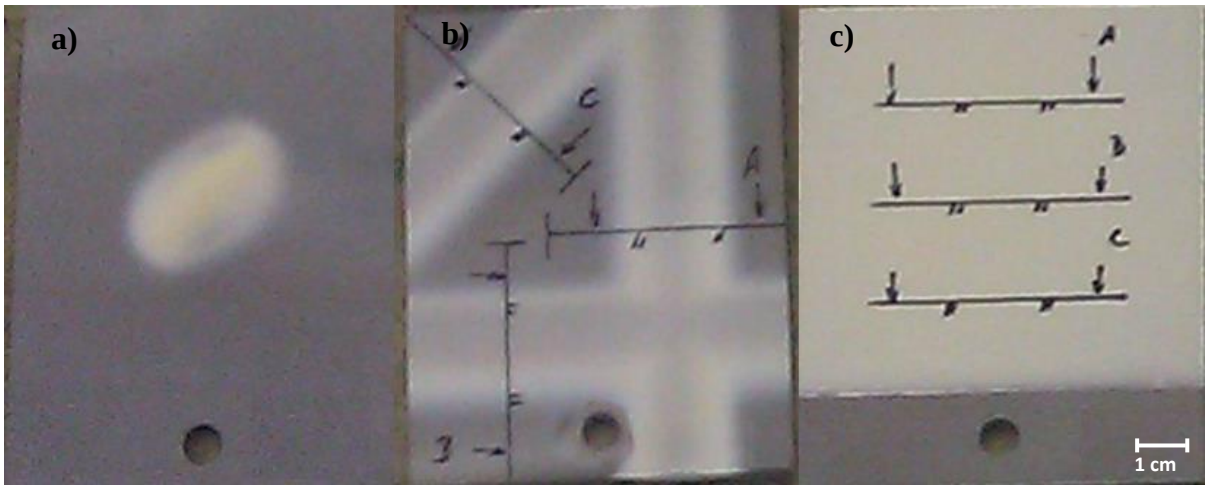

Figure 5.2: Photos of spray patterns: a) single spray spot, b) horizontal, vertical and tilted spray profiles, c) complete coating layer.

5.2 Measurement and characterization of the spray spot and profile

Different methods can be used for the investigation of the macroscopic geometry of the spray pattern deposited. In particular, these methods are optical or tactile profilometry and metallographic cross sectioning. All of these methods have their own advantages and disadvantages. The major advantage of the profilometry methods is an ability to capture three-dimensional structure of the coating pattern. The disadvantage of these methods is caused by the need to keep the substrate surface unchanged before and after the measurement procedure. This is difficult enough in practice due to the occurrence of distortion and bending of the substrates caused by inhomogeneous heating and cooling of the substrate during the spray process. A complex and insufficiently accurate procedure for the mathematical calculation of substrate curvature is typically used to take into account the effect of substrate distortion on the measured coating pattern shape. The metallographic cross sectioning, which is a commonly used and well established method to investigate micro and macro structure of the thermal spray coatings, overcomes this difficulty. This method enables direct visual measurements with a microscope of coating thickness at multiple points of the coated substrate. The local measurements on a two-dimensional section of the coating pattern make this method inapplicable for evaluation of the 3D spray spot pattern. On the other hand, metallography is well applicable to measuring thickness distribution in a 2D profile. In particular, a metallographic sectioning across the profile length makes possible a measurement of thicknesses with some selected spatial step and makes it possible to capture thickness distribution in the spray profile pattern. Furthermore, as discussed in Chapter 1.2.4, metallography is a well established method to evaluate thickness and microstructure of the complete coating layer. Hence it is advantageous to use the same method to gain the model data from the profiles, to calculate and predict layer coating thickness, which is evaluated by metallographic techniques.

In order to establish thickness distributions resulting from the measured thickness values, the mathematical reverse solution method was applied. In this method, a thickness distribution in the basic spray spot and profile patterns is described by an equation which depends on a selected number of initially unknown model variables. The values of these variables are found by the requirement of minimization of deviations for experimental and model thickness values at the measurement points. These variables represent a complete set of physical values which characterize the spray spot. A corresponding parametric model is used further to describe the nominal condition of the spray spot and to acquire the experimental data to verify the equations, reflecting changes of the spray spot geometry with variation of the spraying conditions.

5.3 Mathematical approach for definition of model parameters by inverse problem solution

Thickness distribution in the spray spot is characterized by a complete set of model parameters, represented by the nominal deposition efficiency A, standard deviations of thickness along the main axes σ_x and σ_y, displacements x_0, y_0 and angle of rotation of the single spray spot α_0 in the reference coordinate system. The definition of these characteristics can be done with the method of inverse problem solution. In this method these variables represent unknown variables of the model. Their values are to be found to satisfy the requirement of the best fit to the measurement result. Parametric dependence of thickness distribution in the spot on the process variables set $\{A_0, x_0, y_0, \sigma_x, \sigma_y, \alpha_0\}$ is described by the equation (3.49). For a particular coating pattern, this equation is a functional dependence on the model parameters and coordinates of measurement points $\{x_i, y_i\}$:

$$h = h(x_i, y_i, A_0, x_0, y_0, \sigma_x, \sigma_y, \alpha_0). \tag{5.1}$$

Here index i refers a number of the measurement point. The solution for the model parameters to fulfill the requirement of the best fit to the experimental result can be mathematically formulated to find the model parameters set which minimize a standard deviation of the experimental and model results. This will minimize following objective function:

$$F = \frac{1}{2}\sum_{i=1}^{N}\left(h(x_i, y_i, h_0, x_0, y_0, \sigma_x, \sigma_y, \alpha_0) - h_i\right)^2 -> \min. \tag{5.2}$$

Here h_i is a single thickness measurement result at a point with the number i and N is the total number of measurement points. A necessary condition to achieve a local minimum of the objective function $F(A_0, x_0, y_0, \sigma_x, \sigma_y, \alpha_0)$ is simultaneous equality to zero of partial derivatives with respect to each model variable. Let us introduce a vector of the unknown model variables in the form:

$$p_k = (A_0, x_0, y_0, \sigma_x, \sigma_y, \alpha_0). \tag{5.3}$$

The requirement of the local minimum of the objective function $F(p_k)$ we can write as:

$$\frac{\partial F}{\partial p_k} = \sum_{i=1}^{N}\left(h(x_i, y_i) - h_i\right)\frac{\partial h(x_i, y_i)}{\partial p_k} = 0 \quad . \tag{5.4}$$

The equations (5.4) represent a system of nonlinear algebraic equations. These equations, taking into account (3.49), in an explicit form cannot be solved with analytic methods. Due to this fact, numerical methods must be applied for their effective solution. There are various

methods developed to solve the systems of nonlinear equations and finding of local extremes of functions of multiple variables. Some applications of numerical methods to solve a numerical minimization problem are discussed in [59]. In this paper, the gradient descent method was utilized for the solution of the system (5.4). This is a relatively simple but adequately effective iterative method. The gradient descent method is based on the fact that the objective function of multiple variables approaches a local minimum, and at the same time fulfills requirements (5.4), in the direction of negative gradient of the objective function.

At the first iteration, an initial vector $p_k^{(0)}$ of the system variables is taken as a first assumption for the solution of the equations system. At any subsequent iteration, the next approach to the system solution is calculated along the gradient of the target function according to the following equation:

$$p_k^{(m+1)} = p_k^{(m)} - \lambda_k \frac{\partial F^{(m)}}{\partial p_k}. \tag{5.5}$$

Here m is a number of the iteration. The sequence of vectors $p_k^{(m)}$ converges to the local minimum of the target function. In order to achieve a convergence of the solution, the parameters λ_k must be properly chosen. In particular, the values of λ_k must be small enough to ensure smooth convergence but at the same time large enough to achieve the local minimum of the function within a reasonable number of iterations. For the practical realization of the numerical solution, the derivatives of the coating thickness in (5.4) were substituted by their finite differences at each iteration step:

$$\frac{\partial h}{\partial p_k} = \frac{h(p_k + \Delta p_k) - h(p_k)}{\Delta p_k}. \tag{5.6}$$

The increments of the arguments Δp_k were chosen as small enough constant values which ensure satisfactory accuracy of calculation of the corresponding derivatives. The iterative sequence was stopped if the variables vector after certain number if iterations do not change considerably. This criterion of achievement of iterative solution convergence can be written in the following form:

$$\left| p_k^{(m+1)} - p_k^{(m)} \right| < \delta_k. \tag{5.7}$$

Here δ_k are allowable uncertainties in the definition of the solution for the vector p_k.

In order to realize the numerical solution to find the optimal spray spot configurations which correspond to the thickness measurement results, the Visual Basic (VBA) program was created within the Microsoft Excel environment. The VBA program makes it possible to determine the parameters set (5.1) with an input of a 2D matrix of the thickness values in the spray spot or with an input of a 1D vector of thickness values in three spray profiles.

5.4 Characterization of spray spot

In order to quantify spray spots, the measurement data were obtained with optical profilometry. The thickness measurements were performed with a white light interferometer device of type FRT MicroProf 100 at the Fraunhofer IPK lab. The thickness values were extracted from the 3D scanning data and mathematically treated. A data input for the numerical solution to quantify corresponding spray spot characteristics represents a square matrix h_i of the thickness values, measured at the points with selected coordinates $\{x_i, y_i\}$. The VBA routine, which realizes the iterative solution of the inverse problem based on the equations (5.4-5.7) and taking into account the definition of the thickness distribution according to the model (3.45), gives as an output the values of the optimal parameters set $\{A_0, x_0, y_0, \sigma_x, \sigma_y, \alpha_0\}$. These parameters set ensure the best fit of the measured thickness distribution and the thickness distribution provided by the model. The results of thickness measurements of the spray spots corresponding to the spraying parameters s1 and s2 from Table 5.1 are presented in Figure 5.3. The quality of the tactile scanning result was sufficient to enable fitting of the experimental results for both single and double spray spots with model equations (3.45) with acceptable accuracy. On the other hand, due to the substrate curvature, the definition of the substrate interface was found to be difficult enough. A certain arbitrariness in the definition of the initial substrate surface led to variability of definition of the spray spot geometry parameters (5.3). Furthermore, multiple local minimums of the objective

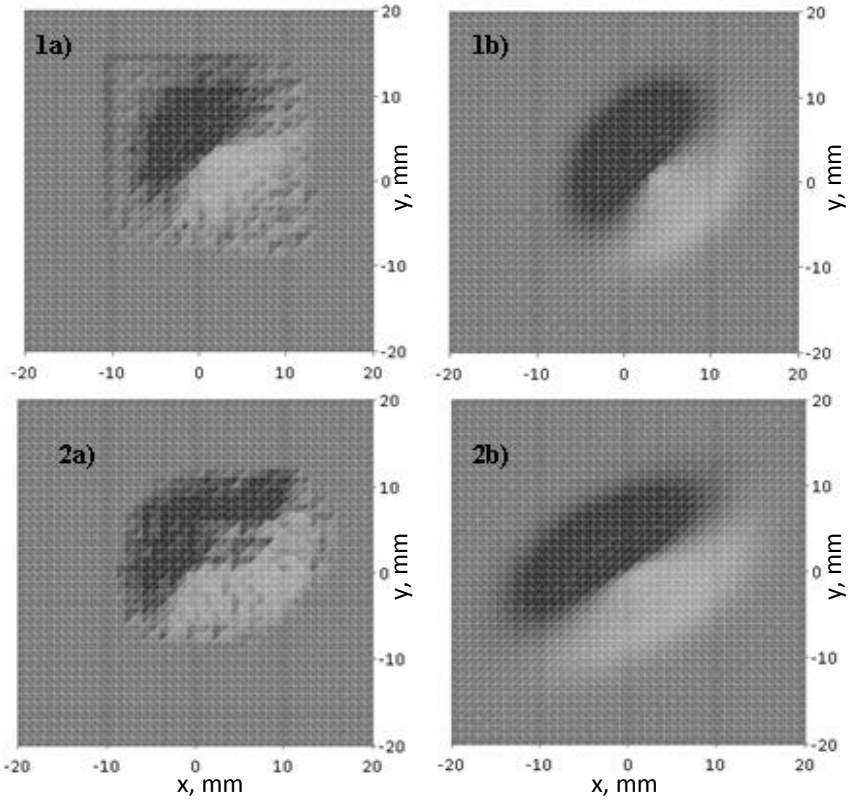

Figure 5.3: Reconstruction of spray spots produced with: 1-single and 2-double injection; a) tactile scanning result and b) model result based on inverse problem solution.

function (5.2) were found for the double spray spot, which corresponded to various parameters sets. Additionally, low stability of the inverse problem solution was related to high noise in the scanning measurement data, visible in the Figure 5.3a, caused by coating roughness. Both these factors led to a multi-variant solution for the parameters of the double injection spot. In order to avoid these difficulties, a more accurate, alternative method to establish spray spot parameters based on evaluation of several linear spray profiles with metallographic techniques was developed and discussed in the next chapter.

5.5 Characterization of spray profile

The spray profile represents a 2D coating pattern with a constant thickness distribution along the profile axis and a bell-like form in a perpendicular cross section. The spray profiles applied by vertical, horizontal and tilted spray paths of the spray gun over the flat substrate with parameters p1.1 from Table 5.1 are shown in Figure 5.2b. The direction of spray gun motion can be characterized in the coordinate system connected to the flat plate shown in Figure 5.1. In this coordinate system, the horizontal profile-A is sprayed along the line which makes an angle 0°, vertical-B an angle 90° and the third profile-C an angle 45° with the x-axis of the flat plate. In all tests done with variation of the spray angle, the tilting of the spray gun is performed in the direction of the y-axis (in the y-z plane). The parameters set $\{A_0, x_0, y_0, \sigma_x, \sigma_y, \alpha_0\}$, which describe a corresponding spray spot, can be defined uniquely by analysis of the spray profiles applied in at least three different directions. Thickness distributions $h_i^{(l)}$ in each spray profile with a number $l = 1..3$ at selected measurement points x_i represent a data input for a numerical solution to quantify model parameters. In addition to the thickness measurement values, the process parameters (powder feed rate $\dot{M}$, coating density ρ_{coat}, spray gun speed v and the number of injectors N) must be entered to characterize the spraying conditions. The VBA routine to realize the iterative solution (5.4-5.7) is used with implementation of model definition of the spray profile according to the equation (4.7). The output of the numerical routine is the optimal $\{A_0, x_0, y_0, \sigma_x, \sigma_y, \alpha_0\}$ set of parameters which give the best fit to the experimental result for all three spray profiles.

Measurements of thickness distribution in spray profiles p1.1-p1.11, p2.1 were performed with metallographic techniques at the Siemens TACR coating facility. The thickness was directly measured on the metallographic cross sections at selected locations. The metallographic sections were prepared by cutting each profile across the profile axis as presented in Figure 52b. The coating thickness in each profile was measured optically with a microscope at positions with a spatial step of 2mm. The starting point for the measurement

series was selected at the outer edges of the flat plate. In order to establish the displacements of the spray profile from the spray jet axis, the displacement of the TCP position of the spray gun from each edge of the plate was controlled for each of three spray profiles. An example of the metallographic sections of the spray profiles is presented in Figure 5.4. It can be seen that profile a - in the 90° direction has broader thickness distribution with a lower maximum in comparison with the profiles b (0°) and c (45°) directions, which have narrower distributions with a higher maximum. This behavior is a result of mass conservation, which requires the same amount of powder deposited per time unit, which can be characterized by the area under the thickness distribution curve. Corresponding metallographic results of the thickness distribution in all three profiles for the sample p.1.1 is presented in Figure 5.5. The zero value

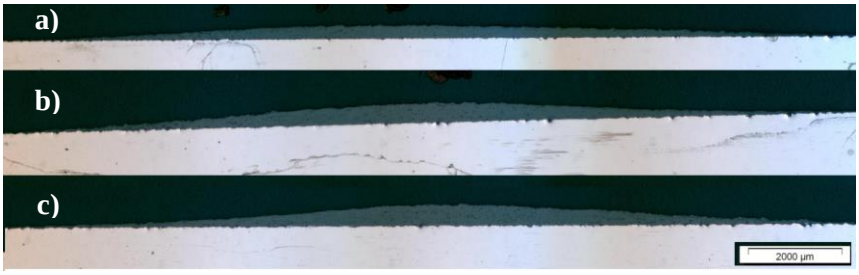

Figure 5.4: Metallographic sections of spray profiles on Plate p1.1 applied along: a) 90°, b) 0° and c) 45° directions.

Parameter	value
feed rate, g/min	nom
efficiency, %	**43,1**
speed, mm/s	nom
distance, mm	nom
tilting betax, °	0
tilting betay, °	0
sigmax, mm	**5,44**
sigmay, mm	**3,50**
elipse alfa0, °	**31**
deflection X, mm	**2,59**
deflection Y, mm	**4,16**
Coat. density, g/cc	5,5
number repetitions	40
Injectors	**1**

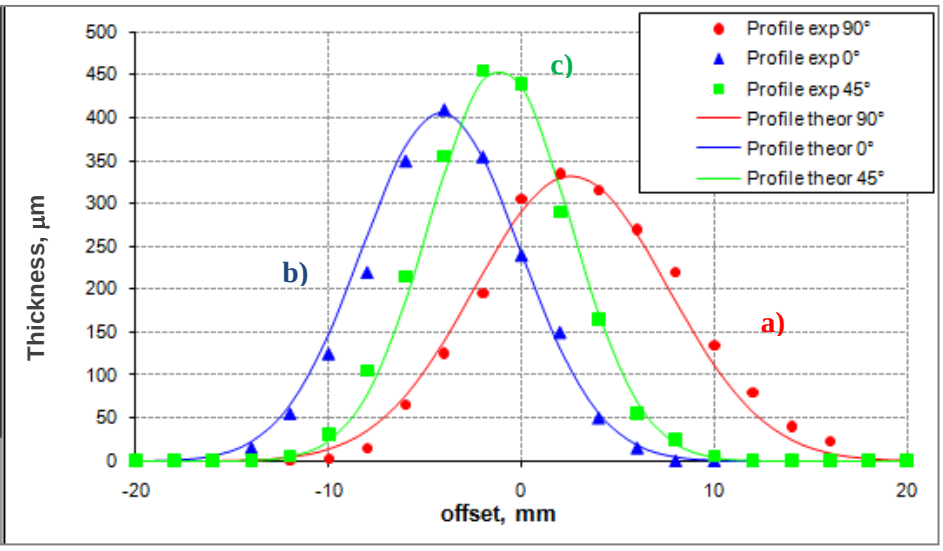

Figure 5.5: Measured and model curves for thickness distribution in spray profiles p1.1 applied along: a) 90°-vertical, b) 0°-horizontal and c) 45°- tilted directions.

of the offset represents a position of the TCP for each spray profile. The direction of measurement was chosen from the middle of the substrate to the edges for each profile. This direction defined a sign of the profile offset on the thickness distribution graph. The maximum position of the spray profiles defined the displacement of the profile from the spray jet axis. As can be seen from the graph both horizontal and vertical profiles exhibit considerable shifts

from the TCP positions, which are described by x_0 and y_0 model parameters. The width of each profile is defined by standard deviations σ_x and σ_y and the direction of the spray gun motion (α=90°, 0° and 45°) in relation to the direction of the major axis of the spray spot which depends on the spot rotation angle α_0. The area under the spray profile curve is determined by deposition efficiency factor A_0. The complete model parameters set $\{A_0, x_0, y_0, \sigma_x, \sigma_y, \alpha_0\}$, which minimizes standard deviation of model and experimental values, is calculated based on thickness measurement data of all three profiles.

Corresponding calculations of the model parameters, which describe the spray conditions from Table 5.1 are shown in Figures 5.6 -5.9. As can be seen from graph 5.6, the values of

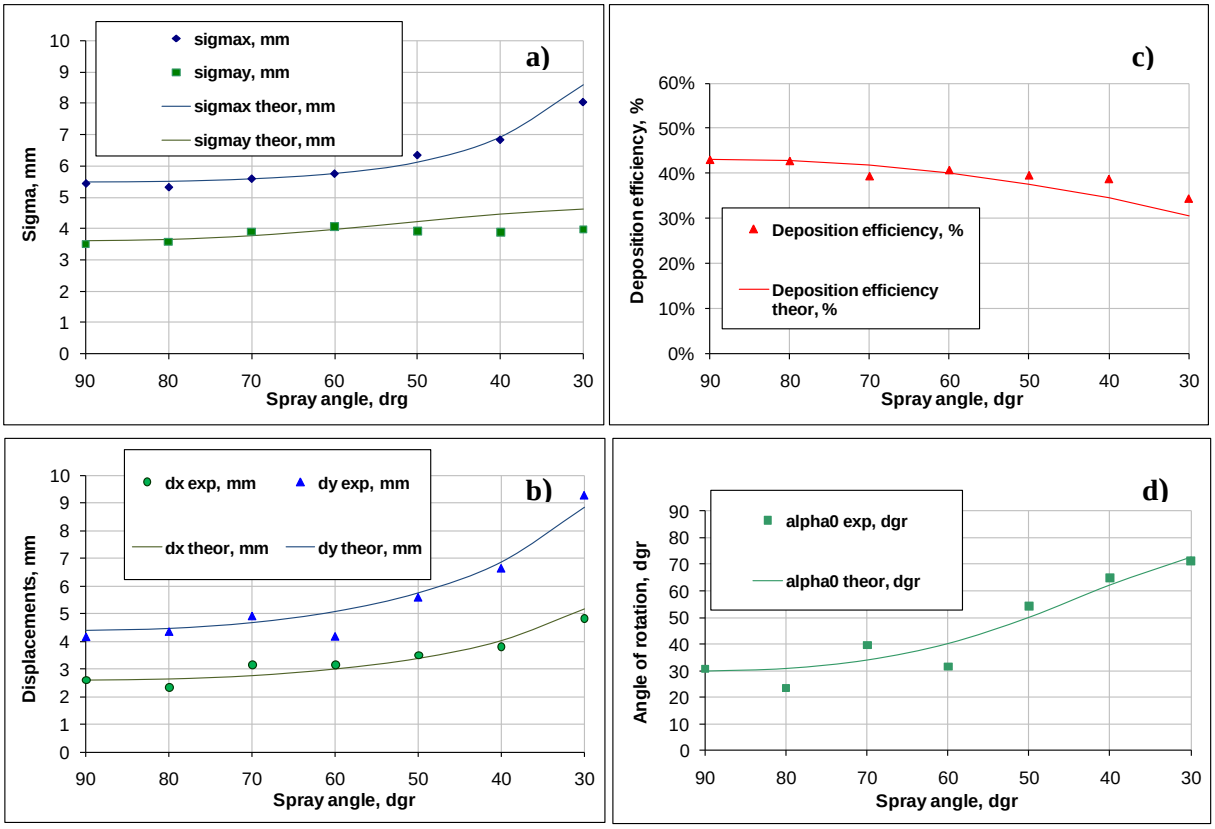

Figure 5.6: Measurement results and prediction curves for the dependence of model parameters on spray angle: a) standard deviations, b) displacements from TCP, c) deposition efficiency, d) angle of spray spot rotation.

standard deviation σ_x along the major axis of the spray spot ellipse increases with the spray angle. The standard deviation along the minor axis σ_y increases as well due to a partial tilting of the spray gun into the direction of the minor axis.

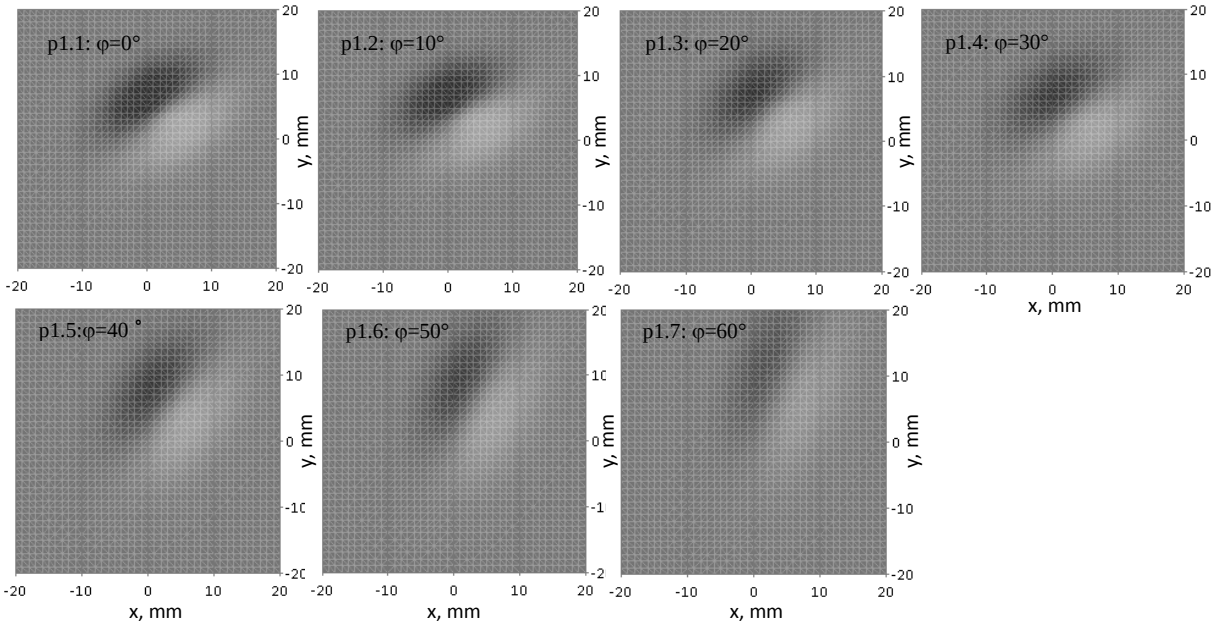

Figure 5.7: Change of the single spray spot geometry with increase of the spray angle, based on measurement of p1.1-p1.7 profiles and spot reconstruction based on the model.

At the same time the spray spot exhibits an additional rotation in the direction of the spray gun tilting, as it is visualized in Figure 5.7. The angle of spray spot rotation increases from the initial value of $\alpha_0 \approx 30°$ at the normal gun orientation up to $\alpha_0 \approx 70°$ for the flat spray angle of φ=60°. The increase in the major standard deviation in combination with rotation of the spray spot in the direction of the gun tilting causes a broadening of the horizontal spray profile with an increase in the spray angle. The displacements of the spray profile increase as well with the spray angle, which causes an increase of the spray spot and profile shift from the TCP position. The dependence of spray spot deviations and displacements is nonlinear, with slight changes at spray angles close to the normal gun orientation, with a rapid increase at higher spray angles over 30°. The deposition efficiency is decreasing with increase of the spray angle, which causes a decrease in maximum profile thickness and corresponding area under the profile curves. The theoretical calculation was done with an input of nominal parameters of the spray profile p1.1 into the equation 3.42 for the comparison with measured and quantified spot parameters. The measurement values of the model parameters are in a good agreement with the corresponding theoretical prediction.

The dependence of the spray spot characteristics on the spray distance is shown in the Figure 5.8. As can be seen from the graphs, the standard deviations increase with the distance with dependence close to the linear. This effect results in an increase in spray spot size with distance from the gun. At the same time, the displacements from the TCP position increased, causing an increase of spray spot shift from the spray jet axis. The deposition

efficiency drops with distance from the gun according to the close to hyperbolic dependence. This dependence supports corresponding model assumption. The angle of the spray spot rotation is assumed to be independent of the spray distance, which is confirmed by the experimental data points on the graph.

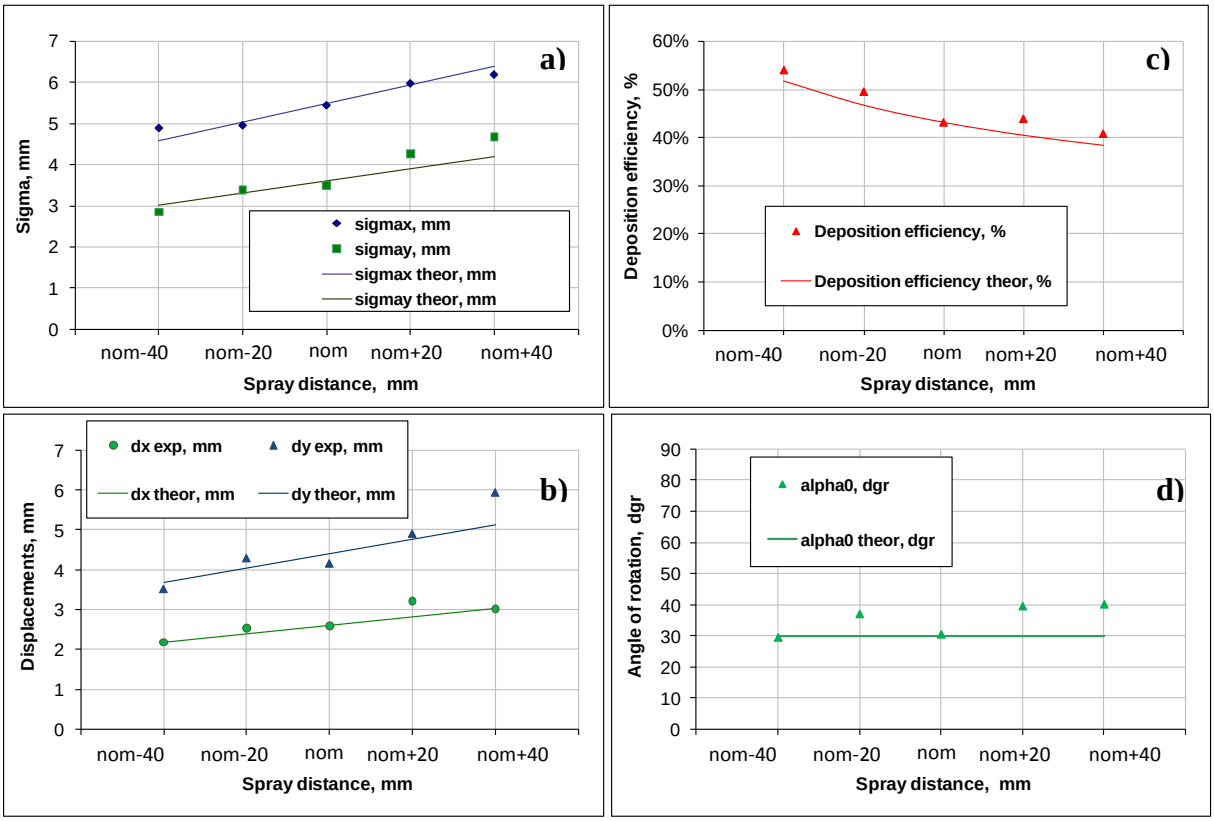

Figure 5.8: Measurement results and prediction curves for the dependence of model parameters on spray distance: a) standard deviations, b) displacements from TCP, c) deposition efficiency, d) angle of spray spot rotation

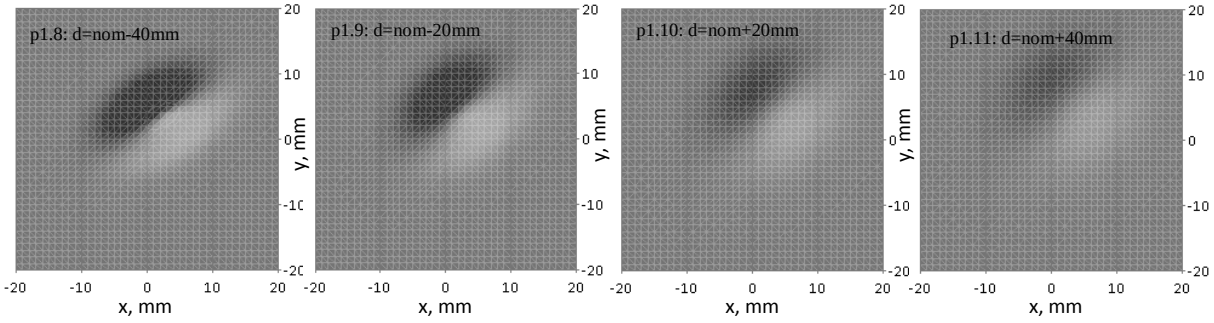

Figure 5.9: Models of the spray spots, constructed based on the measurement data from spray profiles deposited with variation of distance d .

Corresponding visualization of the spray spot geometry, reconstructed from the profile measurements and fitting to the model equation is presented in the Figure 5.9.

In the practical cases, the spray paths to coat substrates are applied along the horizontal or vertical directions. In these cases the thickness distribution in the resulting coating layers are determined by effective standard deviations of thickness in 90° and 0° spray profiles respectively. The effective standard deviations for the profiles applied in an

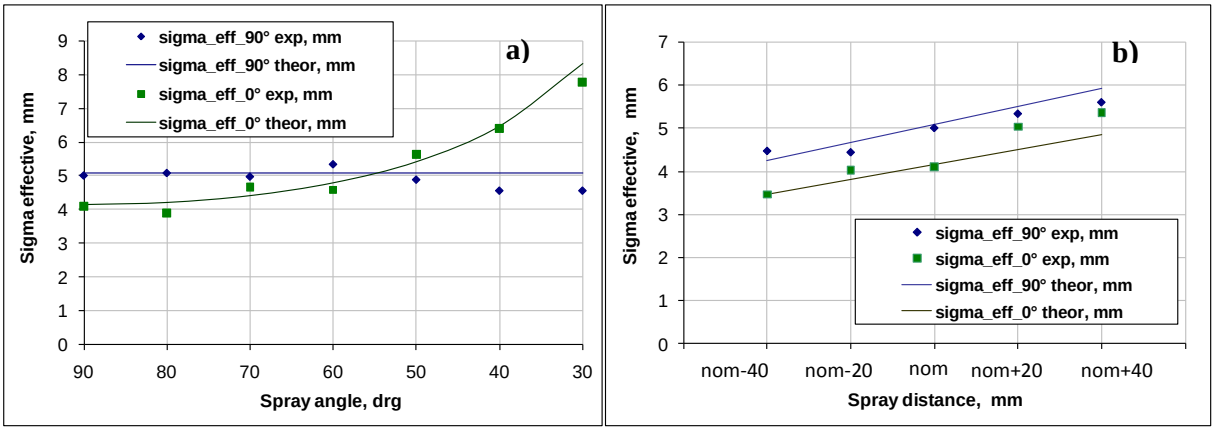

Figure 5.10: Dependence of effective standard deviation for vertical and horizontal profiles on a) spray angle and b) spray distance.

arbitrary direction can be calculated according to the equation (4.9). The experimental and predicted values of effective standard deviations by spraying of horizontal and vertical spray profiles are shown in dependence on the spray angle and distance in Figure 5.10. As can be seen from the graph, only the standard deviation of the horizontal spray profile applied perpendicularly to the gun tilt direction increases with the spray angle, which causes broadening of the profile. The thickness standard deviation in the vertical spray profile applied in the direction of the spray gun tilt stays unchanged. Both the standard deviations increase linearly with the spray distance, which results in an increase in profile width at higher distances from the spray gun.

The double spray profiles were produced in trial p2.1 by activation of the second powder port with the same values of the feed rate as used in the tests p1.1-p1.11. With the same spray program the profiles that were vertical, horizontal and tilted under 45° to the x-axis were produced at the flat plate. The resulting thickness distribution, measured with metallography on the corresponding cross sections of the profiles is shown in Figure 5.11. As can be seen from the data table, summarizing the optimal model parameters set, the deposition efficiency by spraying of the double spot is approximately the same as by spraying of the corresponding spot with a single injector, presented in Figure 5.5. The standard deviations σ_x and σ_y (sigmax and sigmay) along the major axes for one separated spot and for the both single spots, contributing to the double spot pattern are found to be quite close to each other. The displacements x_0 and y_0 (deflectionX and deflectionY) of the

Parameter	value
feed rate, g/min	2x nom
efficiency, %	41,2
speed, mm/s	nom
distance, mm	nom
tilting betax, °	0
tilting betay, °	0
sigmax, mm	4,92
sigmay, mm	3,71
elipse alfa0, °	42
deflection X, mm	4,30
deflection Y, mm	3,60
Coat. density, g/c	5,5
number repetitions	40
Injectors	2

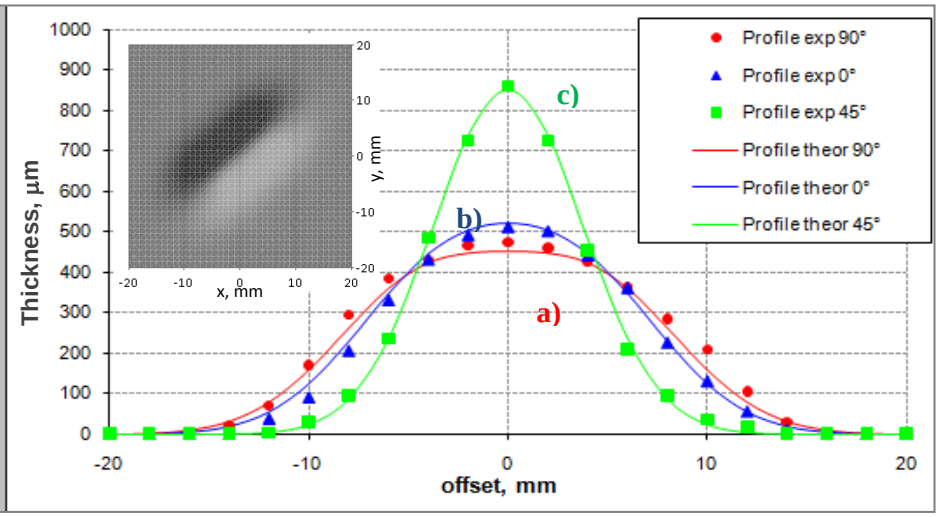

Figure 5.11: Measured and model curves for thickness distribution in double spray profiles p2.1 applied along: a-90° (vertical), b-0° (horizontal) and c-45° (tilted) directions with reconstruction of the corresponding double spray spot.

single and double spots from the TCP target position are found to be different. This can be a result of interaction of both single powder jets within a common powder jet with each other and with the plasma gas swirl produced by the spray gun. Another explanation is related to possible variation of the spray spot configuration during the lifetime of the nozzle. In both cases, the double injection spray spot can be evaluated as a sum of single spots with parameters, which can vary from the parameters of the corresponding separated single injection spot. As can be seen from the graphs, the double injection spray spot produced with selected spray parameters belongs to the type 1 geometry discussed in the Chapter 3.5, with a common maximum in the middle for all orientations of the spray gun motion. This can be explained by analysis of ratio between displacement and standard deviation of the single spots. As can be seen from the table in Figure 5.11, for the double spot we have $x_0 < \sigma_x$ and $y_0 < \sigma_y$, which, based on the results discussed in Chapter 3.5, ensures a sufficient overlapping of the single profiles, producing a double profile with a common single maximum.

The presented experimental results are in good agreement with the model assumptions for behavior of the spray spots and profiles, which confirms validity of the basic model and applicability for various spraying conditions.

5.6 *Verification of model for flat substrates*

The final result of coating process is a deposition of a continuous coating layer onto the substrate. Thickness distribution in the coating layer on a flat substrate, as shown in Chapter 4.2, can be analytically calculated based on equation (4.18) if the model parameters set (5.3)

are known for a particular spray process. In the series of spray trials shown in Table 5.1, the coating layers were deposited with various settings of the spray angle and spray distance in order to confirm the deposition model assumptions. As can be seen from the equation (4.18) the layer thickness is defined by deposition efficiency, feed rate, coating density, gun speed and paths' offset distance, and does not depend on the standard deviations in the particular spray profile. The input of model parameters describing the spray spot applied with nominal spray parameters was done by evaluation of p.1.1 profiles from Table 5.1. Based on known model parameters set the layer thickness was calculated based on equation (4.18) taking into account model dependence (3.17) of deposition efficiency on the spray angle and distance. The calculated values are compared with the measurement results for the layer thicknesses, obtained by metallographic evaluation of the cross sections of the coated samples l1-l6. An example of the optical image of coating layer obtained by the cross sectioning of the coating layer is shown in Figure 5.12. Three cross sections were done for each sample, according to the preparation plan shown in Figure 5.2c. The layer thickness was calculated by averaging of thickness values measured at three points at each cross section over all three cross sections. Corresponding measurement and prediction results for the dependence of layer thickness on the spray angle and distance are presented in Figure 5.13.

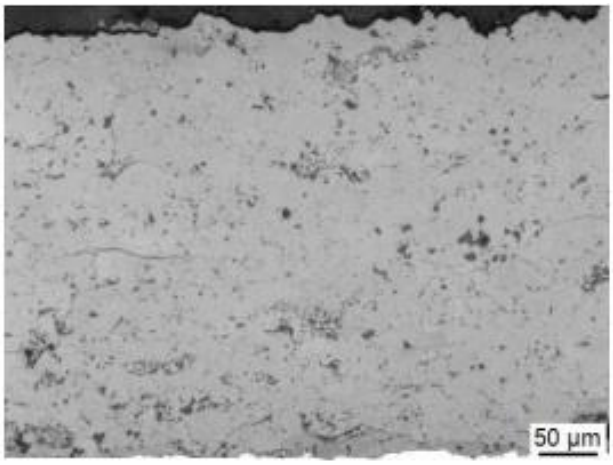

Figure 5.12: Metallography image of the cross section of the TBC coating layer.

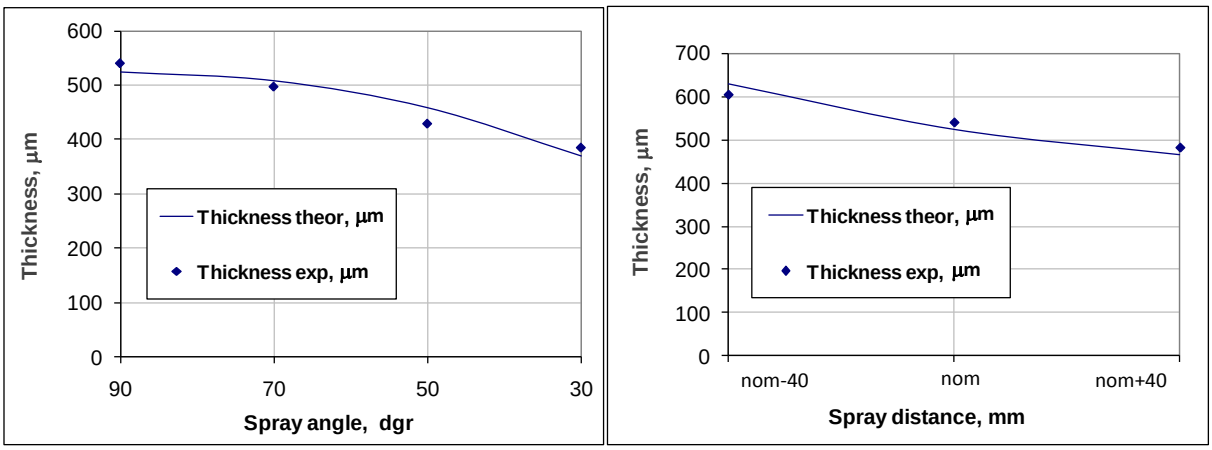

Figure 5.13: Dependence of layer thickness on a) spray angle and b) spray distance.

As can be seen from the graphs, the experimental values in all tests agree not only qualitatively but also by quantities with the theoretical values, predicted by relation (4.18), which represents a direct result of the developed coating deposition model. The dependences of the layer thickness on the spray angle and distance reflect the dependence of the deposition efficiency on these parameters, shown in Figures 5.6c and 5.7c. This is a confirmation of the assumption of the semi-empirical dependence (3.17) of the deposition efficiency on the spray angle and distance.

5.7 Verification of model for cylindrical substrates

The effect of the substrate curvature on the thickness result, discussed in chapter 4.3, was verified experimentally by spraying onto the cylindrical samples with various curvature (c1-c3 described in the Table 5.1). The cylindrical samples with diameters of 10mm, 15mm and 30 mm (with curvature radiuses of 5mm, 7.5mm and 15mm respectively) were sprayed with the same gun settings and spray conditions as spray profile p1.1 and l1 from the Table 5.1. The coating layer was applied by a series of vertical spray paths of the spray gun. The neighboring spray paths were displaced from each other by the path offset of $p = \pi$ =3.14 mm, the sample was turned over the symmetry axis after application of each subsequent path. The selected path offset enabled uniform distribution and an even number of spray paths over the circumference of the samples with constant spacing. The number of spray paths needed for a full coverage of the samples circumference was equal to $N = 2\pi R / p$, which results in a number of paths of 10, 15 and 30 for the selected three cylindrical samples. In particular, normal orientation of the spray gun in relation to the substrate surface with the nominal spray distance was maintained during application of each spray path to deposit a coating layer. The coated cylindrical samples c1-c3 are presented in Figure 5.14. Coating thickness was evaluated by metallographic technique on the three cross sections of the samples as shown in this figure. The thickness was measured over the circumference of the samples. The average value over three cross sections and measurement points were calculated and compared with the prediction result. The prediction of the coating thickness on the curvature substrate can be done by an input of

Figure 5.14: Coated cylindrical substrates with various diameters.

the model parameters, obtained for example by quantification of the spray profile and performing calculations with equation (4.32). Taking as an input the nominal values of the model parameters from the measurements done on the nominal spray profiles p1.1 shown in Figure 5.5, the theoretical layer thicknesses were calculated and plotted for the various values of the substrate diameters in Figure 5.15. The theoretically predicted thicknesses are compared in this figure with the corresponding metallographic result obtained by direct thickness measurement on cylindrical samples c1-c3. As can be seen from the graphs, the prediction curve fits experimental results for the selected samples of 10, 15 and 30 mm diameters very well.

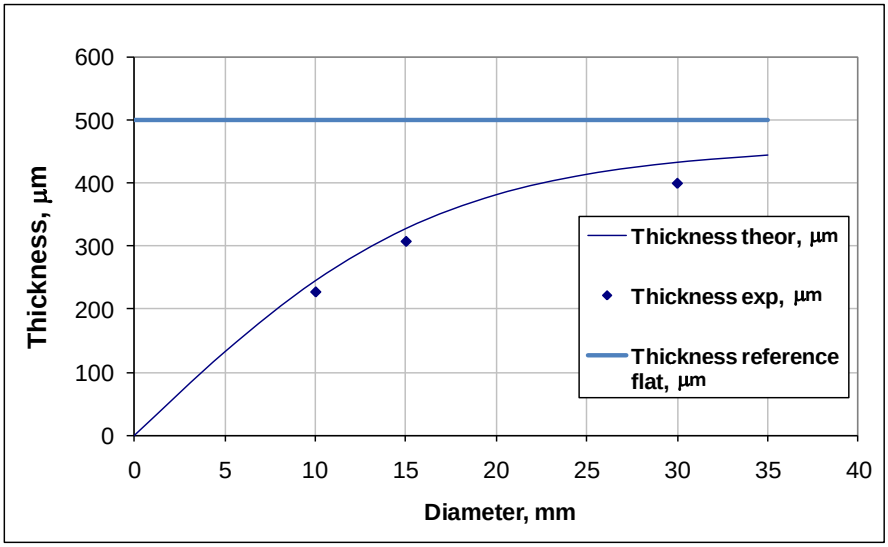

Figure 5.15: Dependence of coating thickness on substrate diameter: theoretical curve and experimental results.

In the case is the reference layer thickness is known for the flat substrate, the equation (4.32) can be used alternatively to (4.27) to predict thickness on the corresponding curvature substrate, coated with the same spray parameters. In particular the calculated values of the correction factor which link the layer thickness on a flat and on a curved substrate can be extracted from Figure 4.10 by utilization of particular R/σ_{eff} ratio for the cylindrical samples. The value of the effective Gaussian standard deviation σ_{eff} of coating thickness in the vertical spray profile is shown in the Figure 5.8 as value for the 90°-spray profile.

For the selected spray process, this value is equal $\sigma_{eff} \approx 5$mm, hence R/σ_{eff} =1, 1,5 and 3 for the selected cylindrical substrates. In Figure 5.16, the dependence of ratio of thickness on the curvature and flat substrate on the ratio of sample radius to effective standard deviation (see Figure 5.8) is presented in comparison with corresponding experimental data. The solid points on the graph depict the ratio of measured thickness on the cylindrical substrate to the calculated value of thickness on the flat substrate. The unfilled points are calculated for the base line thickness measured on the flat substrate. As can be seen from Figures 5.15 and 5.16, the theoretical prediction gives slightly higher thickness

values than metallographic measurements. This can be caused by an assumption that the spray spot and corresponding vertical profile is not displaced from the center line of the spray jet, hence meeting the target substrate surface with a maximum peak of the Gaussian thickness distribution in the theoretical calculation. In practice the vertical spray profile is displaced with the displacement of $x_0 \approx 2.5$ mm. This displacement can certainly cause the reduction of coating layer thickness. Regardless of slight differences of theoretical prediction and experimental result, which are about 10% for the performed tests, the theoretical model predicts a trend of layer thickness change with substrate diameter with good accuracy. This agreement of theoretical and experimental results is a confirmation of the validity of the model assumptions for the cylindrical substrates.

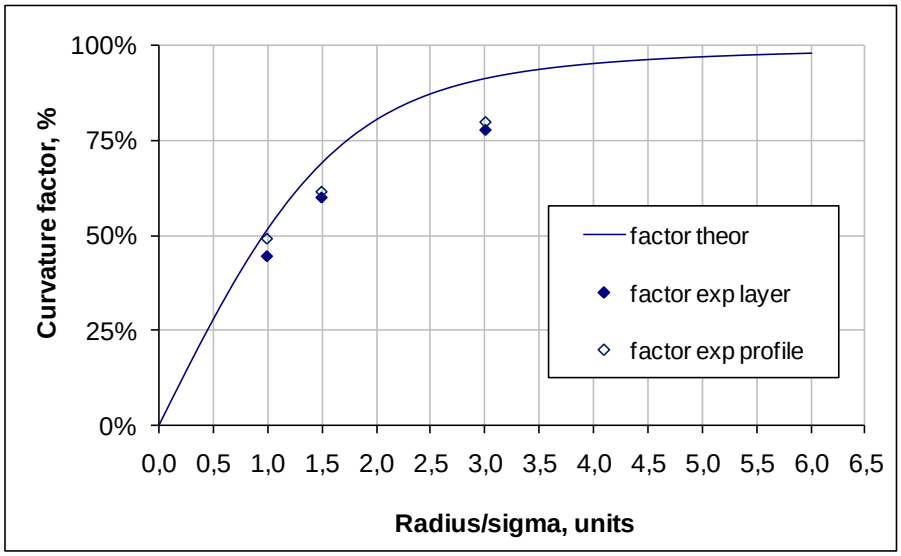

Figure 5.16: Dependence of theoretical ratio of thicknesses on curvature and flat substrates on radius to sigma ratio.

6 Offline programming and coating simulation with RobCad software

Implementation of the RobCad software enables to perform robot path planning and coating thickness simulation within the virtual cell. The virtual cell in RobCad represents a CAD model of the actual spray booth. The spray booth to deposit coatings with APS process at Siemens TACR facility is presented in Figure 6.1. The virtual model of the booth with equipment for APS and HVOF coating processes including robot manipulator with additional rotational axes, spray guns and components to be coated with corresponding toolings and fixtures is established and introduced into the graphical simulation system of RobCad at Siemens TACR. The production work cells were used to implement and verify the coating model discussed in Chapters 3 and 4.

The RobCad software package includes the Paint module, which was originally developed for simulation of painting process. The coating thickness distribution can be simulated by the Paint module with an input of the thickness distribution in a basic paint profile. The ability of the software to simulate an accumulation of thickness, provided by application of an arbitrary number of spray profiles, allowed RobCad to be applied with the Paint module for the simulation of thermal spray process. Corresponding software algorithms were developed and implemented into the programming code to enable simulation of much more complex spray patterns deposited by thermal spray processes taking into account dependences on process parameters and conditions. Major aspects and simulation results for atmospheric plasma spray (APS) process to deposit 8YSZ TBC coating are discussed further in this chapter.

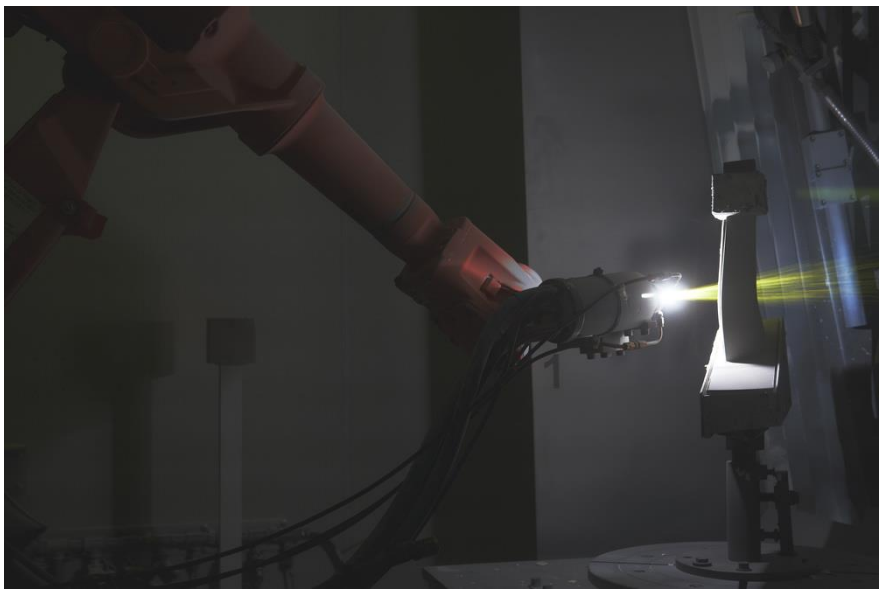

Figure 6.1: Deposition of TBC coating with atmospheric plasma spray process on gas turbine vane at TACR coating facility.

6.1 Spray robot programming in RobCad

Robot motion control in RobCad is achieved by programming of sequences of robotic locations. The tip of the working tool attached to the spray gun must pass these locations. In the case of thermal spraying, the working tool is represented by the spray gun. At each robot location a tool center point (TCP) position and orientation must be set. The TCP is an important object in robot programming, which represents a frame with an attached coordinate system. Usually the z-axis of the TCP frame coincides with the symmetry axis of the spray gun and defines the axis of the spray jet. The axes x and y of TCP frame lie in the perpendicular plane. The TCP frame can be attached directly to the spray gun tip or displaced by a certain distance from it. It is advantageous from the programming point of view to place a TCP frame at the distance equal to the nominal spray distance from the spray gun. The placement of the TCP used in the verification trials with RobCad is presented in

Figure 6.2. It is desirable from the processing point of view to maintain normal orientation of the spray gun in respect to the substrate surface. The normal orientation ensures the maximal deposition efficiency and nominal values of the coating properties such as coating porosity and interface roughness. From the geometrical standpoint this requirement is equivalent to setting of the z - axis of the TCP frame along to the normal vector to the substrate surface. It is easy to achieve the normal orientation of the gun for simple substrate geometry, for example by spraying on a flat, or close to flat, substrate surface. In a general case, an arbitrary orientation of the spray gun and corresponding TCP frame can be used by spraying of a particular substrate, and hence an arbitrary spray angle must be considered by the simulation model. The case of the spray gun tilting to the substrate surface is presented in Figure 6.2. In this example the z - axis of the TCP frame is tilted in the lane (y, z) around the x axis of the reference frame which is placed in the middle of the substrate with a normal orientation.

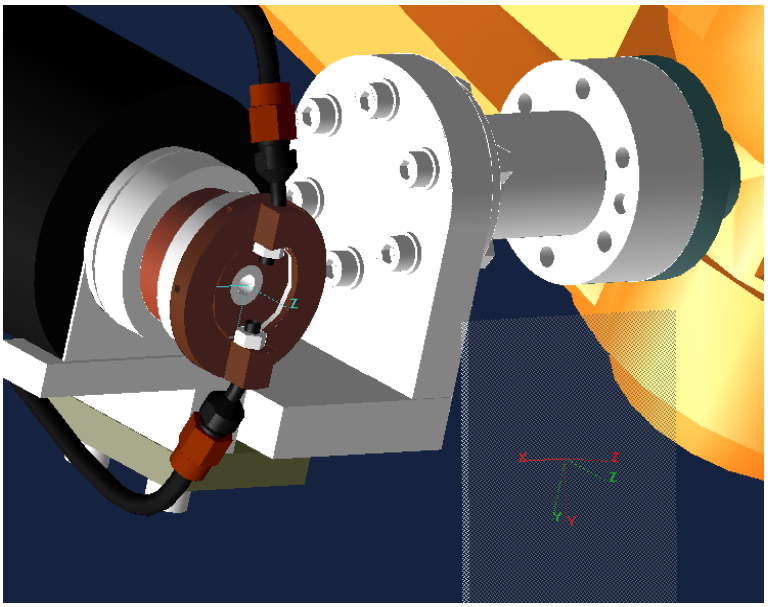

Figure 6.2: Orientation of TCP frame in case of tilting of the spray gun relative to the substrate surface.

The robotic locations, connected with each other, form the spray paths. All spray paths needed to coat a particular component form the coating program. After the generation of the coating program, the robot motion will be performed with the help of the robot controller software. This calculation of joints configuration to perform the motion path is provided by inverse kinematics algorithms, by the robot controller. Once the program is created in the RobCad environment, it can be translated into the native controller language and downloaded to the actual robot memory to perform motion program in the booth. During program execution in the spray booth, the positioning instructions are provided by the motion attributes at each location to control the robot motion. The robot performs motion of the spray gun from a current location to the next one according to these attributes. The location settings include in particular the type, position, orientation of the TCP, configuration of the robot joints and external axes. Furthermore, the TCP speed must be selected together with

the motion type selected to reach the destination location. For this reason the joint type, linear type or circle motion types can be used. The zone attribute must be selected to define how accurately the robot has to achieve the destination location. A typical spray path performs a gun motion along a raster-like trajectory. The path consists of a number of locations placed on both sides of the substrate. Each row of locations is displaced at a constant offset distance from the neighboring rows. In later verification trials with Robcad, linear motion with a constant speed and normal orientation of the TCP frame was used to apply various coating patterns to the flat substrates.

In order to enable a robotic simulation in combination with coating simulation, the Robcad software should be set up and properly configured. Following configuration steps must be performed to set up the work cell:

- Set up of the robot model in RobCad work cell and attachment of the spray gun model. In addition auxiliary manipulators such turntables must be modeled and programmed as external robotic axes to perform motion of the component holder.
- Input of the CAD model of the component into the RobCad environment. Typical format of the model is an IGES file.
- Completing the exact CAD models of the component holder and needed auxiliary tools. The modeling could be done with the internal RobCad design module or with the help of the external software with a subsequent import into RobCad. The holder, tools and a component must be assembled together and attached to the turntable.
- Calibration and the adjustment of the virtual RobCad work cell. The calibration procedure is necessary to ensure that the offline programmed robotic path and programmed robotic locations meet their real counterparts in the actual spray booth.

The calibration procedure uses a specific robot path with three locations attached to a component and chosen at selected characteristic points on the component. These three locations should be created in RobCad and downloaded to the booth. The robot with a distance measurement tool mounted onto the robot or spray gun should be moved to these locations in the real booth. If the RobCad location does not match the real position, the robot with the measurement tool will be moved manually to the correct position. This new manually adjusted position will be stored together with the initial location in the robotic controller memory for each of the three locations. Thus, the three pairs of the programmed and adjusted locations will be created. This pairs of locations will be uploaded back to the RobCad. The work cell calibration utility will analyze the calibration locations pairs to compute a displacement vector. This utility shifts the component with the attached tools and paths according to the displacement vector in the RobCad work cell.

6.2 Application of the Robcad/Paint software for coating thickness simulation

The coating thickness simulation is performed by RobCad software with the reprogramming of the Paint module according to the model equations developed. The Robcad software allows to simulate coating distribution on the part, resulting from arbitrary motion of the TCP frame. The TCP frame is connected to the spray gun and moves along the robot path following the programmed locations at selected speed.

The spray programs to apply profiles and complete coating layers onto the flat substrates discussed in the Chapter 5 were generated with OLP technique in RobCad. Examples of the robot programs to apply these coating patterns with subsequent thickness simulation for the 8YSZ coating sprayed by the APS process are presented and discussed in [60-62]. Applied simulation procedure is described in the patent [63]. In particular, in order to produce three spray profiles in directions that are vertical, horizontal and tilted under 45° at the flat plates, the spray path presented in Figure 6.3 was used. Figure 6.4 shows the coating program to apply complete coating layer. The trajectory of the TCP frame is shown by the dashed line. Corresponding target locations are depicted by rectangular frames. The stand-off distance and gun

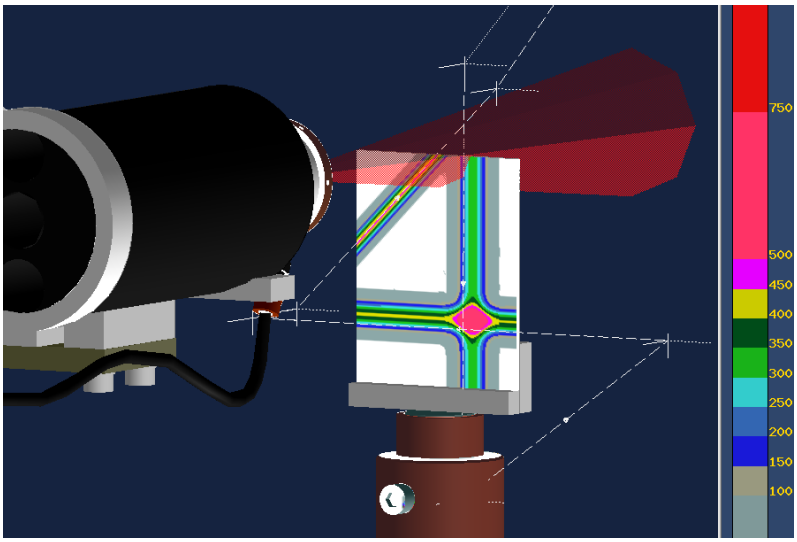

Figure 6.3: Thickness simulation in Robcad of asymmetrical single spray profile.

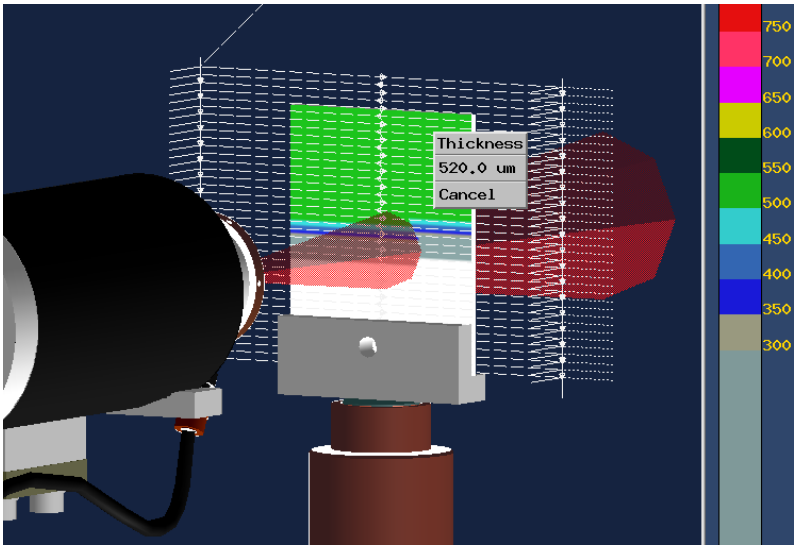

Figure 6.4: Simulation of coating layer deposition on flat plate with a raster spray program.

orientation were programmed to stay constant and equal to their nominal values during the spraying onto the substrate. In order to keep the gun speed constant on the plate, the turning points of the gun are put far enough away from the plate to prevent acceleration and deceleration of the gun on the substrate to be coated.

After performing of the robot motion simulation, corresponding result of thickness simulation appears on the substrate surface in the form of a color map, which defines thickness distribution at each substrate point. The color scale at the images represents thickness given in micrometers. Parameters of the spray spot used for these simulations were chosen according to the values shown in the Figure 5.5. These values represent nominal parameters of the selected spray process. As it is visible from the thickness mapping shown in the Figure 6.3, the thickness distribution varies in the vertical, horizontal and tilted profiles. This reflects asymmetrical behavior of the spray profile in respect to the direction of the gun motion. The numerical values of thickness agree with the theoretical and experimental thickness values of each profile (see Figure 5.5) what verifies the parameters input and confirms correctness of RobCad simulation for the profiles.

The simulation result which predicts coating layer thickness on the flat substrate is presented in the Figure 6.4. Here, the coating layer is formed by superposition of multiple spray profiles under nominal conditions. As it is visible from the color map, the numerical value of layer thickness calculated by RobCad is in a good agreement with the corresponding theoretical and experimental values shown in the Figure 5.13. This result demonstrates capability of RobCad to simulate coating layers and correctness of the layer thickness prediction.

6.3 Simulation of coating deposition for turbine parts

Implementation of the coating thickness simulation in addition to the OLP robot programming enables a full process development cycle within the virtual environment of Robcad software. A realistic prediction and analysis of the coating distribution resulting from the motion of the spray gun can be performed without a real spray trial in the production booth. Based on the analysis of the simulated thickness result, necessary adjustments of the spray program can be made off-line. A verification of the adjustments is performed by a subsequent thickness simulation. Thus, as presented in Figure 6.5, an iterative process of coating program development is performed off-line within the Robcad virtual cell.

Developing the robot path for complex surfaces of turbine components such as blades and vanes represents a challenging task. Generation of the spray program must take into account the geometrical and mechanical constraints resulting from the component surface

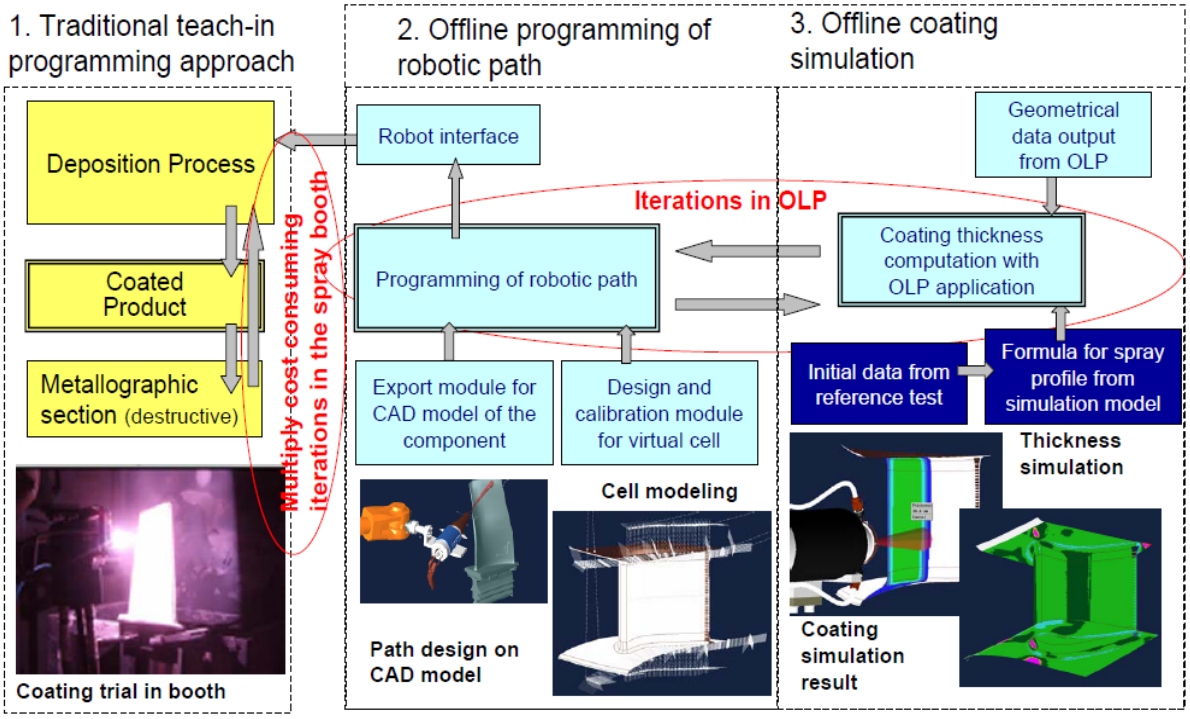

Figure 6.5: Conceptual diagram of coating process development with application of off-line programming and coating thickness simulation in RobCad software.

contour, reachability of points on the surface, and allowable target robot configurations. Furthermore, mechanical imitations for the robot joints motion can make it difficult to maintain selected gun speed by motion along the programmed trajectory. For a complex surface with a defined curvature, implementation of a simple meander-like design of the spray path can not achieve a necessary level of coating thickness uniformity. The adaptive algorithms of path generation must be used based on the geometrical analysis of the CAD model of particular component. The most important target of the spray path development is to achieve a uniform thickness at selected segments of the component surface. Due to complexity

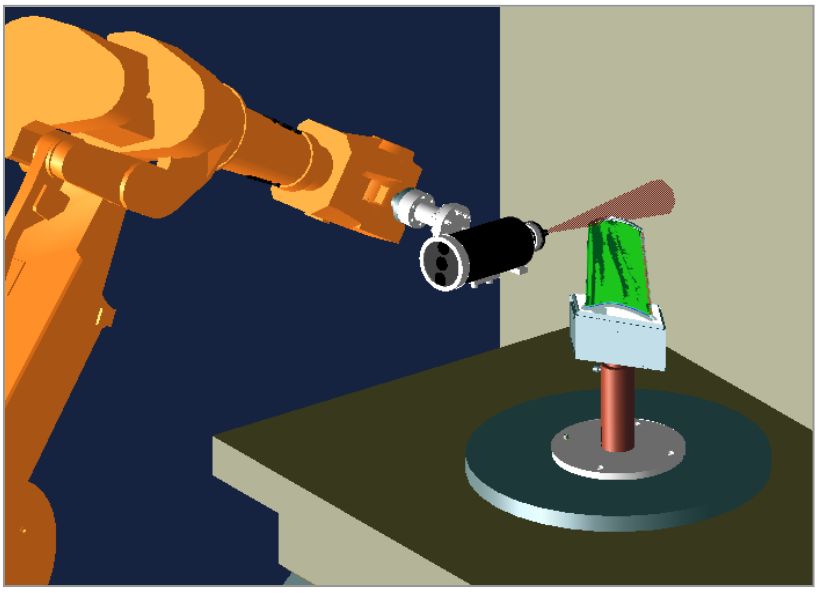

Figure 6.6: Coating simulation in Robcad virtual cell for a turbine blade.

of turbine components' geometry and existence of spray process drifts, certain thickness tolerances are defined to meet component functionality criteria. In order to meet these tolerances, a robust spray program and stable spray process had to be developed and utilized to coat turbine components with very narrow tolerance ranges. An off-line simulation of the coating thickness makes it possible to predict and analyze the coating distribution on the component. Based on this analysis, the spray path segments which cause deviation of thickness from the requested tolerances can be identified and changed to achieve improvement in thickness distribution. As presented in the Figure 6.6 the mapping of thickness distribution on the turbine blade, which appears after the OLP simulation of the robot motion, makes it possible to identify the problematic areas on the part and perform needed improvement of the spray program.

A comparison of predicted and corresponding measured thickness distribution along middle cut of the blade airfoil shown in Figure 6.6 is presented in Figure 6.7. As can be seen from the graph, the simulation predicts measurement results with a high accuracy in most areas of the airfoil. Based on the realistic prediction of the coating result by simulation, an iterative process of spray path improvement is performed in the RobCad virtual cell until the thickness of all coated surfaces achieves required tolerances. This iterative process which involves development, verification and adjustment of the spray path within OLP environment reduces substantially the number of intermediate spray trials in the spray booth, substituting them by simulations.

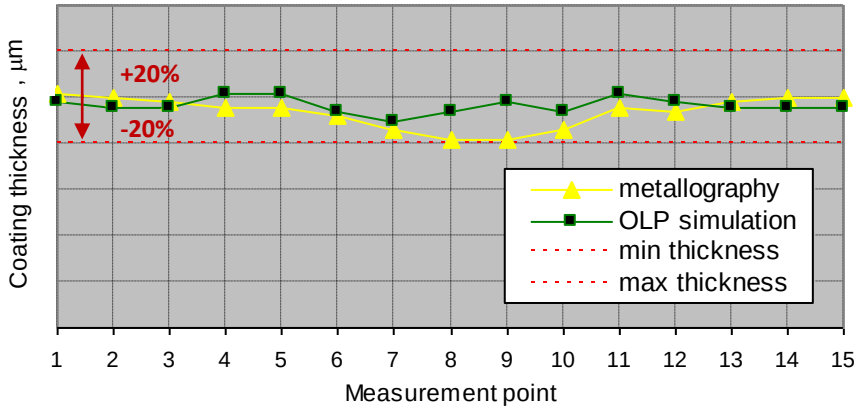

Figure 6.7: Comparison of measured and simulated thickness result for airfoil section of the turbine blade.

7 Conclusion and further perspectives

7.1 Conclusion

A model of thermal spray deposition process was developed to simulate a coating distribution on the various substrates. The non-approximate physical character of the spray profile modeling avoids a lot of experimental trials to gain initial data. On the other hand,

experimental input from the reference test of some complex process properties such as spray efficiency and standard deviations of thickness in the spray profile make the model straightforward enough for practical implementation. This compromise and combination of theoretical background and empirical input allow an exact, self consistent and practically useful simulation procedure to be created. The model includes generic features of the spray processes, which makes it easily transferable for different coating processes.

Some peculiarities of the thickness distribution in the asymmetrical APS spray spot and profile patterns were analytically investigated and their influence on the coating layer formation was discussed. In particular, a model parameters set was established to enable a full description of the basic spray pattern represented by the spray spot. These parameters are deposition efficiency, standard deviations of thickness along the main axes of the spot ellipse, displacements of the spot from the spray jet axis and angle of the spot rotation, measured in a selected reference coordinate system on a flat substrate. These parameters represent physical characteristics of the deposition process which can be determined with well developed methods in the experiment. The dependences of the model parameters on the spraying conditions was modeled, taking into account geometry considerations related to conical form of the spray jet and assumptions of dependence of the deposition efficiency on the spray angle and distance. Some practical cases of spraying with double and multiple injectors were considered by an analytical description of the double and multi-injection spray spots. In particular, a form of the multi-injection spray spot was investigated in dependence on the characteristics of the contributing single spots. Using an analytic character of the model the thickness distribution in the linear spray profile and complete coating layer was calculated and analyzed for flat and cylindrical substrates. The direct expressions were developed to calculate the layer thickness in dependence on feed rate, path offset and gun speed for the deposition process with known model parameters set.

The basic results, which follow from the developed model, were verified experimentally for a deposition of 8YSZ TBC coating with APS process onto the flat and cylindrical substrates. A method based on reverse problem solution was developed to quantify the experimental spray spot parameters by analysis of measured thickness distributions in the spray spot and profiles. The measurements were done on the spray spots by mechanical profilometry and on spray profiles by metallographic technique. The parameters set, which describe the spray profiles, obtained by metallographic measurements, deposited with various spray angle and distance were in a good agreement with corresponding theoretical values, predicted by the model. It was shown that the model equation for the coating layer thickness gives an accurate prediction of the corresponding experimental thickness values. Furthermore, a dependence of the layer thickness on the curvature was verified by

comparison of theoretical and experimental thickness result for cylindrical samples with various diameters. The experiential series discussed showed an applicability of the theoretical model for the selected APS process with high prediction accuracy.

An application of the developed model enables thickness distribution to be calculated in all possible coating patterns generated by the arbitrary motion of the spray gun over the substrate surface along the selected trajectory with variable gun speed. The model equations were entered into the off-line simulation software RobCad by reprogramming of the Paint thickness simulation module. The input of the model into the simulation software enabled a realistic prediction of the coating thickness with a high accuracy on free-form substrate surfaces. Simulation results for flat substrates and a test turbine component for the APS TBC spray process were presented and compared with experimental data.

An implementation of the off-line programming in combination with coating thickness simulation in the coating development process enables a full cycle digital development of the spray process, meeting the strict thickness requirements and at the same time bringing significant reduction in development effort and time.

7.2 Future perspectives

As it is shown, the developed model reflects substantial features of the coating pattern formation on various substrate surfaces for the selected APS spray process to deposit selected 8YSZ TBC coating. The generic character of the model enables an application and verification of the model for further processes such as LPPS, HVOF to increase confidence of model assumptions and results. In general, each model represents an approximation of the real processes with own assumptions and compromises. In particular, the presented model requires an experimental input of the nominal parameters: deposition efficiency, thickness standard deviations, spot displacements and angle of rotation. Furthermore an assumption of dependence of these parameters on the spray angle and distance in general needs an experimental input as well. These parameters have to be established prior to the analytical prediction of the coating layer thickness on the flat substrates and numerical prediction for the free-form substrates with off-line simulation software. The metallographic methods used to gain the nominal profile parameters have limited accuracy for single measurements related to a limited number of measurement points, where thickness is visually evaluated. Hence it would be important to develop extended test methods and experimental design to improve accuracy and at the same time not increasing efforts to conduct experiments. Alternatively, it is reasonable to link the model parameters with the spray gun settings, such as torch current and power, process gases and carrier gas flow

rates. In addition, substrate morphology and thermal flow must be taken into account by this model. This linking will avoid a need to perform the spray trials and measurements to gain the nominal model parameters. On the other hand, such whole process modeling will require extended theoretical investigations in frames of fluid dynamics and thermodynamics, which can make the resulting model complex enough for practical use.

It is known that the parameters of the spray process are subject to fluctuations and vary, for example, with the operation time of the electrodes of the plasma gun. These fluctuations can affect the input of the nominal process parameters, which are captured by a single measurement done on the cross section of the spray profiles. The effect of short term fluctuations in the time range of milliseconds must be studied and a method to take them into account must be developed. The long term variations which take place within the nozzle lifetime can affect the overall coating result. Long term change of the spray gun characteristics leads to long-term changes of the in-flight particles' characteristics such as distribution of mass, velocity and temperature of the powder particles. These in-flight characteristics, in frames of the current model, define the distribution of powder flux in the spray jet and affect the deposition efficiency on the substrate surface. Changes of the spray spot as a result of variation of in-flight characteristics will lead to change of the corresponding thickness of a coating profile and consequently in the complete coating layer, especially for the substrates with a high curvature. On the other hand, there are various monitoring technique based particle sensors such as Accuraspray, Spraywatch, DPV200 (see Chapter 1.2.5), developed for the on-line monitoring of in-flight coating characteristics. Establishing the dependence between the spray spot model parameters with in-flight characteristic of the powder particles jet, provided by particle sensors, will enable changes in the final coating layer thickness to be predicted. An implementation of on-line monitoring with off-line programming and simulation techniques is potentially very promising and important, especially for serial production of the coatings for turbine components, to ensure stability of the deposit properties during the lifetime of the coating equipment. The visionary target is to provide a closed cycle process control system, which makes it possible to perform corrective actions on the spray parameters to bring the spray spot into the initial form if the particles sensor detects corresponding process variation.

A further practically important extension of the off-line programming is an application of the adaptive algorithms for the automatic robot path generation for a particular component to be coated for a selected CAD component geometry with implementation of the coating thickness simulation as discussed in [64]. In the end, development of the corresponding software tools will enable full automation of the process of spray program generation with an adaptive process adjustment and control.

References

[1] J. S. Christof Lechner, Stationäre Gasturbinen, Springer Heidelberg Dordrecht London New York, 2010, p. 1101

[2] H. Kurz, State of the art combined cycle & steam power plants, Siemens presentation at Hannover messe, Hannover, 2009.

[3] R. Subramanian, A. Burns, W. Stamm, Advanced Multifunctional coatings for land-based industrial gas turbines, Proceedings of ASME Turbo Expo 2008: Power for Land, Sea and Air GT 2008, June 9-13, 2008, Berlin, Germany

[4] M. Oechsner, Property Variations in Thermal Barrier Coatings and their Impact on Gas Turbine Design, Presentation at ICTM Conference 2013, Aachen, Germany

[5] R. Rajendran, Gas turbine coatings - an overview, Eng. Fail. Analys. 26 (2012) 355–369

[6] Kang N Lee, The Gas Turbine Handbook- Protective Coatings for Gas Turbines

[7] A. Evans, J. Hutchinson, The mechanics of coating delamination in thermal gradients, Surface & Coatings Technology 201 (2007) 7905–7916

[8] K. Schneider, V. Belashchenko et al., Thermal Spraying for Power Generation Components, WILEY-VCH Verlag, 2006

[9] R. Tucker, Thermal Spray Coatings, ASM Handbook, Vol. 5: Surf. Engineering, 1994

[10] H. Grunling, W. Mannsmann, Plasma sprayed thermal barrier coatings for industrial gas turbines: morphology, processing and properties, J. de Physique 111, Vol. 3 (1993) 903-912

[11] G. Mauer, R. Vassen, D. Stoever, Atmospheric plasma spraying of yttria-stabilized zirconia coatings with specific porosity, Surface & Coatings Technology 204 (2009) 172–179

[12] M. Oska, E. Turunen, et. al., Optimization and Characterization of High Velocity Oxy-fuel Sprayed Coatings: Techniques, Materials, and Applications, Coatings 1 (2011) 17-52

[13] G. Moskal, B. Witala, A. Rozmuslowska, Metallographic preparation of the conventional and new TBC layers, Archives of Mat. Science and Eng. Vol. 39 Issue 1 (2009) 53-60.

[14] G. Antou, G. Montavon, Quantifying Thermal Spray Coating Architecture by Stereological Protocols: Part II. Key Points to be Addressed, JTTEE5 16:168–176

[15] A. Kanta, G. Montavon, et. al., Intelligent system for prediction and control: Application in plasma spray process, Expert Systems with Applications 38 (2011) 260–271

[16] W. Zhang, S. Sampath, A Universal Method for Representation of In-Flight Particle Characteristics in Thermal Spray Processes, JTTEE5 18:23–34

[17] J. Fincke, W. Swank, et. al., Diagnostics and control in the thermal spray process, Surface and Coatings Technology 146 –147 (2001) 537–543

[18] A. Vaidya, V. Srinivasan, et. al., Process maps for plasma spraying of yttria-stabilized zirconia: An integrated approach to design, optimization and reliability, Materials Science and Engineering A 497 (2008) 239–253
[19] P. Fauchais, Understanding plasma spraying, J. Phys. D: Appl. Phys. 37 (2004) 86–108
[20] F. Qunbo, W. Lu, W. Fuchi, 3D simulation of the plasma jet in thermal plasma spraying, Journal of Materials Processing Technology 166 (2005) 224–229
[21] E. Pfender, Plasma jet behavior and modeling associated with the plasma spray process, Thin Solid Films, 238 (1994) 228-241
[22] H. Xiong, L. Zheng, Three-dimensional simulation of plasma spray: effects of carrier gas flow and particle injection on plasma jet and entrained particle behavior, International Journal of Heat and Mass Transfer 47 (2004) 5189–5200
[23] V. Hurevich, A. Gusarov, I. Smurov, Simulation of coating profile under plasma spraying conditions, Proceeding: International Thermal Spray Conference 2002 (DVS-ASM)
[24] M. Vardelle, A. Vardelle, P. Fauchais, et. al., Controlling Particle Injection in Plasma Spraying, JTTEE5 10:267-284
[25] P. Wang, S. Yu, H. Ng, Particle velocities, sizes and flux distribution in plasma spray with two powder injection ports, Materials Science and Engineering A 383 (2004) 122–136
[26] S. Sampath, X. Jiang, Splat formation and microstructure development during plasma spraying: deposition temperature effects, Mat. Science and Eng. A304–306 (2001) 144–150
[27] M. Mellali, P. Fauchais, A. Grimaud, Influence of substrate roughness and temperature on the adhesion/cohesion of alumina coatings, Surf. and Coatings Techn. 81 (1996) 275 286
[28] S. Sampath, X. Jiang, Substrate temperature effects on splat formation, microstructure development and properties of plasma sprayed coatings Part I: Case study for partially stabilized zirconia, Materials Science and Engineering A272 (1999) 181–188
[29] L. Bianchi, A. Leger, et. al., Splat formation and cooling of plasma-sprayed zirconia, Thin Solid Films 305 (1997) 35-47
[30] C. Kang, H. Ng, Splat morphology and spreading behavior due to oblique impact of droplets onto substrates in plasma spray coating process, Surface & Coatings Technology 200 (2006) 5462 – 5477
[31] C. Kang, H. Ng, S. Yu, Plasma spray deposition on inclined substrates: simulations and experiment, JTEE5 16:261-274
[32] G. Montavon, S. Sampath, et. al., Effects of the spray angle on splat morphology during thermal spraying, Surface and Coatings Technology 91 (1997) 107-l 15
[33] A. Kout, T. Wiederkehr, H. Müller, Efficient stochastic simulation of thermal spray processes, Surface & Coatings Technology 203 (2009) 1580–1595

[34] A. Kulkarni, A. Vaidya, et. al., Processing effects on porosity-property correlations in plasma sprayed yttria-stabilized zirconia coatings, Mat. and Engineer. A359 (2003) 100-111
[35] S. Mihm, Influence of the anode nozzle design to the APS coating process, Proceeding of Turbine Forum 2012
[36] A. Zagorski, F. Szuecs, et. al., Experimental study of substrate thermal conditions at APS and HVOF, Proceeding of International Spray Conference ITSC 2003
[37] S. Guessasma, F. Trifa, et. al., Al2O3–13% weight TiO2 deposit profiles as a function of the atmospheric plasma spraying parameters, Materials and Design 25 (2004) 307–315
[38] F. Trifaa, G. Montavon, et. al., Geometrical features of plasma-sprayed deposits and their characterization methods, Materials Characterization 54 (2005) 157– 175
[39] F. Trifa, G. Montavon, C. Coddet, On the relationships between the geometric processing parameters of APS and the Al2O3–TiO2 deposit shapes, Surface & Coatings Technology 195 (2005) 54– 69
[40] S. Leigh, C. Berndt, Evaluation of off-angle thermal spray, Surface and Coatings Technology 89 (1997) 213-224
[41] E. Lugscheider, R. Nickel, Finite element simulation of a coating formation on a turbine blade during plasma spraying, Surface and Coatings Technology 174 –175 (2003) 475–481
[42] S. Duncan, P. Jones, P. Wellstead, Robot Path Planning for Spray Coating: A Frequency Domain Approach, Proceeding of the American Control Conference 2004
[43] A. Kout, H. Müller, Parameter optimization for spray coating, Advances in Engineering Software 40 (2009) 1078–1086
[44] J. Goedjen, R. Miller, W Brindley, A simulation technique for predicting thickness of thermal sprayed cotings, Technical Memorandum NASA 1995
[45] D. Stepanenko, Modeling of spraying with time-dependent material feed rate, Applied Mathematical Modelling 31 (2007) 2564–2576
[46] A. Hansbo, P. Nylen, Models for the simulation of spray deposition and robot motion optimization in thermal spraying of rotating objects, Surface and Coatings Technology 122 (1999) 191–201
[47] Fasching, M; Prinz, et. al., University.Engineering Design Research Center., Optimization of robotic trajectories for thermal spray shape deposition (1991). Robotics Institute. Paper 680. http://repository.cmu.edu/robotics/680M
[48] E. Abele, M. Weigold, S. Rothenbücher, Modeling and Identification of an Industrial Robot for Machining Applications, Annals of the CIRP Vol. 56/1/2007
[49] A. Olabi, R. Beare, et. al., Feed rate planning for machining with industrial six-axis robots, Control Engineering Practice 18 (2010) 471–482

[50] Z. Pan, J. Polden, et. al., Recent progress on programming methods for industrial robots, Robotics and Computer-Integrated Manufacturing 28 (2012) 87–94

[51] R. Gadow, A. Candel, M. Floristán, Optimized robot trajectory generation for thermal spraying operations and high quality coatings on free-form surfaces, Surface & Coatings Technology 205 (2010) 1074–1079

[52] R. Bernhardt, G. Schreck, C. Willnow, The virtual robot controller (VRC) interface, Proceeding of ISATA 2000

[53]. Lehtla. Introduction to robotics. TTU, Dept. of Electrical Drives and Power Electronics. Tallinn, 2008. 96 p.

[54] Digital manufacturing environment for robotic workcells verification and off-line programming, Web: http://www.siemens.com/plm

[55] S. Deng, d. Fang, et.al., Application of external axis in robot-assisted thermal spraying, JTTEE5 21 (2013) 1203-1215

[56] S. Deng, Z. Cai, et. al. Application of robot offline programming in thermal spraying, Surface & Coatings Technology 206 (2012) 3875–3882

[57] D. Conner, P. Atkar, et. al., Development of Deposition Models for Paint Application on Surfaces Embedded in R3 for Use in Automated Path Planning, online publication: Carnegie Mellon University, Pittsburgh PA 15213, USA

[58] P. Atkar, D. Conner, et. al., Uniform Coverage of Simple Surfaces Embedded in R3 for Auto-Body Painting, online publication: Carnegie Mellon University, Pittsburgh PA 15213

[59] L. Sheiko, A. Sadovoy, Yu Troschenkov, O Kulyk, Influence of grain boundaries on orientation of spontaneous magnetization inside domains in the Fe – 3% Si ferromagnetic sheets, J. Phys. D. Appl. Phys., 35 (2002), 1 - 3.

[60] A. Sadovoy, R. Subramanian, S. Kyeck, A. Borchardt, Optimization of thermal spray process development by off-line programming with coating thickness simulation, Proceedings 10th International Conference THE A Coatings 2013, Aachen, Germany

[61] J. Richter, A. Sadovoy, A. Borchardt, C. Degel, R. Wilkenhöner, B. Basdere, Advanced Manufacturing and Control of TBC Systems, Presentation at Japanese-German TBC Workshop, Munich, June 25 – 27, 2013

[62] R. Subramanian, A. Sadovoy, N. Hitchman, J. Richter, A. Vaidya, Coatings Reliability for Gas Turbine Components, Presentation at ASM/TTS Thermal Spray Coatings Conference, GE Global Research Center, NY, October 8-9, 2013

[63] A. Sadovoy, R. Subramanian, Method for simulation of the thickness of a coating, Patent US2010/024260, Issued Feb. 16 2010

[64] A. Sadovoy, R. Subramanian, D. Thomaidis, Method and device for coating path generation, Patent US2012/0156362, Issued Jun. 21, 2012

Publications list

Related to thesis topic

[1] A. Sadovoy, R. Subramanian, S. Kyeck, A. Borchardt, Optimization of thermal spray process development by off-line programming with coating thickness simulation, Presentation and Proceedings "10th International Conference THE A Coatings 2013", Aachen, Germany

[2] J. Richter, A. Sadovoy, A. Borchardt, C. Degel, R. Wilkenhöner, B. Basdere, Advanced Manufacturing and Control of TBC Systems, Presentation at Japanese-German TBC Workshop, Munich, June 25 – 27, 2013

[3] R. Subramanian, A. Sadovoy, N. Hitchman, J. Richter, A. Vaidya, Coatings Reliability for Gas Turbine Components, Presentation at ASM/TTS Thermal Spray Coatings Conference, GE Global Research Center, NY, October 8-9, 2013

[4] A. Sadovoy, R. Subramanian, Method for simulation of the thickness of a coating, Patent US2010/024260, Issued Feb. 16 2010

[5] A. Sadovoy, R. Subramanian, D. Thomaidis, Method and device for coating path generation, Patent US2012/0156362, Issued Jun. 21, 2012

Previous publications

[5] L. Sheiko, A. Sadovoy, Yu Troschenkov, O Kulyk, Influence of grain boundaries on orientation of spontaneous magnetization inside domains in the Fe – 3% Si ferromagnetic sheets, J. Phys. D. Appl. Phys., 35 (2002), 1 - 3.

[6] L. Sheiko, A. Sadovoy, Saturation Magnetization Distribution in the Vicinity of a Grain Boundary in a Plate of a Triaxial Silicon-Iron-Type Ferromagnet, Physics of the Solid State Translated from Fizika Tverdogo Tela (Russia), Vol. 43, No. 8, 2001, pp. 1567–1571.

[7] L. Sheiko, A. Sadovoy, G. Brekharya, Calculation of magnetostatic energy f_m related to small-angled grain boundaries in three-axis ferromagnetics such as silicon steel, J. Phys. D. Appl. Phys., 34 (2001), 303-306.

[8]. L. Sheiko, G. Brekharya, O. Kulyk, A. Sadovoy. Experimental investigation of μ^*- effect near the grain boundaries in grain-oriented silicon steel sheets JMMM, 215-216, 86-88 (2000)

[9] Sheiko, G. Brekharya, A. Sadovoy, S. Gaiduk, O. Kulyk, Investigations of magnetostatic fields related to grain boundaries in silicon steel sheets, J. Phys. D. Appl. Phys., 32 (1999), 2851-2855.

Lebenslauf

Alexandr Sadovoy

Diplom - Physiker

Geboren
19. Januar 1978
in Saporoshje, Ukraine

Anschrift
Danckelmannstraße 57
14059 Berlin
Deutschland
Tel.: +493068077002
Mobile: +491732984113
Email: alexandr_sadovoy@yahoo.com

Berufspraxis

1/2009-bis jetzt: Siemens AG
Experte für Beschichtungstechnologien für Gasturbinenbauteile bei der Siemens AG in Berlin. Leitung von R&D- und Qualifizierungsprojekten für die Entwicklung von Beschichtungsprozessen und Technologien, insbesondere im Bereich vom thermischen Spritzen von metallischen und keramischen Hochtemperaturbeschichtungen.

2/2003- 12/2008: Coatec GmbH
Entwicklungsingenieur bei der Fa. COATEC GmbH & Co. KG (Praxair Surface Technologies) in Schlüchtern. Entwicklung und Optimierung von Beschichtungen mit dem CVD (Chemical Vapor Deposition) Verfahren zum Schutz der Turbinenkomponenten gegen Oxidation und Heißgaskorrosion.

09/2000 - 12/2002: Aspirantur
Aspirantur auf dem Lehrstuhl der Physikalischen Materialwissenschaft in der Staatlichen Universität Saporoshje in der Ukraine. Forschungsarbeit auf dem Gebiet der numerischen und analytischen Simulationen von magnetostatischen Effekten in Softmagnetwerkstoffen. Vorbereitung einer Dissertationsarbeit zum Thema „Einfluss der Korngrenzen auf die Domainstruktur und Eigenschaften der softmagnetischen Werkstoffe“.

09/1995 - 06/2000 - Studium
Studium an der Physikfakultät der Staatlichen Universität Saporoshje in der Ukraine, Fachgebiet Festkörperphysik. Das Studium ist mit Diplom des Spezialisten „mit Auszeichnung“ abgeschlossen.